IOAKEIM SIOUTIS

SOFC test rig development and evaluation of electrode materials

SCHOOL OF MECHANICAL ENGINEERING

Sector: Thermal Engineering

Laboratory of Steam Boilers and Thermal Plants

Supervisor: Prof. Dr.-Ing. Sotirios Karellas, NTUA Professor

Athens 2022

ΙΩΑΚΕΙΜ ΣΙΟΥΤΗΣ

Ανάπτυξη πειραματικής διάταξης για κελιά καυσίμου στερεού ηλεκτρολύτη και αξιολόγηση υλικών ηλεκτροδίων

ΣΧΟΛΗ ΜΗΧΑΝΟΛΟΓΩΝ ΜΗΧΑΝΙΚΩΝ

Τομέας: Θερμότητας

Εργαστήριο Ατμοκινητήρων και Λεβήτων

Επιβλέπων: Σωτήριος Καρέλλας, Καθηγητής ΕΜΠ

Αθήνα 2022

--- κενή σελίδα ---

Solemn Declaration for plagiarism and copyright theft:

I have read and understood the rules for plagiarism and how to properly cite the sources contained in the Diploma Thesis writing guide. I declare that, as far as I know, the content of this Thesis is the product of my own work and there are references to all the sources I have used.

The views and conclusions contained in this Thesis are those of the author and should not be construed as representing the official positions of the School of Mechanical Engineering or the National Technical University of Athens.

Full Name: Ioakeim Sioutis

Υπεύθυνη δήλωση για λογοκλοπή και για κλοπή πνευματικής ιδιοκτησίας:

Έχω διαβάσει και κατανοήσει τους κανόνες για τη λογοκλοπή και τον τρόπο σωστής αναφοράς των πηγών που περιέχονται στον οδηγό συγγραφής Διπλωματικών Εργασιών. Δηλώνω ότι, από όσα γνωρίζω, το περιεχόμενο της παρούσας Διπλωματικής Εργασίας είναι προϊόν δικής μου εργασίας και υπάρχουν αναφορές σε όλες τις πηγές που χρησιμοποίησα.

Οι απόψεις και τα συμπεράσματα που περιέχονται σε αυτή τη Διπλωματική εργασία είναι του συγγραφέα και δεν πρέπει να ερμηνευθεί ότι αντιπροσωπεύουν τις επίσημες θέσεις της Σχολής Μηχανολόγων Μηχανικών ή του Εθνικού Μετσόβιου Πολυτεχνείου.

Ονοματεπώνυμο: Ιωακείμ Σιούτης

Acknowledgements

The research for this diploma thesis took place in the Technical University of Clausthal in the Materials Science and Engineering department. I would like to thank Prof. Dr. Ing. Argirusis Christos and Dr.-Ing. Georgia Sourkouni, for the help and the guidance through all the diploma research. I would also like to thank Ph.D. candidates Kalogirou Charalampia Stamatia and Mechili Maria for their advice and support during the whole research period.

Table of Contents

Abstract

Fuel cell technologies are a research field that gains more and more popularity as hydrogen seems to be a sustainable green source of energy for the near future. Among several types of fuel cells, Polymer Electrolyte and Solid Oxide fuel cells are considered the ones with the most potential for high performance. Solid oxide fuel cells currently present the best efficiency and performance results. However, the solid oxide fuel cells require a challenging testing procedure, as they operate in high temperatures (650 ^{o}C -1000^{o}C). In this research, the main goal is to set a testing rig for solid oxide fuel cells as well as a user-friendly software that controls and stores the results of the testing rig. The testing rig consists of a fuel cell fixture that can stand the high temperatures of testing, a furnace system that is controlled by a PID controller, a DC load that is used to draw current from the fuel cell, a potentiostat that performs characterization-techniques measurements and flow valves that control the fuel feed in the anode and the cathode side of the fuel cell. Moreover, the software, which was developed in the LabVIEW program controls all the instruments above, had a graphic environment that presents all the useful information and measurements of the running SOFC experiment, and stores all the measurements automatically with a titling system that helps to the best organization of the results. Furthermore, different electrodes materials are tested in order to evaluate the functionality of both the testing rig and the software, as well as to get a holistic view of the fuel cell working principles. The testing rig will be the foundation for further future testing that will aim not only at the research and development of electrodes and electrolyte materials but also at the utilization of alternative fuels such as ammonia (NH_3) or hydrocarbons.

Περίληψη

Η ανάπτυξη κελιών καυσίμου είναι ένα επιστημονικό πεδίο που κερδίζει όλο και περισσότερο έδαφος. Η χρήση υδρογόνου τόσο για την παραγωγή όσο και την αποθήκευση ενέργειας φαίνεται να είναι η λύση στην μελλοντική βιώσιμη πράσινη οικονομία. Υπάρχουν πολλά διαφορετικά είδη κελιών καυσίμου, καθένα από τα οποία λειτουργεί με διαφορετικό τρόπο και παρουσιάζει τα δικά του πλεονεκτήματα και μειονεκτήματα. Παρ' όλα αυτά δύο είδη εξ' αυτών φαίνεται να παρουσιάζουν ιδιαίτερο ενδιαφέρον λόγω της καλής τους απόδοσης, τα κελιά καυσίμου πολυμερικής μεμβράνης τα οποία δουλεύουν σε χαμηλές θερμοκρασίες (περίπου 60 ^{o}C και τα κελιά στερεού ηλεκτρολύτη, τα οποία δουλεύουν σε υψηλές θερμοκρασίες (στο εύρος των 650 ^{o}C -1000 ^{o}C). Τα κελιά στερεού ηλεκτρολύτη κατέχουν προς το παρόν τον μεγαλύτερο βαθμό απόδοσης και είναι ιδανικά για χρήσεις συμπαραγωγής ενέργειας. Όπως βέβαια είναι φυσικό η λειτουργία σε τόσο υψηλές θερμοκρασίες επιφέρει πολλές δυσκολίες στην πειραματική διαδικασία αξιολόγησης των κελιών καυσίμου. Στα πλαίσια αυτής της διπλωματικής κατασκευάζουμε μια πειραματική διάταξη για την διεξαγωγή ερευνών στον τομέα των κελιών στερεού ηλεκτρολύτη καθώς και ένα λογισμικό το οποίο θα μπορεί να ελέγχει όλες τις μεταβλητές του πειράματος, να παρουσιάζει ευκρινώς και αποτελεσματικά όλες τις πληροφορίες, τα μετρούμενα αποτελέσματα του πειράματος αλλά και να αποθηκεύει με συστηματικό τρόπο όλα τα αποτελέσματα των πειραμάτων. Η πειραματική διάταξη αποτελείται από μια συσκευή συγκράτησης του κελιού, έναν φούρνο ο οποίος ελεγχεται από έναν αναλογικό ολοκληρωτικό διαφορικό (PID) ελεγκτή, από ένα προγραμματιζόμενο ηλεκτρονικό φορτίο το οποίο θα αντλεί φορτίο από το κελί και έναν ποτενσιοστάτη ο οποίος χρησιμοποιείται για ειδικά πειράματα χαρακτηρισμού του κελιού καυσίμου, και από τις βαλβίδες ελέγχου παροχής των καυσίμων που παρέχονται στο κελί. Μετά την ολοκλήρωση του λογισμικού και την κατασκευή της πειραματικής διάταξης έγιναν δοκιμές με κελιά στερεού ηλεκτρολύτη προκειμένου να επιβεβαιωθεί ότι η διάταξη και το λογισμικό δουλεύουν απρόσκοπτα. Τα κελιά που κατασκευάστηκαν δεν είχαν στόχο τη δημιουργία κάποιου κελιού με πρωτοποριακά υλικά και πολύ υψηλή απόδοση. Αντίθετα κατασκευάστηκαν από έτοιμα υλικά ηλεκτροδίων και έτοιμα δισκία ηλεκτρολύτη προκείμένου να αποκτηθεί μια γενική εικόνα γύρω από την λειτουργία, την κατασκευή και την πειραματική διαδικασία κελιών στερεού ηλεκτρολύτη. Η πειραματική διάταξη και το αντίστοιχο λογισμικό αποτελούν την βάση για μελλοντική έρευνα τόσο στον τομέα των υλικών που χρησιμοποιούνται σαν ηλεκτρόδια και σαν ηλεκτρολύτες στα κελιά, όσο και στον τομέα των διαφορετικών καυσίμων που μπορεί να χρησιμοποιηθούν με τα κελιά στερεού ηλεκτρολύτη όπως η αμμωνία (NH_3) και διάφοροι υδρογονάνθρακες.

List of Abbreviations

AFC	Alkaline Fuel Cell
ASCII	American Standard Code for Information Interchange
ASR	Area Specific Resistance
CC	Constant Current
CV	Cyclic Voltammetry
DAQ	Data Acquisition
DC	Direct Current
DMFC	Direct Methanol Fuel Cell
EDX	Energy Dispersive X-ray
EIS	Electrochemical Impedance Spectroscopy
GDC	Gadolinium Doped Ceria
GEIS	Galvanostatic Electrochemical Impedance Spectroscopy
HOR	Hydrogen Oxidation Reaction
LSCF	Lanthanum Strontium Cobalt Ferrite
LSCV	Lanthanum Strontium Chromium Vanadium
LSGM	Lanthanum Strontium Gallium Magnesium
LSM	Lanthanum Strontium Manganite
MCFC	Molten Carbonate Fuel Cell
OCV	Open Circuit Voltage
ORR	Oxygen Reduction Reaction
PAFC	Phosphoric Acid Fuel Cell
PEIS	Potentiostatic Electrochemical Impedance Spectroscopy
PEMFC	Polymer Membrane Fuel Cell

SCPI	Standard Commands for Programmable Instruments
ScSZ	Scandia Stabilized Zirconia
SEM	Scanning Electron Microscope
SOFC	Solid Oxide Fuel Cell
STP	Standard Temperature and Pressure
TEC	Thermal Expansion Coefficient
YSZ	Yttrium Stabilized Zirconia

1. Introduction

1.1 Problem Statement

A fuel cell is a device that converts the chemical energy of hydrogen (or other fuels) through an electrochemical reaction to electricity. In a fuel cell, hydrogen is combined with oxygen to generate electricity, heat, and water. A fuel cell is like a battery except that it does not need periodically recharge. Instead, it will continue to produce electricity as long as a fuel source is provided. A single fuel cell can generate only about some mW however; multiple cells are connected in series or parallel to form a stack that can produce from 1W to 10MW. The basic structure of a fuel cell is composed of an anode, a cathode, and an electrolyte that separates the previous two. The electrolyte is a material with ion conductivity but no electrical conductivity so as to prevent a short circuit between the anode and the cathode. The anode and cathode should acquire both electronic and ionic conductivity. Anode and cathode are the electrodes where the electrochemical half-reactions occur.

$$H_2 \rightarrow 2H^+ + 2e^- \quad (1.1)$$

$$\frac{1}{2}O_2 + 2H^+ + 2e^- \rightarrow H_2O \quad (1.2)$$

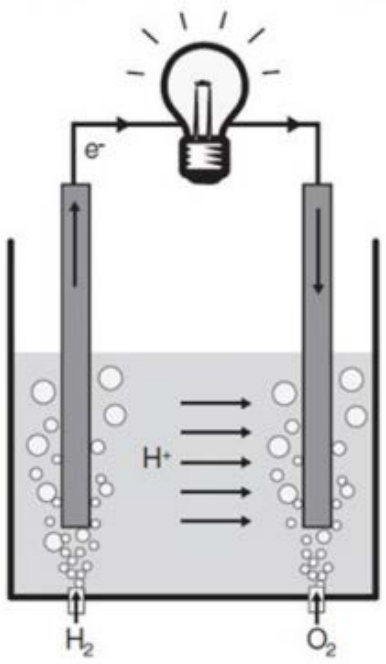

Figure 1.1 Simple Fuel cell structure [1]

Figure 1.1 displays the basic working principles of a fuel cell [1]. In the left electrode, the hydrogen splits into protons (H+) and electrons (as described in equation (1.1)). Due to the electrolyte's ion conductivity and electrical insulation, the H+ protons can flow through the electrolyte. Thus, the electrons can flow only through the wire that connects the two electrodes. When the electrons end on the right electrode, they will recombine with both the H+ protons and the oxygen and they will form water (as described in equation (1.2)). Introducing a load in the wire path (for example a light bulb in figure 1.1) is what will result in power production from the fuel cell.

1.1.1 Fuel cell advantages and disadvantages

Fuel cells present many advantages; consequently, they are under intense research and development recently. Firstly, fuel cells are environmentally friendly, as in most cases the only products of the electrochemical reaction are pure water and heat. Moreover, since they produce directly electrical energy, they are far more efficient than combustion engines. Another benefit is that fuel cells can be solid-state, which means they have no moving parts. As a result, they are reliable and work silently. Additionally, the power and the capacity of fuel cells are independent of their size/weight, while in batteries there is a strong dependency. Last but not least, the recharging/refueling time of fuel cells is much faster than that of the batteries.

On the other hand, hydrogen commercial availability and storage systems constitute a crucial problem of fuel cells. Despite that alternative fuels (such as methanol, gasoline, ammonia, etch.) can be used, they usually require a reforming step before entering the fuel cell, which implies complicated systems and more efficiency factors. Furthermore, hydrogen is a fuel with low volumetric energy density. For that reason, combustion engines and batteries have better volumetric power densities than fuel cells. Finally, yet importantly, fuel cells are sensitive to environmental poisons and rapidly transit phenomena.

1.1.2 Types of fuel cells and their working principle

There are five categories of fuel cells, in which the main differences rely on the electrolyte material, the operating temperature, and the fuels which they can work with:

1. PEMFC (Polymer Membrane Fuel Cell)
2. PAFC (Phosphoric Acid Fuel Cell)

3. AFC (Alkaline Fuel Cell)
4. MCFC (Molten Carbonate Fuel Cell)
5. SOFC (Solid Oxide Fuel Cell)

The table below describes the characteristics of each fuel cell type.

Table 1.1 Types of fuel cells

Type	***Op. Temp. (°C)***	***Electrolyte***	***Fuel***
PEMFC	50-100	Polymer Membrane	H_2, CH_3OH
PAFC	120-200	Liquid H_3PO_4	H_2
AFC	60-220	Liquid KOH	H_2
MCFC	550-650	Molten Carbonate	H_2,CH_4
SOFC	650-1000	Ceramic	H_2,CH_4,NH_3

- PEMFC

As the name implies, PEMFCs use a thin polymer membrane as an electrolyte (the most common material for PEMFC electrolyte is Nafion™). Hydrogen is supplied in the anode of the cell where the HOR (hydrogen oxidation reaction) takes place. The ionic charge carrier is the H+ protons that migrate through the electrolyte on the cathode side. Subsequently, the H+ protons react with the O2 in the cathode where the ORR (oxygen reduction reaction) happens and as a result, water and heat are produced. PEMFC is an attractive type of fuel cell since it can work in low temperatures.

$$Anode: H_2 \rightarrow 2H^+ + 2e^-$$

$$Cathode: \frac{1}{2}O_2 + 2H^+ + 2e^- \rightarrow H_2O$$

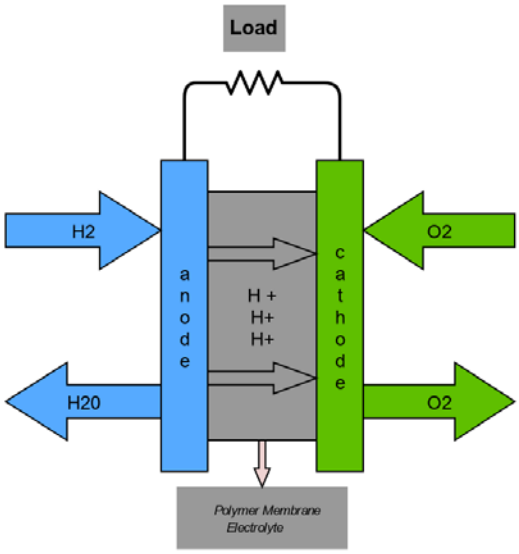

Figure 1.2 Polymer Electrolyte Membrane Fuel Cell

A variation of PEM fuel cells is the DMFC (Direct Methanol Fuel Cells). In DMFCs, instead of hydrogen, methanol is fed directly into the anode of the fuel cell. The use of methanol solves many problems concerning the storage and the use of compressed hydrogen. However, DMFCs have low fuel efficiency because of the methanol crossover in the membrane of the fuel cell. Another problem is that carbon dioxide is formed in the anode side. DMFCs are used in applications with low power demands over a long time.

$$Anode: CH_3OH + H_2O \rightarrow CO_2 + 6H^+ + 6e^-$$

$$Cathode: \frac{3}{2}O_2 + 6H^+ + 6e^- \rightarrow 3H_2O$$

- PAFC

Phosphoric Acid fuel cells work in the same principle as Polymer electrolyte fuel cells with the difference that the electrolyte is phosphoric acid. This type of fuel cell operates at higher temperatures than PEMFC and is used widely in CHP plants.

$$Anode: H_2 \rightarrow 2H^+ + 2e^-$$

$$Cathode: \frac{1}{2}O_2 + 2H^+ + 2e^- \rightarrow H_2O$$

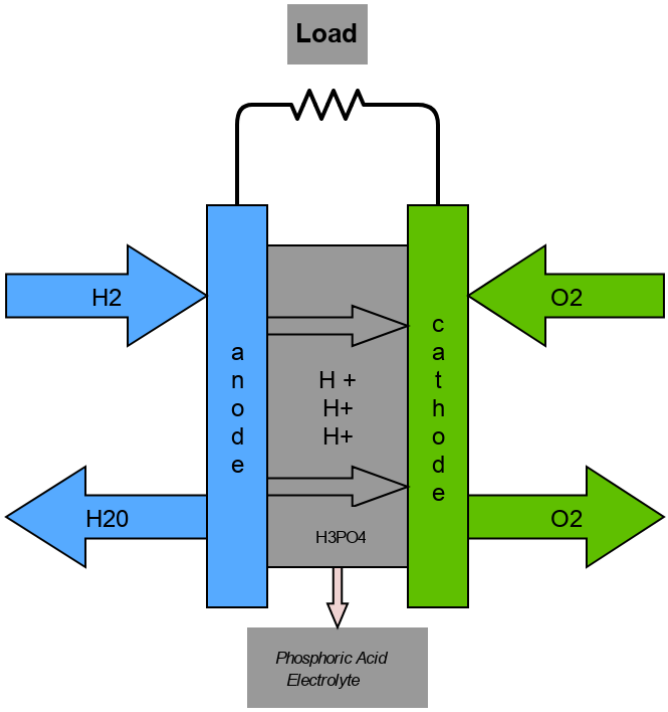

Figure 1.3 Phosphoric Acid Fuel Cell

- AFC

  Alkaline Fuel Cells use a Potassium Hydroxide solution as an electrolyte. This type of fuel cell shows high electrical efficiency, 50-60%. Additionally, AFCs can work with Nickel catalysts and as a result, the cost of their production is low. However, they are susceptible to carbon dioxide contained in the air. The carbon dioxide reacts with the electrolyte and forms an insoluble carbonate. For that reason, AFCs are fed with pure oxygen. There are three main configurations of AFC:

  Static electrolyte (the electrolyte is contained in matrix material between the electrodes)

  Mobile electrolyte (the electrolyte is circulated inside the cell)

  Dissolved fuel (the fuel, which can be ammonia or hydrazine is dissolved in the electrolyte).

$$Anode: H_2 + 2OH^- \rightarrow 2H_2O + 2e^-$$

$$Cathode: \frac{1}{2}O_2 + H_2O + 2e^- \rightarrow 2OH^-$$

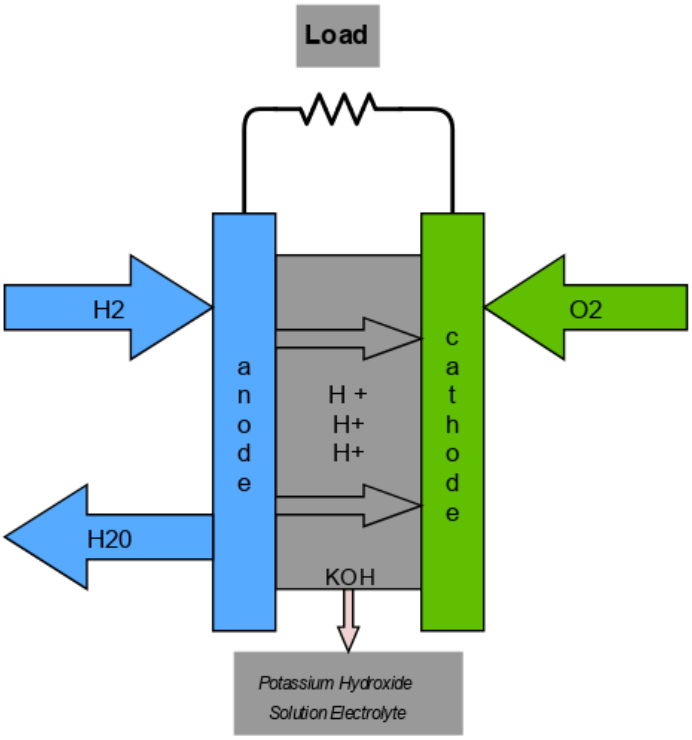

Figure 1.4 Alkaline Fuel Cell

- MCFC

Molten Carbonate Fuel Cells are high-temperature fuel cells which deliver an efficiency of about 55%. The electrolyte of MCFCs consists of a liquid mixture of sodium and potassium carbonates. A lithium aluminum oxide (LiOAlO2) ceramic matrix is used to hold the liquid electrolyte in high temperatures. These fuel cells can work with hydrocarbon fuels. The electrolyte uses carbonate ions (CO_3^{2-}) as charge carrier ions, so it is essential to feed CO2 to the cathode. When hydrocarbons are used

as a fuel, they are reformed within the fuel cell into hydrogen and carbon monoxide which is then oxidized and fed back to the anode as carbon dioxide.

$$Anode: H_2 + CO_3^{-2} \rightarrow H_2O + CO_2 + 2e^-$$

$$Cathode: \frac{1}{2}O_2 + CO_2O + 2e^- \rightarrow CO_3^{-2}$$

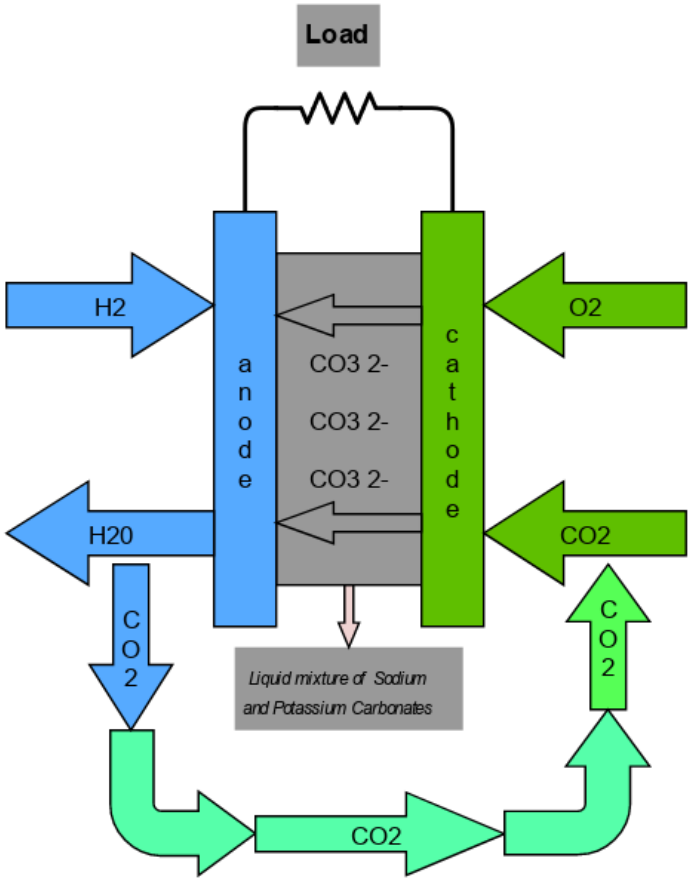

Figure 1.5 Molten Carbonate Fuel Cell

- SOFC

Solid oxide fuel cells are the cells that operate at the highest temperatures. The electrolyte is usually made of ceramic materials, with the most popular one being YSZ (Yttrium Stabilized Zirconia). Solid oxide fuel cells show numerous benefits as they are not susceptible to CO or CO2. Due to the high working temperature and with the suitable catalysts fuel such as methane or ammonia can be reformed into hydrogen and carbon dioxide or nitrogen directly in the cell. As a result, SOFC can work with a wide range of fuels. Another advantage of SOFC is that they have neither corrosive electrolytes nor any moving parts. Consequently, they show reliable, quiet, and last long operation. Last but not least, SOFCs do not require expensive catalysts as well as there is plenty of knowledge in the production of the ceramic materials from which they consist.

There are two configurations of SOFC: Oxygen ion-conducting and Hydrogen proton-conducting. Despite that from the thermodynamic aspect, proton-conducting SOFC can achieve a higher potential the proton-conducting electrolyte research and manufacturing is in an initial stage without consistent results.

H-SOFC	O-SOFC
$Anode: H_2 \rightarrow 2H^+ + 2e^-$ $Cathode: \frac{1}{2}O_2 + 2H^+ + 2e^- \rightarrow H_2O$	$Anode: H_2 + O_2^{-2} \rightarrow H_2O + 2e^-$ $Cathode: \frac{1}{2}O_2 + 2e^- \rightarrow O_2^{-2}$

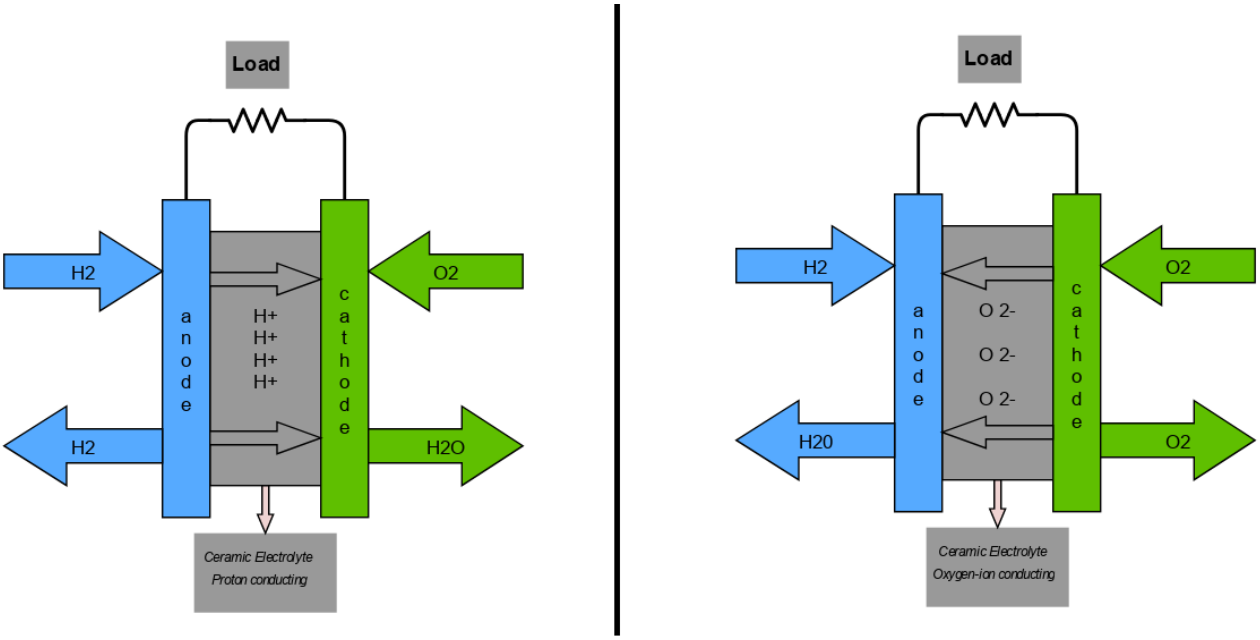

Figure 1.6 Solid Oxide Fuel Cell

1.2 Project Objective and Constraints

First of all, the main goal is to fabricate a rig for reliable and consistent measurements of the voltage, the current, the temperature and the flow rate of the fuel gases. Moreover, to create an application that can easily control the measurement instruments and systematically store the data from the experiments. After developing the testing facility, the goal is to fabricate fuel cells with various anode and cathode materials (the electrolytes are bought as 25mm discs) and evaluate their performance. Due to the strictly limited time schedule to six months, as the whole research is taken place in TU Clausthal University via Erasmus+ program, the aim is to get a holistic view of solid oxide fuel cells, how they work, how they are fabricated and how they are tested and not to create a novel high-performance fuel cell. Furthermore, the testing facility will be the foundation for future test, research and development in the field of electrodes and electrolyte materials for SOFC.

2.Fuel Cell Modeling

2.1 Thermodynamics

The first law of thermodynamics states that energy can neither be created nor destroyed. From another view, energy can be transferred between a closed system and its surroundings via heat or work.

$$dU = dQ - dW \ (2.1)$$

Gibbs free energy, denoted as G, is defined as the enthalpy minus the temperature multiplied by the entropy of a system. Gibbs free energy indicates when a chemical reaction is spontaneous or nonspontaneous. A nonspontaneous reaction occurs only with external energy input and has positive Gibbs energy. A spontaneous reaction occurs without any external energy input and has negative Gibbs energy. Gibbs free energy gives essential information for the electrochemical systems as it calculates the maximum amount of energy that is available to do electrical work.

$$G = H - TS \ (2.2)$$

Differentiating the equation (2.2) results in:

$$dG = dH - T\,dS - S\,dT \ (2.3)$$

Assuming that the mechanical work is produced solely from the expansion of the system against pressure. Then:

$$dW_{\mathrm{mech}} = p\,dV \ (2.4)$$

so from eq. (2.1)

$$dU = dQ - dW_{elec} - p\,dV \ (2.5)$$

Furthermore, enthalpy is defined as:

$$H = U + pV \ (2.7)$$

And the differentiation of eq. (2.7) gives:

$$dH = dU + p\,dV + V\,dp \ (2.8)$$

At this stage, because the calculations concern a fuel cell model, a reasonable assumption is that during the reaction we have a constant-temperature, constant-pressure process. Thus, according to the second thermodynamic law for a reversible heat transfer under constant pressure:

$$dQ = T\,dS \ (2.9)$$

Combining equations 2.3, 2.5, 2.8, 2.9 we get:

$$dG = Vdp - S\,dT - dW_{elec} \ (2.10)$$

However, for a constant-temperature, constant-pressure process dp = 0 and dT = 0.

Thus:

$$dG = -\,dW_{elec} \ (2.11)$$

Calculating now the electrical work done by a moving charge Q:

$$W_{elec} = EQ \ (2.12)$$

Where:

E is the electrical potential difference measured in Volts.

Q is the moving charge, which in the case of fuel cells is carried by electrons.

$$Q = nF \ (2.13)$$

Where:

n is the number of electrons transferred

F is the Faraday's constant

Given that at STP conditions Gibbs free energy change of the reaction $H_2 + \frac{1}{2}O_2 \rightarrow H_2O$ is -237 kJ/mol. Then the maximum voltage that can be generated by a hydrogen oxygen fuel cell working in STP conditions is:

$$E^0 = \frac{-\,dG}{nF} = 1{,}23\ V \ (2.14)$$

Temperature and pressure are crucial variables in the operation of fuel cells. Generally, an increase in the working temperature and pressure of the fuel cell will result in better efficiency. From the thermodynamics aspect, an increase in the temperature will result in a slight decrease in the reversible voltage. Moreover, an increase in the pressure will result in a slight increase in the reversible voltage. However, it is worth noticing that changes in the temperature and pressure have a negligible effect on the thermodynamic reversible voltage calculations.

Last but not least, changes in the concentration of the electrodes affect the reversible voltage. The chemistry of a system is quantified as chemical potential. Chemical potential changes result in changes in the Gibbs free energy and consequently in reversible voltage changes [3].

$$\mu_i^a = \left(\frac{\partial G}{\partial n_i}\right)_{T,p,n\neq i} \quad (2.15)$$

Where:

μ_i^a is the chemical potential of species i in phase a,

$\left(\frac{\partial G}{\partial n_i}\right)_{T,p,n\neq i}$ expresses the difference created in Gibbs free energy for an infinitesimal increase in the quantity of species i, under constant temperature, pressure and all the quantities of other species.

The connection of the phase a and the chemical potential of species i is calculated from the following equation:

$$\mu_i = \mu_i^0 + RT \ln a_i \quad (2.16)$$

Where a_i is calculated according to the following table:

Table 2.1 Activity a calculation

Chemical nature	**a_i =**	**Description**
electrons in metals	1	
pure components	1	e.g. activity of platinum in a platinum electrode
ideal gas	p_i/p^0	where pi is the partial pressure of the gas and p^0 is standard state pressure
non ideal gas	$\gamma(p_i/p^0)$	where $\gamma \in (0,1)$ is the coefficient that describes the departure from ideality
dilute	c_i/c^0	where ci is the molar concentration of the species and c^0 is the standard state concentration
non ideal solutions	$\gamma(c_i/c^0)$	where $\gamma \in (0,1)$ is the coefficient that describes the departure from ideality

Assuming a chemical reaction on a molar basis for species K:

$$1K + lL \rightarrow mM + nN \ (2.17)$$

Then via equations (2.14, 2.15, 2.16) results to:

$$E = E^0 - \frac{RT}{nF} \ln \frac{a_M^m \, a_N^n}{a_K^1 \, a_L^l} \quad (2.18)$$

Generalizing equation (2.18) for a system with an arbitrary number of products and reactants results to Nernst's equation:

$$E = E^0 - \frac{RT}{nF}\ln\frac{\prod a_{products}^{u_i}}{\prod a_{reactants}^{u_i}} \quad (2.19)$$

Additionally, to fully describe the thermodynamic behavior of the cell accounting both temperature and pressure variations, combining the equations (2.10, 2.14 and 2.19):

$$E = E^0 - \frac{RT}{nF}\ln\frac{\prod a_{products}^{u_i}}{\prod a_{reactants}^{u_i}} + \frac{\Delta S}{nF}(T - T_0) \quad (2.20)$$

2.2 Kinetics

There are two types of reactions regarding the phase of the reactants and products: heterogeneous and homogeneous. In the homogeneous reaction, both the reactants and products are in the same phase while in heterogeneous they are in a different phase. The electrochemical processes described in this thesis are heterogeneous. As a result, they occur in the boundary layer where the electrode and the electrolyte intersect. Because electrochemical reactions occur at specific surfaces, the current which is produced is highly dependable from the active surface. In order to neutralize the geometrical effect of the fuel cell in our calculations we introduce the current density j (A/cm^2) which is basically:

$$j = \frac{i}{A} \quad (2.21)$$

According to the band theory of solids, the available energy states form bands instead of discrete energies as in the free atom case, assuming there are conduction and valence bands. In insulators, there is a large gap between electrons of the valence band and electrons of the conduction band. In conductors, the two bands are overlapping as shown in the picture below.

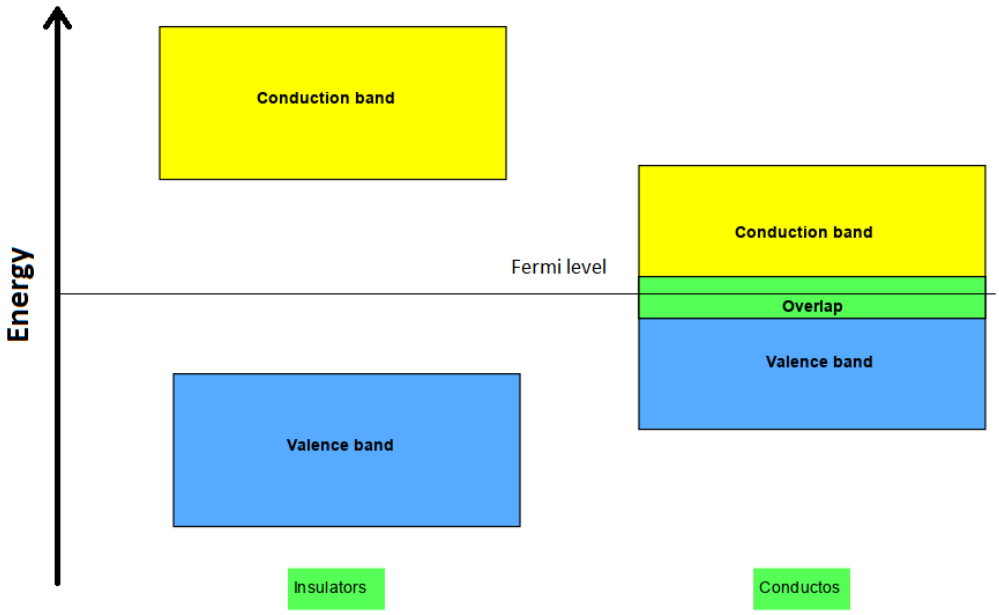

Figure 2.1 Band theory graph

Fermi level is the chemical potential. By controlling the electrode potential, we can control the direction of the electrochemical reaction (for example, whether oxidation or reduction will occur).

In every chemical reaction, there is a finite number that defines the rate at which the reactants are converted into products. Moreover, for a chemical reaction to take place, the reactants should overcome the reaction's activation energy. The probability of this process determines the reaction rate. The reactions can be analyzed in several basic steps. Therefore, the slowest step of the reaction will determine the reaction rate. A characteristic example of the potential energy graph is shown below:

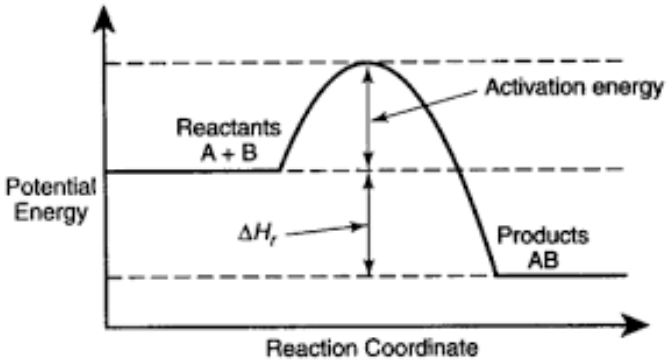

Figure 2.2 Activation energy

According to statistical mechanics [3], the probability (P_{act}) of finding species that have overcome the activation barrier is exponentially dependent on the activation barrier size (E_a).

$$P_{act} = e^{-E_a/(RT)} \quad (2.22)$$

As a result, the reaction rate can be written as:

$$J_1 = c_R^* \cdot f_1 \cdot P_{act} \Rightarrow J_1 = c_R^* \cdot f_1 \cdot e^{-E_a/(RT)} \quad (2.23)$$

Where:

J_1 is the reaction rate,

c_R^* is the reactant surface concentration (mol/cm^2)

f_1 is the the decay rate of species to form products

Taking into consideration both the forward and the reverse reaction, the net reaction rate is calculated as:

$$J_{net} = J_1 - J_2$$

$$J_{net} = c_R^* \cdot f_1 \cdot e^{-E_a/(RT)} - c_P^* \cdot f_2 \cdot e^{-(E_a - \Delta h_f)/(RT)} \quad (2.24)$$

Defining the reaction rate per unit area, in the same way as the current density is defined:

$$J = \frac{dN}{A\,dt} = \frac{i}{nF\bar{A}} = \frac{j}{nF} \quad (2.25)$$

Where:

dN/dt is the reaction rate

n is the number of electrons transferred

F is the Faraday's constant

From equation (2.24) we can convert reaction rate to current density as:

$$j_{net} = n \cdot F \cdot [c_R^* \cdot f_1 \cdot e^{-E_a/(RT)} - c_P^* \cdot f_2 \cdot e^{-(E_a - \Delta h_f)/(RT)}] \quad (2.26)$$

It is worth mentioning that the j_{net} should be equal to zero at thermodynamic equilibrium.

As figure 2.2 indicates, the activation barriers for the forward versus the reverse reaction are unequal. Hence, the forward reaction rate will be faster than the reverse reaction rate. This difference in the rates will lead to the accumulation of e^- in the metal of the electrode and H^+ in the electrolyte. This charge build-up will lead to a potential difference $\Delta\phi$ in the interface of the electrode and the electrolyte which will counterbalance the chemical free energy. The graphs below represent the process described.

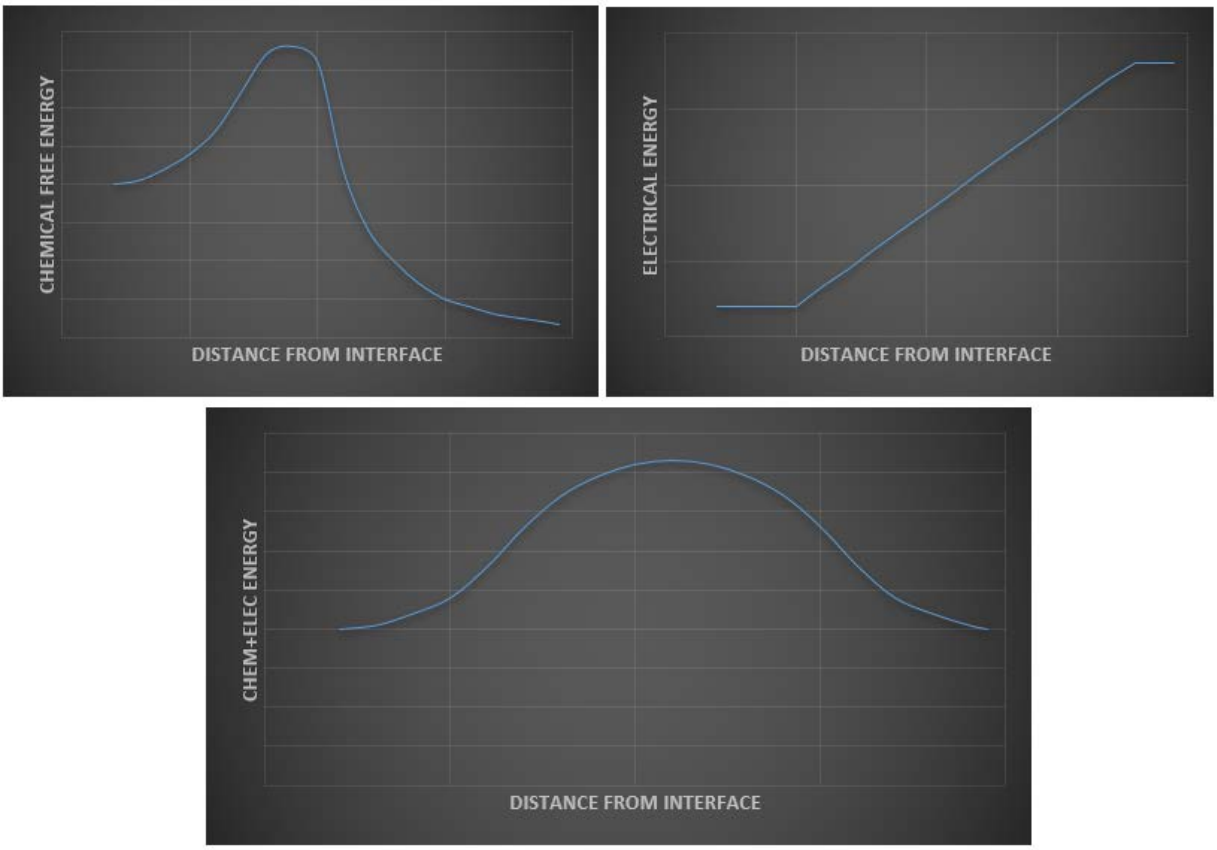

Figure 2.3 Activation energy equilibrium

Observing the graphs above, we can state that in order the equilibrium to be achieved the forward activation barrier decreases by η_{act} (where η_{act} is the voltage loss due to activation), and the reverse activation barrier increases by $(1-a)\cdot\eta_{act}$ (where a is a coefficient that expresses the symmetry of the activation barrier and it varies from 0,2 to 0,5). Therefore, the net current density is calculated as:

$$j = j_0\left(e^{anF\eta_{act}/(RT)} - e^{-(1-a)nF\eta_{act}/(RT)}\right) \quad (2.27)$$

Where j_0 is the current density of the equilibrium for both forward and reverse reaction.

Finally, taking into account the concentrations of the reactant and product species, results to the Butler Volmer equation:

$$j = j_0^0 \left(\frac{c_R^*}{c_R^{0*}} \cdot e^{anF\eta_{act}/(RT)} - \frac{c_P^*}{c_P^{0*}} \cdot e^{(a-1)nF\eta_{act}/(RT)} \right) \quad (2.28)$$

Many conclusions can be drawn from the Butler Volmer equation. First of all, it is observed that the current produced by the electrochemical reaction is exponentially increasing with the activation overvoltage η_{act} . Moreover, it is worth mentioning that the kinetics of the electrochemical reaction induce an exponentially shaped loss. This loss will be observed later in the characteristic j-V fuel cell curve. Furthermore, because current density is analogous to j_0 the higher the j_0 the higher the performance of the fuel cell. Thus, the ways that lead to j_0 increase are the following:

- Decreasing the activation barrier of the reaction. This can be achieved by using highly catalytic materials for electrodes.
- Increasing the reactants' concentration. By increasing the fuel cell's operation pressure, a higher reactant concentration is achieved.
- Increasing the working temperature.
- Increasing the reaction sites. By using highly porous electrode the reaction sites are increased.

Last but not least, it is worth mentioning that there are two useful simplifications/approximations of Butler Volmer equation known as Tafel equations. For very low activation overvoltage values (around 15 mV) the following equation results:

$$j = j_0 \frac{nF\eta_{\text{act}}}{RT} \quad (2.29)$$

The above equation indicates that current density is linearly dependent on the activation overvoltage.

As for the high activation overvoltage (around 100 mV) the Butler Volmer equation is simplified to:

$$j = j_0 \left(e^{anF\eta_{act}/(RT)} \right) \quad (2.30)$$

2.3 Charge Transport

Two types of charge transport occur inside the fuel cell, ion and electron charge transport. These two types work in a completely different way, mainly because of the big difference in the mass of electrons and ions. Ion charge transport is much more difficult than electron charge transport. In order to study the charge transport phenomenon lets define first some fundamental concepts.

Flux (J) defined as the quantity that flows through a certain surface at a certain time, divided by the surface area and time. Charge flux, which represents a current density is defined as:

$$j = z_i F J \quad (2.31)$$

Where:

z_i = the amount of charge carried by a charged species

F = Faraday's constant

J = molar flux

There are three different processes with which the charge can be transported:

1. Conduction. The driving force of this process is the electrical potential gradient $dV \,/\, dx$ and the coupling coefficient is the conductivity (σ). Conduction is described from the following equation:

$$J = \frac{\sigma}{|z_i|F}\frac{dV}{dx} \quad (2.32)$$

2. Diffusion. The driving force of this process is the concentration gradient $dc \,/\, dx$ and the coupling coefficient is diffusivity (D). Diffusion is described from the following equation:

$$J = -D\frac{dc}{dx} \quad (2.33)$$

3. Convection. The driving force of this process is the concentration gradient $dp\ /\ dx$ and the coupling coefficient is viscosity (μ). Convection is described from the following equation:

$$J = \frac{Gc}{\mu}\frac{dp}{dx} \quad (2.34)$$

Where:

G = geometric constant

c = the concentration of the transported species

From all the processes above the most dominant is the conduction.

Assuming that we have a disc with radius R and thickness L. Then the area of the disc from which the current flows is $A = \pi R^2$ and the charge transport according to eq. (2.32):

$$j = \sigma\frac{V}{L} \Rightarrow V = j\frac{L}{\sigma} \Rightarrow V = i\left(\frac{L}{A\sigma}\right) \quad (2.35)$$

It is observed that the charge transport induces an ohmic loss ($R = \frac{L}{A\sigma}$). This voltage loss arises because of the conductor's intrinsic resistance to charge transport.

Both electron and ions transport create an ohmic loss which is defined as:

$$\eta_{ohmic} = iR_{ohmic} = i(R_{elec} + R_{ionic}) \quad (2.36)$$

Moreover, from equation (2.35) we can conclude that the ohmic resistance of the fuel cell is highly dependable from the geometry of the electrode. For that reason, in order to be able to compare the performance of different fuel cells we introduce the area specific resistance (ASR_{ohmic}) which is simply:

$$ASR_{ohmic} = A_{Cell} \cdot R_{ohmic} \quad (2.37)$$

2.4 Mass Transport

Mass transport is the last aspect that contributes to the fuel cell model. As has been mentioned above, the concentrations of the reactants and the products within the catalyst layer are crucial variables that affect the performance of the fuel cell. More specifically, concentrations of products and reactants have been included in the Nernst equation as well as in the Butler Volmer equation.

Assuming in the Nernst equation (2.19) that we have single reactant species and that the concentration voltage loss is attributed only to the depletion of the reactants in the catalyst layer (we neglect the accumulation of the product species). Then:

$$\eta_{conc,thermo} = E^0_{Nernst} - E^*_{Nernst} \Rightarrow$$

$$\eta_{conc,thermo} = \frac{RT}{nF} \ln \frac{c^0_R}{c^*_R} \quad (2.38)$$

Where:

c^0_R = catalyst layer reactant concentration

c^*_R = bulk reactant concentration

From equation (2.33) assuming a steady-state situation we have:

$$J = -D^{eff} \frac{c^*_R - c^0_R}{\delta} \Rightarrow j = nFD^{eff} \frac{c^*_R - c^0_R}{\delta} \quad (2.39)$$

Where:

Deff = effective reactant diffusivity

From equation (2.39) we can define the limiting current density (j_L), which is the current density that causes the reactant concentration to be equal to zero ($c^*_R = 0$). Therefore:

$$j_L = nFD^{eff} \frac{c^0_R}{\delta} \quad (2.40)$$

Finally, the equations (2.38, 2.39, 2.40) result to:

$$\eta_{conc,thermo} = \frac{RT}{nF} \ln \frac{j_L}{j_L - j} \quad (2.41)$$

As far as the effect of concertation to the reaction rate is concerned, previously (eq. 2.30) the activation loss is defined as:

$$\eta_{act} = \frac{RT}{anF} \ln \frac{j c_R^*}{j_0 c_R^0} \quad (2.42)$$

Calculating now the incremental voltage loss due to the concentration:

$$\eta_{conc,kinetic} = \eta_{act}^* - \eta_{act}^0 = \frac{RT}{anF} \ln \frac{c_R^0}{c_R^*} = \frac{RT}{anF} \ln \frac{j_L}{j_L - j} \quad (2.43)$$

Finally, combining the concentration effect in thermodynamics and kinetics we end up with the total concentration loss which is expressed as:

$$\eta_{conc} = \frac{RT}{nF} \left(1 + \frac{1}{a}\right) \ln \frac{j_L}{j_L - j} \quad (2.44)$$

Considering the analysis above, we conclude that the objective of the fuel cell's intake design is to keep the c_R^0 at a constant and high value within the fuel cell flow channels.

2.5 Fuel cell model

Taking into consideration all the paragraphs above, the equation that describes the fuel cell's performance is:

$$V = E_{Thermo} - \eta_{act} - \eta_{ohmic} - \eta_{conc} \quad (2.45)$$

In other words, the voltage which is produced from a fuel cell is the result of the theoretical thermodynamic potential, minus the kinetic, charge and mass transport losses. In the reality one additional form of loss exists and it is associated with undesired side reactions, gas crossover and current leakage. Furthermore, in this model it is assumed that water is present only as gas, which is an accurate assumption for the Solid Oxide fuel cells. The fuel cell's model can be also graphically represented from the characteristic V-I curve. A typical V-I curve has the following form.

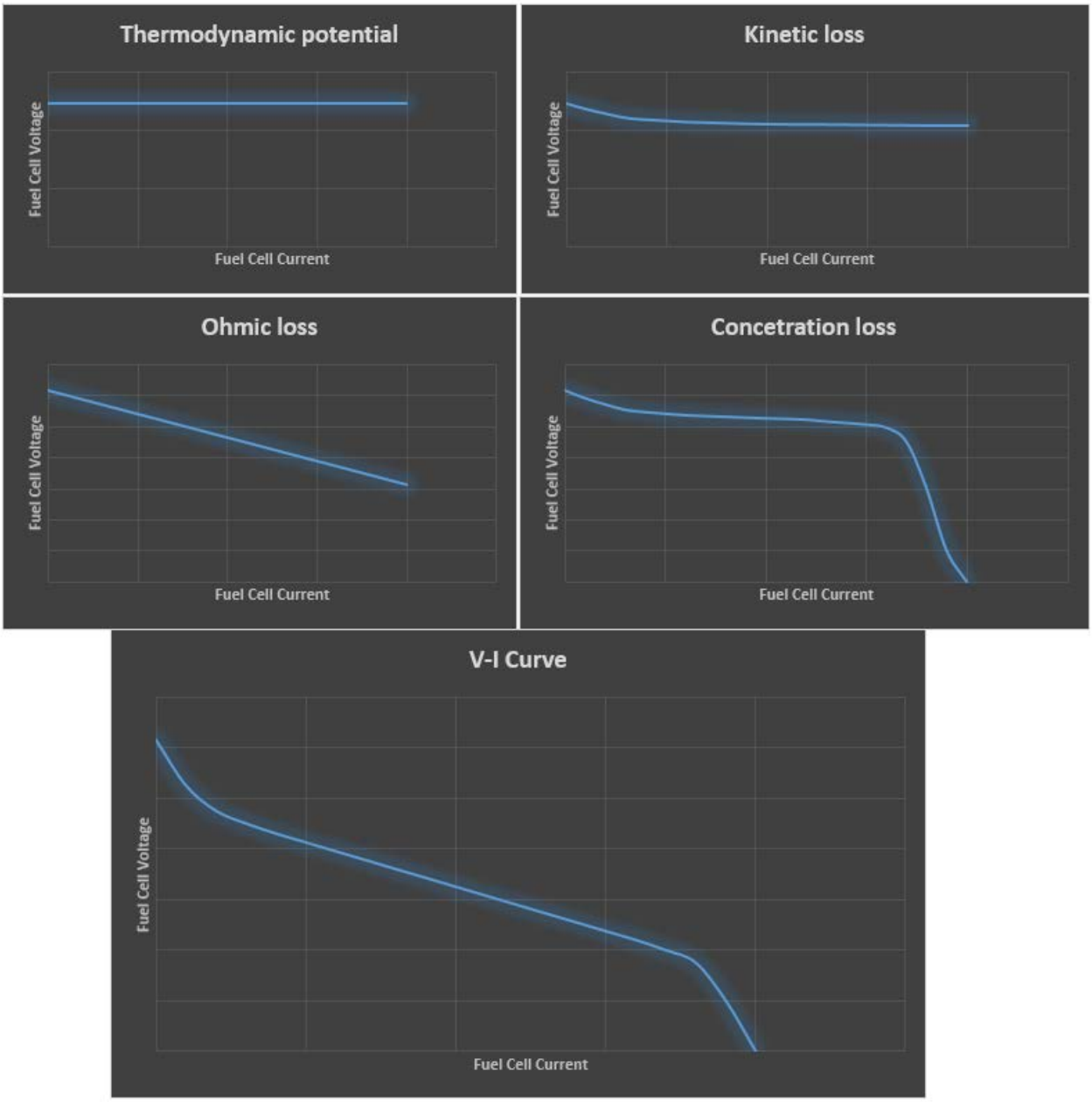

Figure 2.4 Fuel Cell V-I curve

Taking into consideration the modeling analysis of the fuel cells, the following results, concerning mostly the fabrication and the geometry of the fuel cell, emerge.

Electrodes:

The electrochemical reaction takes place only in the triple-phase boundaries (TPBs), i.e. the zone where the gas, the electrolyte (which is only ion conductive, or else the anode will be short-circuited with the cathode) and the electrically conductive electrode are in contact. For that reason, maximizing the TPBs will improve drastically the performance of the cell. To increase the TPBs the electrodes should be highly porous. Moreover, the thickness of the electrodes is a crucial aspect. On one hand, thicker electrodes will increase the reaction sites, on the other hand increasing the thickness affects negatively the electrodes' diffusivity.

Electrolyte:

To decrease electrolyte resistance, the electrolyte should be as thin as possible. However, the thickness of the electrolyte adds structural integrity to the electrolyte. Additionally, thickness prevents pinholes and non-uniformities to be created in the electrolyte's surface which lead to fuel crossover and electrical hot spots. Moreover, there is a physical limit that dictates the lowest thickness of the electrolyte. That is the dielectric breakdown properties of the material according to which the electric field across the electrolyte layer exceeds the dielectric breakdown of the material.

3. Solid Oxide Fuel Cell Materials

Solid oxide fuel cells are fabricated from ceramic materials to withstand the high working temperatures. As is mentioned in the model analysis above, each layer (anode, cathode, and electrolyte) presents alternative demands regarding ion/electrical conductivity and porosity. In addition, all the layers must be chemically and mechanically compatible, as in higher temperatures, the layers expand. In the next paragraphs, the characteristics of each layer will be discussed thoroughly as well as the most commonly applied materials. Last but not least, a brief description of the interconnect materials that are used in solid oxide fuel cell stacks will be provided.

3.1 Electrolyte Materials

As far as conductivity is concerned, the electrolyte layer must have high ionic conductivity and as low as possible electronic conductivity. Electrolytes achieve ion conductivity with the defect hopping mechanism. It is worth mentioning that ceramic materials have significantly lower ionic conductivity compared to polymeric proton conductors that are used in other types of fuel cells like PEMFCs. This is one of the reasons that solid oxide fuel cells must operate at high temperatures. Developing electrolyte materials that can operate with high efficiency in temperatures like (500^{o}C to 800^{o}C) is a growing research field that will revolutionize the use of solid oxide fuel cells [2]. As far as porosity is concerned the electrolyte layer must be dense to prevent gas leakage from the anode to the cathode side of the fuel cell. Moreover, the thickness of the electrolyte layer is of utmost importance. A thick electrolyte layer, on the one hand, presents great mechanical properties for the cell and creates a dense barrier between the anode and the cathode, on the other hand, it will end up creating high ohmic losses. A thin electrolyte layer will definitely increase the efficiency of the fuel cell; however, the structural integrity of the cell can be compromised and there is a possibility of pinholes to be observed in the layer. Consequently, the thickness of the electrolyte layer is a complex problem that can be solved only with optimization methods taking into consideration the sensitivity factor of each variable (resistance, operating temperature, mechanical integrity, surface defects, etch.)

Having referred to the characteristics of solid oxide electrolytes, let's proceed to the most common materials that are used as electrolytes.

3.1.1 Yttria Stabilized Zirconia

Yttria Stabilized Zirconia (YSZ) is probably the most famous electrolyte material for solid oxide fuel cells. Zirconium Oxide (ZrO_2) is doped with a certain amount of Yttrium Oxide (Y_2O_3), to increase the oxygen vacancies and to stabilize the conductive cubic fluorite phase. The process of doping the Zirconium oxide with Yttrium oxide is called aliovalent doping because each time two zirconium cations (Zr 4+) are replaced by two Yttrium cations (Y 3+) and one oxygen site will be left vacant to maintain charge balance [1]. Thus, the ionic conductivity is increased. However, there is a limit for the doping amount of Yttria to zirconia (6-8% molar basis), after that the ion conductivity drops again. The variation of conductivity of YSZ is shown in the diagram below [3] [4] [5] [6].

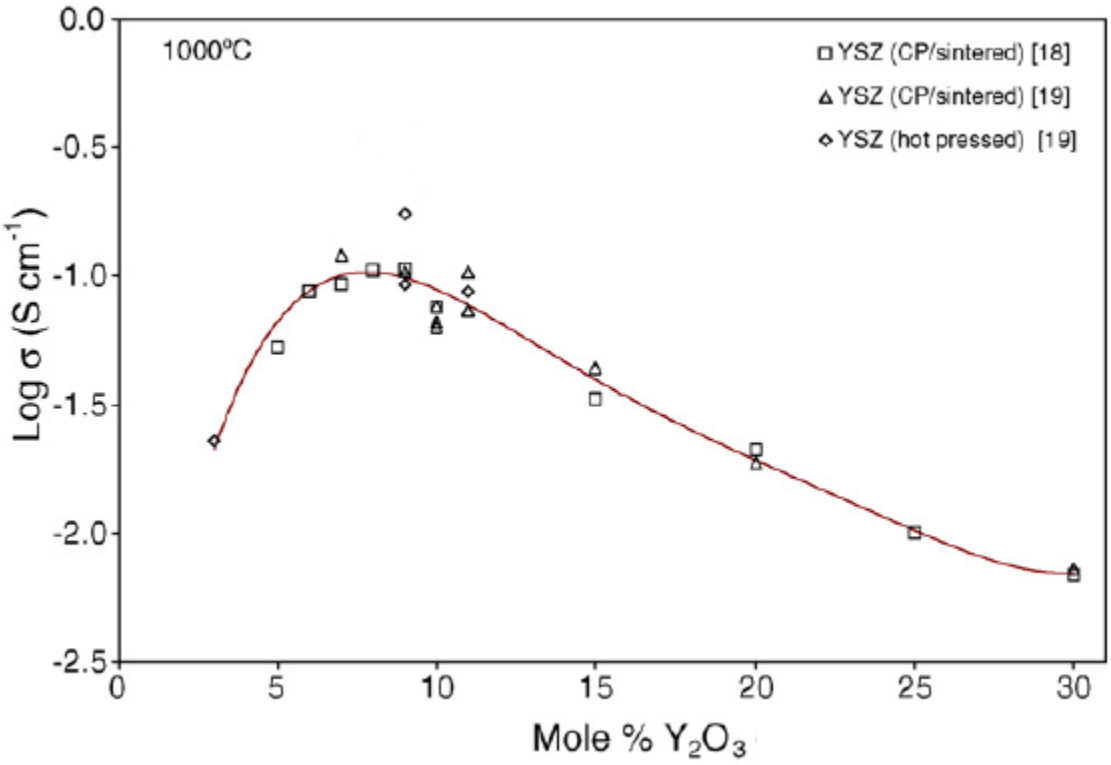

Figure 3.1 Conductivity of Yttria Conductivity at 1000 °C

Except for the Yttrium oxide, other dopants can stabilize Zirconia. One of them that can achieve the same and higher conductivity than Yttria is Scandia. Scandia cations (Sc 3+) size is closer to the Zirconium cations. Thus, less energy is spent on defect association which leads to higher mobility and consequently higher conductivity. However, as the working temperature of the solid oxide fuel cell decreases, the activation energy for conduction in ScSZ increases, resulting in similar or lower conductivity than YSZ below 500 °C [2] [7] [8]. Moreover, Co-doping methods

have also been used in order to improve the conductivity of the electrolyte. A fruitful attempt has been made by adding calcium to YSZ, resulting in lower activation energy for conduction [9].

3.1.2 Doped Ceria

Another common electrolyte material for solid oxide fuel cells is the Doped Ceria. Doped ceria forms a fluorite structure like zirconia. Doped ceria presents higher ion conductivity, especially in lower temperatures than both YSZ and ScSZ and it has been reported that presents lower polarization resistance [10]. Ceria is doped usually with Gadolinium or Samarium because they have a similar size with the ions that they replace. This is the main reason that GDC achieves higher conductivity than the YSZ. Except for the relative charge (Y 3+, La 3+, etch.), the relative size of the dopant plays a crucial role in the final conductivity that the doped material will provide. As it was observed for the YSZ, again the higher the dopant percentage the higher the ionic conductivity is, until a threshold which is about 20%-25%. From that point, the ionic conductivity starts decreasing again [11] [12] [13]. Furthermore, Ceria can be co-doped like zirconia. There have been reports which investigate the performance of co-doped GDC with Praseodymium [14] [15]. The co-doped electrolyte presented superior chemical stability with many cathode materials such as LSM and LSCF to that of YSZ [16] [17]. Till now, Gadolinia or Samaria doped Ceria seems the perfect candidate for a solid oxide fuel cell electrolyte, however, it has some significant disadvantages. At low oxygen partial pressures, like in the anode side of the fuel cell, Ce^{4+} is partially reduced to Ce^{3+} which is resulting in n-type electronic conductivity [1]. Electronic conductivity in the electrolyte will lead to short-circuiting the anode with the cathode. Moreover, Ceria presents chemical expansion under reduction conditions, which can lead to mechanical failure. It has been reported that GDC10 (10% mol doped) is not chemically expanded as the GDC20 [7]. Thus, doped ceria is usually used either in IT-SOFC (intermediate temperature solid oxide fuel cell) or as a bi-layer between the YSZ electrolyte and the cathode, especially in solid oxide fuel cells that work in intermediate temperatures [18]. In the bi-layer configuration many problems can still be created both from the different expansion behavior of the different layers (that will cause mechanical problems) and due to the formation of reaction products in the interface between the layers, which will reduce the ionic conductivity.

3.1.3 Bismuth Oxide

Bismuth Oxide (Bi_2O_3) is a material that presents polymorphism. That means that bismuth oxide has more than one crystal structure, and each structure is forming in different temperatures. Bismuth oxide has a monoclinic crystal structure at room temperature, when in temperatures

between 720 °C - 820 °C presents a cubic fluorite crystal structure. Bismuth oxide has the highest measured ionic conductivity (about 1S/cm) at 750 °C compared both to Yttria stabilized zirconia and Gadolinia doped ceria [19]. There have been many pieces of research exploring doping bismuth oxide in order to stabilize it in lower temperatures. Unfortunately, bismuth oxide is far from commercial use as a solid oxide electrolyte as despite its great ionic conductivity presents some yet unsolvable problems. The most significant problem is that bismuth oxide is metastable at the temperature range of 500 °C - 600 °C and as a result, there is observed a phase transformation which leads to a huge ion conductivity drop. Moreover, bismuth oxide presents electronic conductivity, has high corrosion activity, but poor mechanical properties.

3.1.4 Perovskite Oxides

Perovskite Oxide materials are the materials that have the formula ABX_3. Where A, B are metal atoms, and X is usually Oxygen. The structure of a common Perovskite is shown in the picture below [20].

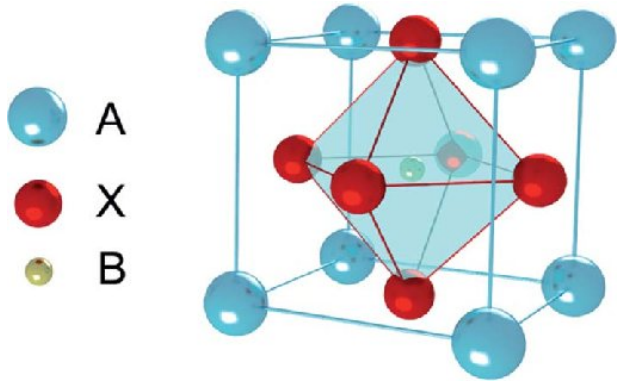

Figure 3.2 Perovskite Oxide Structure

With perovskite oxides, there are numerous combinations of materials that can achieve ion conductivity, since there are two available metal cations for dopant substitutions. Furthermore, Perovskite oxides can present ion conductivity and proton conductivity. Thus, they introduce a new field of research where the solid oxide fuel cell can form the water in the cathode side instead of the anode side. Let's refer briefly to the most common perovskites that are used as SOFC electrolytes.

3.1.4.1 Ion-Conducting Perovskites

One of the most commonly used perovskites in solid oxide fuel cells is lanthanum gallate $LaGaO_3$ because of its great oxygen ion conductivity. Plenty of dopants have been tested for lanthanum substitution with some of that being strontium, calcium, and barium. As in the previous cases, the best performance is observed from the cation that was closer to the size which it will replace, and that is strontium. Moreover, the substitution of gallium with magnesium seems to further improve the performance of the electrolyte (LSGM). The peak substitution percentage per mole was reported to 10-20% for strontium and 15-20% for magnesium [2] [7] [1] [21]. Perovskite electrolytes (LSGM) present many advantages as they have better ion conductivity than Yttria stabilized zirconia (YSZ), especially in intermediate temperatures (around 700 ^oC). However, in these temperatures, they have inferior ion conductivity of gadolinium doped ceria (GDC). Other positive aspects of perovskite electrolytes are their wide range of working temperatures that can maintain their performance and their thermal expansion that is similar to YSZ. On the other hand, despite that, perovskites don't reduce as easily as GDC in lower oxygen partial pressures, thus they don't have any reduction issue in the anode side, they do react with nickel, which is one of the most common anode SOFC elements. To overcome that problem, ceria layers are used to prevent the reaction of the anode material with the perovskite. Furthermore, there is a problem with the volatilization of gallium and the formation of undesirable second phases. Last but not least, LSGM reacts with many cathode materials under oxidizing conditions.

3.1.4.2 Proton-Conducting Perovskites

The proton-conducting electrolytes "reverse" the working principle of solid oxide fuel cells. With the proton-conducting electrolytes, the charge transport is H^+ ions and the H_2O is formed in the cathode side. The hydration of oxygen vacancies with OH^- defects results in the proton conductivity [1]. These defects are created in the perovskite by exposing it to water vapor in high temperatures. It is worth mentioning that the proton conduction occurs due to the lattice diffusion mechanism, thus the high conductivity is independent of the percentage of the humidity. The proton-conducting electrolytes present extremely high conductivity in intermediate temperatures (about 500 ^oC - 600 ^oC) and that is why plenty of research has been done on improving proton conducting electrolytes. Many proton-conducting electrolytes have been tested with $BaCeO_3$ resulting in high conductivity. However, its instability in CO_2 that is contained in the air made the endeavor unrealistic. The most promising perovskite that has been tested is the barium zirconate perovskite doped with yttrium (BZY). BZY has been reported to result in $4.5x10^{-3}$ S/cm at 600 ^oC [22] which is an extremely high conductivity for this temperature. The reasons that keep the proton-conducting electrolytes apart from the commercial-wide use is, first of all, their complicated and not well-established manufacturing procedure. Furthermore, proton-conducting perovskites are also prone to exhibit electronic conductivity.

3.2 Electrode Materials

Electrodes are referred both to the anode and the cathode side of the fuel cell. The demands from the electrode materials, are quite different from the electrolytes'. Electrodes materials are required to offer high electrical conductivity, high catalytic activity as well as high porosity. However, the challenges when choosing an electrode material are extended as the high working temperatures of the solid oxide fuel cells can lead to more problems. First of all, the materials should remain chemically stable at high temperatures. Most metals, that are electrically conductive, lose their stability in the working temperatures of the solid oxide fuel cells. Furthermore, the electrode materials should preserve their mechanical integrity in the high temperatures as well as they must "match" the thermal expansion of the electrolyte material to avoid further tensions. Some additional challenges arise when instead of pure hydrogen, hydrocarbons or ammonia are used as a fuel. When hydrocarbons are used as a fuel, the electrode materials should have fuel flexibility and be tolerant in each fuel's impurities. Moreover, they should be coking resistant as the carbon deposition in the electrode's surface can cause degradation to the fuel cell's performance. Last but not least, as fuel cells are researched for a sustainable transition to hydrogen energy, low cost and materials must be used as electrodes. Rare earth electrode materials may present high performance but their long-term mass production is unsustainable. Having defined the main characteristics of the electrode materials let's proceed further to the materials that are used for the anode and the cathode side of the solid oxide fuel cells.

3.2.1 Anode Materials

3.2.1.1 Cermet Materials

Cermet Materials are ceramic-metallic materials that are widely used in the anode side of the fuel cell. The most common cermet is Ni-YSZ, which is made by mixing nickel oxide (NiO) with yttria stabilized zirconia powders together and sintering them at high temperatures. After that, in the starting procedure of the fuel cell, the anode side is exposed to H_2, thus the NiO is reduced to Ni. Ni-YSZ cermet is a great anode material as it meets all the requirements of the electrode materials that are mentioned above. Nickel provides the electronic conductivity while yttria stabilized zirconia provides both a great mechanical structure that is stable in high temperatures and matches the thermal expansion of the electrolyte (since most of the time the electrolyte is

YSZ) and with its ionic conductivity extends the triple phase boundary which is extremely important for the performance of the fuel cell. Another advantage of the Ni-YSZ cermet is that the nickel does not react with the YSZ despite the high temperatures. Thus, great chemical stability is achieved as well. There are many approaches concerning the porosity of the anode layer. According to research, the goal is to have fine porosity in a thin layer close to the electrolyte and coarse porosity in the thicker outer layer. This strategy maximizes the triple phase boundary zone and therefore maximizes the performance of the fuel cell [23] [24] [25]. The percentage of the nickel that is mixed with the YSZ is another important factor because the amount of nickel affects the electrical conductivity of the anode side. The conductivity versus the amount of nickel mixed with YSZ is shown in the figure below [25]. The optimum balance between the electrical and ionic conductivity seems to be achieved when around 30% percentage of nickel is added.

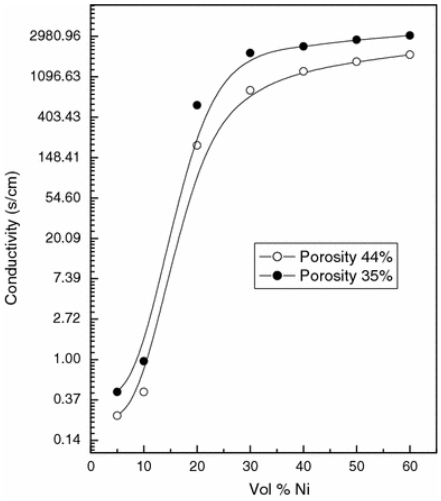

Figure 4.3 Conductivity vs Nickel percentage in Ni-YSZ cermet

On the other hand, Ni-YSZ cermet presents some downgrades. First of all, it is sensitive to carbon exposure. It cannot operate with direct hydrocarbons fuel feed. Moreover, Ni-YSZ has a low tolerance to sulfur impurities. However, several dopants have been tested in order to improve the resistance of Ni-YSZ to carbon deposition, with Mo (molybdenum) and Au (gold) to be the more effective ones.

3.2.1.2 Ceria-Based Materials

Doped ceria anode materials seem to introduce very promising characteristics as anode materials as they don't exhibit any problem with carbon deposition. Therefore, they are excellent materials for anode usage with direct hydrocarbons feed as a fuel. The main problem that doped ceria may present, is that it can be reduced from Ce^{4+} to Ce^{3+}. This reduction results in lattice expansion of

the material which can lead to mechanical failures. However, doping with gadolinium (Gd^{3+}), samarium (Sm^{3+}), or yttrium (Y^{3+}) seems to result in better chemical and dimensional stability. Moreover, as was discussed in the electrolytes' material paragraph, ceria has a different thermal expansion coefficient from YSZ. Thus, combining a doped ceria anode with an YSZ electrolyte can cause mechanical failures. To solve this problem, a small amount of YSZ mixed with the doped ceria anode seemed to have a great result concerning the thermal expansion "match" of the anode and the electrolyte. Furthermore, gadolinium doped ceria (GDC) has been mixed with Ni to form a cermet with superior results to that of Ni-YSZ [23]. Ni-GDC cermet had not only a better performance than Ni-YSZ but also had no problem with carbon deposition.

3.2.1.3 Other Anode Materials

Other potential material candidates for SOFC anodes are the perovskites, tungsten bronze oxides, and pyrochlore-type oxides. The most common perovskites that have been used as anode materials are LSCV- YSZ composites (LSCV is $La_{0.8}Sr_{0.2}Cr_{0.97}V_{0.03}O_3$). LSCV-YSZ composite materials present high electronic conductivity as well as high catalytic activity. They also do not seem to provoke any problem regarding carbon deposition. Moreover, the YSZ mix provides a thermal expansion coefficient close to the YSZ of the electrolyte and thus great compatibility with the electrolyte [26]. Tungsten bronze oxides with general formula $A_2BM_5O_{15}$ (with M = Nb, Ta, Mo, W, and A or B = Ba, Na, etc.) are potential anode materials due to the fact that they exhibit both ionic and electronic conductivity [27]. For the same reason, pyrochlore-type oxide with general formula $A_2B_2O_7$ seems to have a great interest for research.

3.2.2 Cathode Materials

Cathode materials must present both ionic and electronic conductivity as well as high catalytic activity. Due to the high temperatures, on the cathode side, it is more common ceramic materials to be used. As a result, the cathode side exhibits lower electric conductivity than the anode side. Regarding the cathode layer, one crucial factor is the thickness of the layer. The ionic resistance is proportional to the thickness of the cathode while the electronic transport is inversely proportional to the cathode thickness. Consequently, the thickness of the cathode should be taken into serious consideration as it can be the bottleneck that limits the performance of the fuel cell. One of the most common materials that are used in the cathode of solid oxide fuel cells is the lanthanum strontium manganite (LSM) $La_{0.5}Sr_{0.5}MnO_{3-\delta}$. LSM has great chemical stability and exhibits both high electronic conductivity and high catalytic activity. Unfortunately, LSM doesn't provide high ionic activity. For that reason, it can be mixed with YSZ which presents high

ionic conductivity and result in great performance [21]. Another common cathode material is the lanthanum strontium cobalt ferrite (LSCF) $La_{1-x}Sr_xCo_{1-y}Fe_yO_3$. LSCF perovskite (with usually 20% strontium and 80% Ferrite) results in a great performance too especially in lower working temperatures, such as 800 ^oC [28].

3.2.3 Interconnect Materials

Interconnect is the material that is used in a stack configuration and connects the anode of one cell to the cathode of the other cell. Interconnect materials are crucial for the performance of the stack. The interconnect materials require to present excellent electronic conductivity as well as to be stable at both anode and cathode environments since they operate at both of them. Another important factor is that the thermal expansion coefficient of the interconnect material must match the thermal expansion coefficient of the cell, because in a planar cell configuration the interconnect spans in the outer surface of the cell. Thus, a big difference in the thermal expansion coefficient between the interconnect and the cell can cause mechanical failures. Furthermore, the interconnect material must have good thermal conductivity, as in other cases the overall efficiency of the fuel cell is decreased (since the interconnect acts like a thermal barrier between the cells, and more energy must spend to obtain the high temperature in the cells). Moreover, the interconnect must have low permeability of oxygen and hydrogen. Additionally, the interconnect material has to exhibit creep resistance in high temperatures as well as oxidation resistance. Last but not least, the resistance to sulfur and carbon poisoning is vital especially on the occasion that hydrocarbons are used as a fuel. There are two types of materials that meet the above standards: ceramic and metallic interconnects.

Regarding the ceramic interconnect the most common material used is $LaCrO_3$. Pure $LaCrO_3$ has poor air sintering characteristics as well as low electronic conductivity [1]. For that reason, Ca doping is employed and results in high electrical conductivity and excellent air sinterability. Unfortunately, Ca doped $LaCrO_3$ presents also ionic conductivity, which leads to oxygen permeability, while it is expensive to be fabricated [29].

Regarding the metallic interconnect the most common materials are chromium metal alloys. The metallic interconnects exhibit higher electric conductivity than the ceramic ones, higher mechanical stability as well as no oxygen permeability. Another advantage of metallic interconnects is that they possess higher thermal conductivity. On the other hand, metallic interconnects present a high thermal expansion coefficient, which is inevitable to be matched with the thermal expansion coefficient of the ceramic fuel cell. Moreover, volatile chromium species can deposit in the cathode side and cause degradation of the cell.

4. Fuel Cell Characterization

To determine the testing rig demands as well as to figure out the whole testing procedure it is important to know what data must be collected and which techniques must be used to collect them properly. Thus, fuel cell characterization is the process that will be used after the experiments to analyze the results. Moreover, in the process of developing better fuel cells, it is important not only to verify which fuel cell performs best, but also to explore the reasons why. To achieve that, first of all, the main losses of the fuel cell must be clear. These are the activation, the ohmic, and the concentration losses. Additionally, the fuel crossover must be taken into consideration. Determining the size of each loss as well as understanding the effect of each change on the performance of the cell are the steps for improving and developing better fuel cells.

To achieve high performance in a fuel cell many factors must be taken into consideration. On the one side, the raw materials that will be used in the anode, electrolyte, and cathode side of the cell as well as the porosity of each layer must be appropriate. On the other side, the achievement of triple phase boundary zones and the stability of the cell are also of great importance. Hence, there are two approaches to fuel cell characterization: in-situ and ex-situ. In-situ characterization aims to evaluate the behavior of the whole cell as an “assembly”. In in-situ characterization, the voltage, the current, and the time are the main data that are collected and then examined to lead to a conclusion. Ex-situ characterization aims to evaluate the characteristics of separate materials that are going to be used in the fuel cell. Both approaches are equally important. However, for the research of this diploma thesis only in situ methods were conducted in order to characterize the cells. In-situ characterization techniques can also be divided into two main categories: potentiostatic and galvanostatic techniques. In the potentiostatic techniques, the controlled variable is the voltage and the measured variable is the current response. In the galvanostatic techniques exactly the opposite applies. Let’s analyze the most important characterization techniques.

4.1 j-V Measurement

The Current density vs Voltage graph is one of the most common graphs that quantitatively describe the performance of the cell. The j-V measurement is conducted as follows: initially, the cell is rested without any current drawn from its electrodes. At this stage, the OCV (open circuit voltage) is indicated. After that, small steps of current are applied in the electrodes (for instance 10 mA) and in each step there is a resting time (drawing constant current) till the equilibrium has been met and the voltage of the cell is stable. The steps are repeated till the voltage drop reaches values close to zero. The current drawn normalized by the active surface of the cell versus the

equilibrium voltage at each step composes the j-V diagram. From the j-V diagram one can easily observe some vital characteristics of the cell, like its OCV, and its peak power. However, it is possible to make a rough estimation of the activation, ohmic, and concentration losses. Because each loss has a different effect on the diagram's form as it was mentioned in the modeling paragraph and as it is shown in the figure below [30].

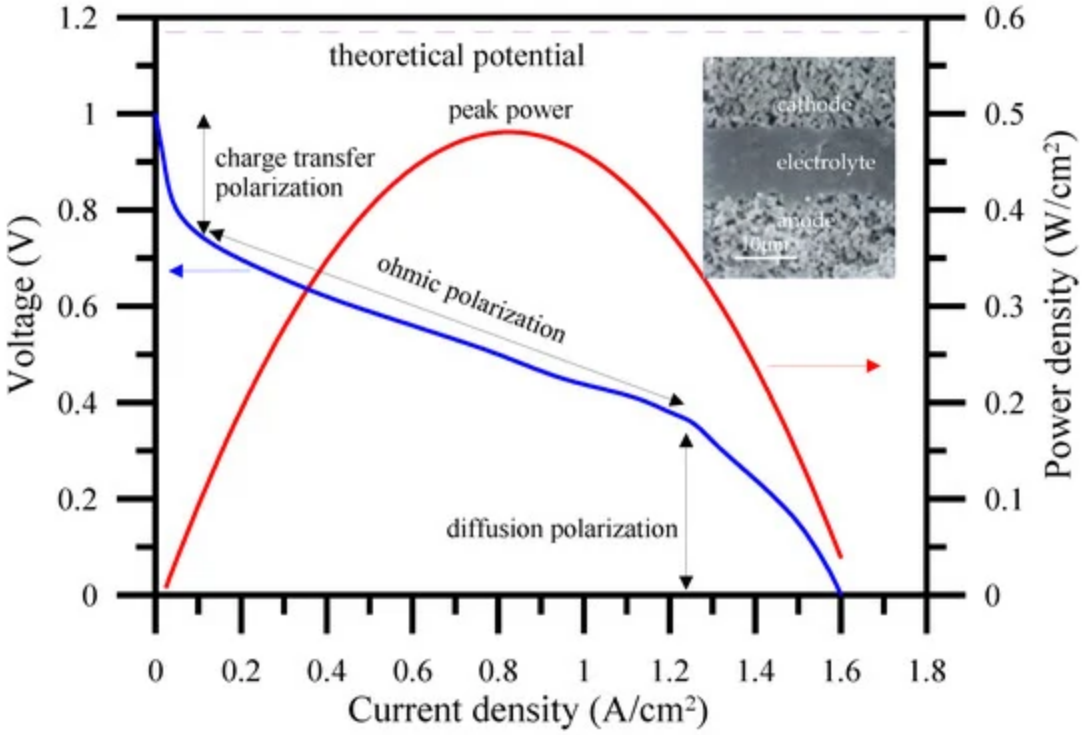

Figure 4.1 j-V curve and the distinct areas of losses [30]

4.2 Electrochemical Impedance Spectroscopy

Impedance is the ratio between a time-dependent voltage and a time-dependent current. It measures the ability of a system to impede the flow of electrical current.

$$z = \frac{V(t)}{i(t)} \quad (4.1)$$

Impedance includes both the resistance and the reactance of a system. Impedance measurements are usually conducted by applying a sinusoidal voltage perturbation $V(t) = V_0 \cos(\omega t)$ (where V_o is the voltage amplitude, ω is the radial frequency, and t is the time) and measuring the resulting current response $i(t) = i_0 \cos(\omega t)$ (where i_o is the current amplitude, ω is the radial frequency, and t is the time). Comparing now the current perturbation with the

voltage, it can be observed that a phase shift occurs. This phase shift can be described by the angle ϕ as is shown in the figure below.

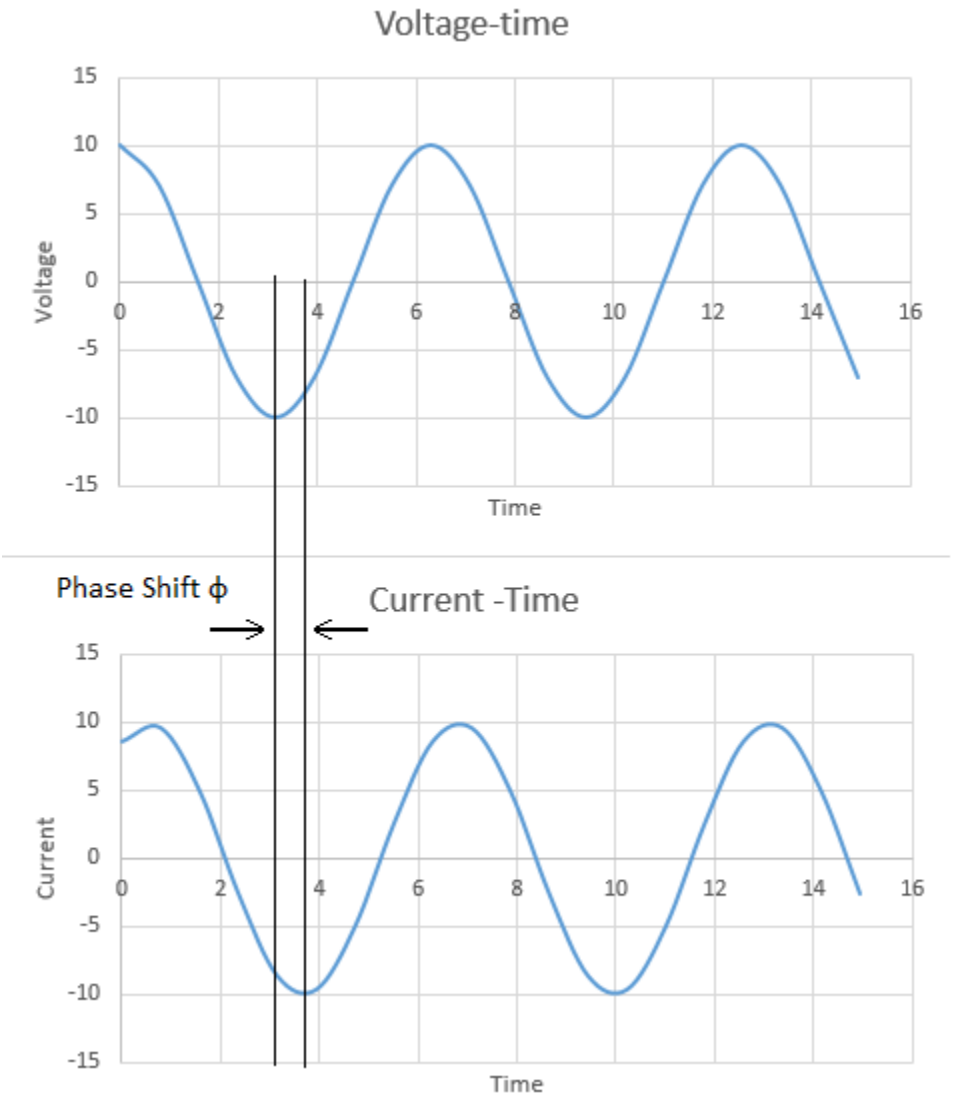

Figure 4.2 Phase shift between voltage and current perturbation in impedance spectroscopy

Embedding the phase shift (ϕ) in the equation (4.1) results in:

$$Z = \frac{V_0 \cos(\omega t)}{i_0 \cos(\omega t - \varphi)} = Z_0 \frac{\cos(\omega t)}{\cos(\omega t - \varphi)} \quad (4.2)$$

Or in phasor representation:

$$Z = Z_0 e^{j\phi} = Z_0(\cos\phi + j\sin\phi) \quad (4.3)$$

As a result, now the impedance can be described from an impedance amplitude (Z_0) and a phase shift (ϕ), or even better from a real and an imaginary component. Usually, impedance spectroscopy data are presented in a Nyquist plot in the real (x) and the minus imaginary (-y) axis. Nyquist plots have the advantage to summarize the impedance behavior in a wide range of frequencies. An example of an impedance spectroscopy Nyquist plot is given in the figure below [31].

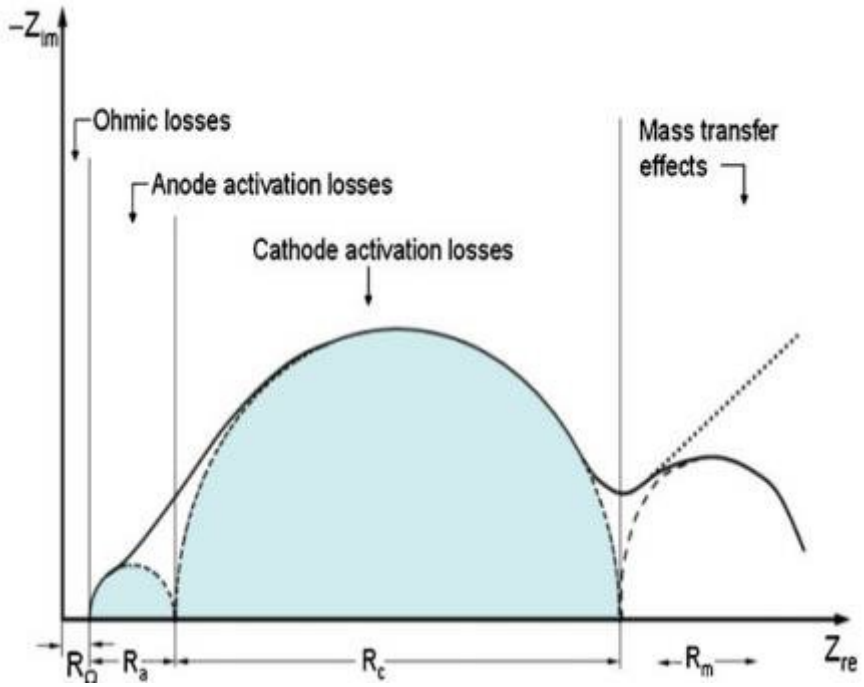

Figure 4.3 Impedance spectroscopy graph [31]

As it can be observed from the figure above, each source of loss forms a semicircular area in the impedance spectrum diagram. Moreover, the cathode activation loss dominates the fuel cell's performance as it is the biggest source of loss. In order to understand how the impedance spectrum is generated, it is essential to model the fuel cell as an equivalent electrical circuit.

As far as the kinetics aspect is concerned the equivalent circuit component is a resistor R_f. That is because according to the Tafel simplification of reaction kinetics:

$$n_{act} = -\frac{RT}{anF}\ln i_0 + \frac{RT}{anF}\ln i \quad (4.4)$$

For small-signal sinusoidal perturbation, the impedance can be approximated as Z=dV/di. Hence,

$$Z_f = \frac{dn_{act}}{di} = \frac{RT}{anF}\frac{1}{i} = \frac{RT}{anF}\frac{1}{i_0 e^{anFn_{act}/(RT)}} \quad (4.5)$$

From equation (4.5) it is apparent that Z_f has no imaginary part. As a result, Z_f is represented by an Ohmic resistance and it can be modeled as a resistor.

As far as the electrochemical reaction interface, that can be modeled as a capacitor with C_{dl} capacity. The capacitive nature of the reaction interface relies on the charge separation that occurs. In the reaction interface electrons are accumulated in the electrode and ions are accumulated in the electrolyte. This behavior is modeled as a capacitor.

As a result, in order to model the electrochemical reaction a capacitor parallel to resistance is used.

$$\frac{1}{Z} = \frac{1}{Z_1} + \frac{1}{Z_2} \Rightarrow Z = \frac{1}{1/R_f + j\omega C_d} \quad (4.6)$$

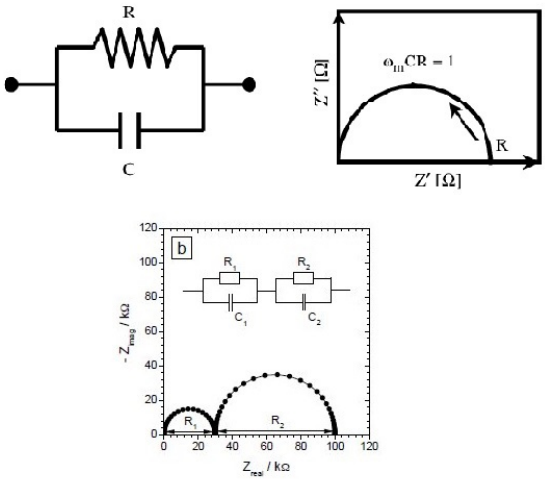

Figure 4.4 Nyquist graph of an RC circuit and Fuel cell electric circuit equivalent [32]

The resulting Nyquist graph of the parallel RC circuit is similar to the resulting impedance measurement of each electrode of the cell. The resemblance is shown in the figure above.

To clarify, the semicircles that are shown in the figure above are not always as distinct (that depends on the capacity of the capacitor which changes from fuel cell to fuel cell). There is the possibility the two circles to interfere, thus the resulting measurement will not form two clear semicircles but the sum of the two losses.

As far as the mass transport phenomenon is concerned, it can be modeled by a Warburg circuit element. Warburg element models a semi-infinite diffusion process which is bounded by a planar electrode on one side. The impedance of a Warburg element is given by the following equation:

$$Z_w = \frac{\sigma_i}{\sqrt{\omega}}(1-j) \quad (4.7)$$

Where σ_i is the Warburg coefficient that characterizes the effectiveness of the species i to a reaction interface and is defined as:

$$\sigma_i = \frac{RT}{(n_i F)^2 A\sqrt{2}}\left(\frac{1}{c_i^0\sqrt{D_i}}\right) \quad (4.8)$$

where:

c_i^0 is the bulk concentration of species i

D_i is the diffusion coefficient of species i

To be more specific, the Warburg element can model the diffusion process of a thick layer, which in the fuel cells' electrodes it is not the case. For that reason, a porous bounded Warburg model is used which has a slightly different form:

$$Z_w = \frac{\sigma_i}{\sqrt{\omega}}(1-j)\tan h\left(\delta\sqrt{\frac{j\omega}{Di}}\right) \quad (4.9)$$

Where:

δ is the diffusion layer thickness

The resulting Nyquist graph of a Warburg element is a straight line with a slope of 1. However, the equivalent circuit of the whole electrochemical procedure, taken into consideration the kinetics, the interface reaction, and the mass transport, is modeled with the Randles circuit and it has the following form [33]:

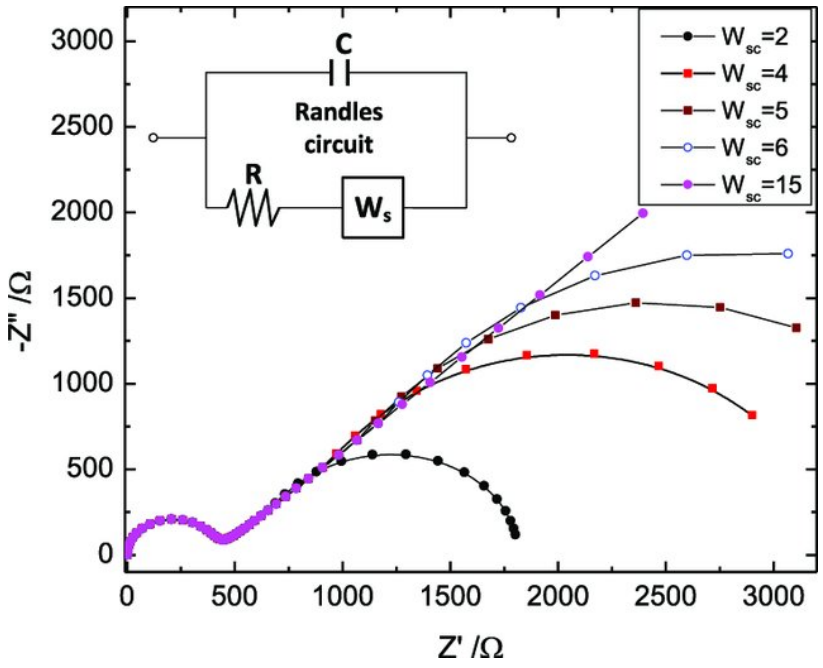

Figure 4.5 Nyquist graph of Randles circuit [33]

Now taking into consideration the ohmic resistance of the electrolyte and the electrochemical reaction in the anode and the cathode (anode mass transfer is negligible), the final model and impedance spectrum that is shown in *figure 4.3* is created. As it is mentioned at the beginning both galvanostatic and potentiostatic electrochemical impedance spectroscopy techniques can be employed to characterize the fuel cell's performance.

4.3 Cyclic Voltammetry

Cyclic voltammetry is used to characterize the catalytic activity of the cell in more detail. In cyclic voltammetry, a linear voltage sweep is applied to the cell and the responding current is measured. The graph with the current versus the voltage that applied is the cyclic voltammogram which usually has a "duck" shape. The duck shape is created because of the two contributions of current. The one contribution is constant and represents the capacitive charging current that flows due to the linear increase of voltage. The other contribution is nonlinear and represents the adsorption reaction that occurs on the cathode catalyst surface. As the voltage increases the current reaches a peak when the catalyst surface is fully saturated with hydrogen and then falls.

The total catalyst surface can be obtained by quantifying the total charge Q_h. In the figure below is cyclic voltammogram is presented [34].

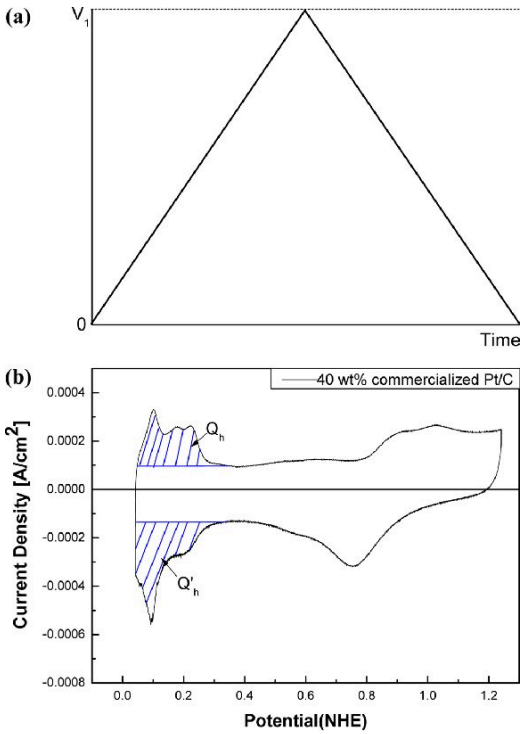

Figure 4.6 Cyclic Voltammogram [34]

5.Testing facility and software

This research aimed to test different anode and cathode materials for solid oxide fuel cells and compare their performance. Moreover, the measurements from the fuel cells were expected to be in the range of 1V and 250 mA. Therefore, it was essential to set a testing rig that can measure consistently and precisely the results of our experiments as well as a software to control all the instruments of the rig.

Figure 5.1 SOFC Testing rig

5.1 Testing rig

A solid oxide fuel cells testing rig must consist of at least the following components:

1. A mounting device for the fuel cell, which can withstand temperatures as high as 1000^{o}C
2. A furnace device with a controller, in order to control the temperature and the temperature ramps of the experiment
3. Flow valves that will control the gases flow
4. A DC load and a Potentiostat (for more specific measurement techniques like impedance spectroscopy measurements)
5. Temperature, Voltage and Current sensors
6. A data acquisition system that will log the data from the sensors above

5.1.1 The mounting device

For the mounting device of the fuel cell, it was used the ProboStat™ device from Norecs. The ProboStat™ is a cell designed for measurements up to 1600 ^{o}C. It consists of several components that can be assembled together and create structures for different experiments. The ProboStat™ is divided into two "main" areas. The upper area in which the fuel cell is mounted and is placed into the furnace, and the lower area where all the sensors and gas feed lines are connected. The lower area is placed outside the furnace. Therefore, all the electrical connections and the gas feed plastic tubes are remaining at the environmental temperature without any risk of melting in the high temperatures that the fuel cell works. The ProboStat™ requires additionally an external cooler that recirculates cold water in the lower area for extra cooling.

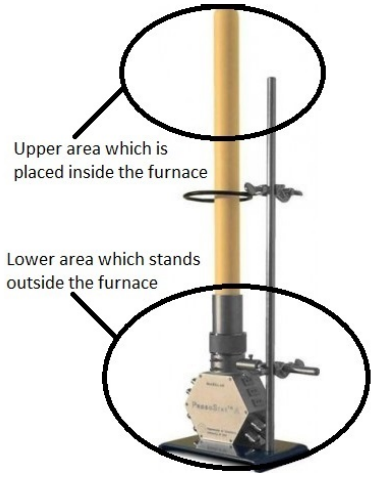

Figure 5.2 The ProboStat™

Inside the ProboStat™, a long ceramic tube, separates the area of anode and cathode. Inside this ceramic tube there is connected one thermocouple that measures the inner temperature, and a contact electrode that provides electrical connection of the anode side with the base of the ProboStat™. Moreover, there is a ceramic feed line that provides the anode with hydrogen. Outside the ceramic tube there is a gas line that feeds with oxygen the cathode, and contact electrode that connects the cathode with the base of the ProboStat™, and a thermocouple that measures the temperature on the cathode side. Finally, all these components are placed into an outer protective either glass or ceramic tube. Below there are pictures of the several components for more clarity.

Figure 5.3 Upper area of the ProboStat™

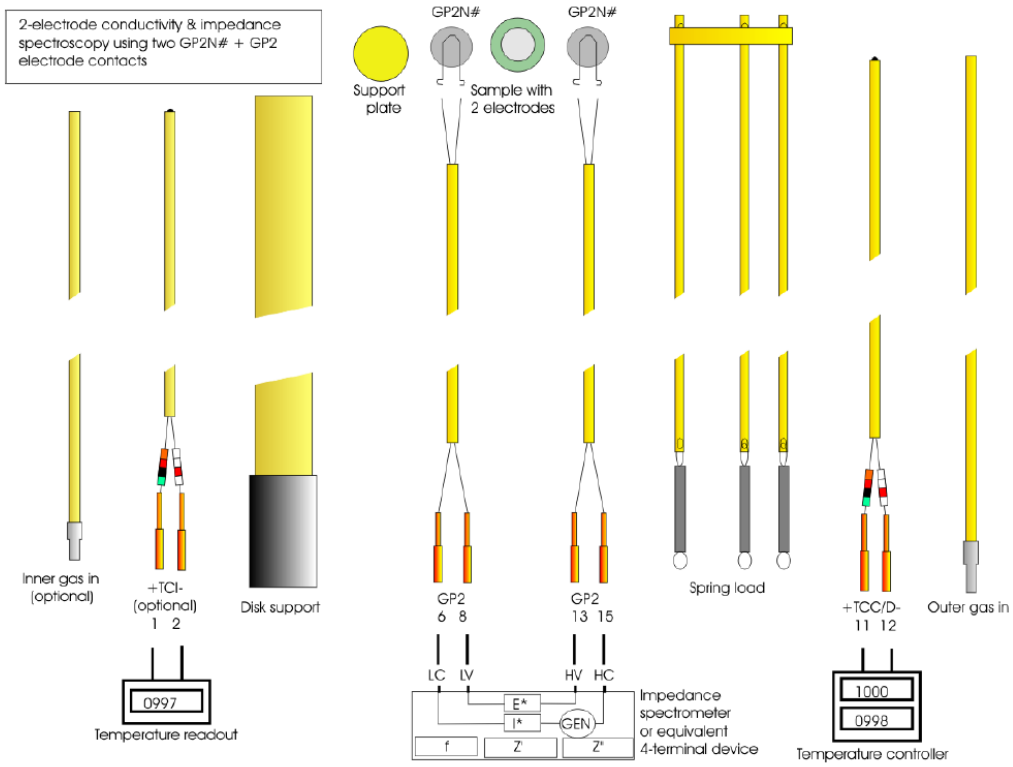

Figure 5.4 ProboStat™ connection graph

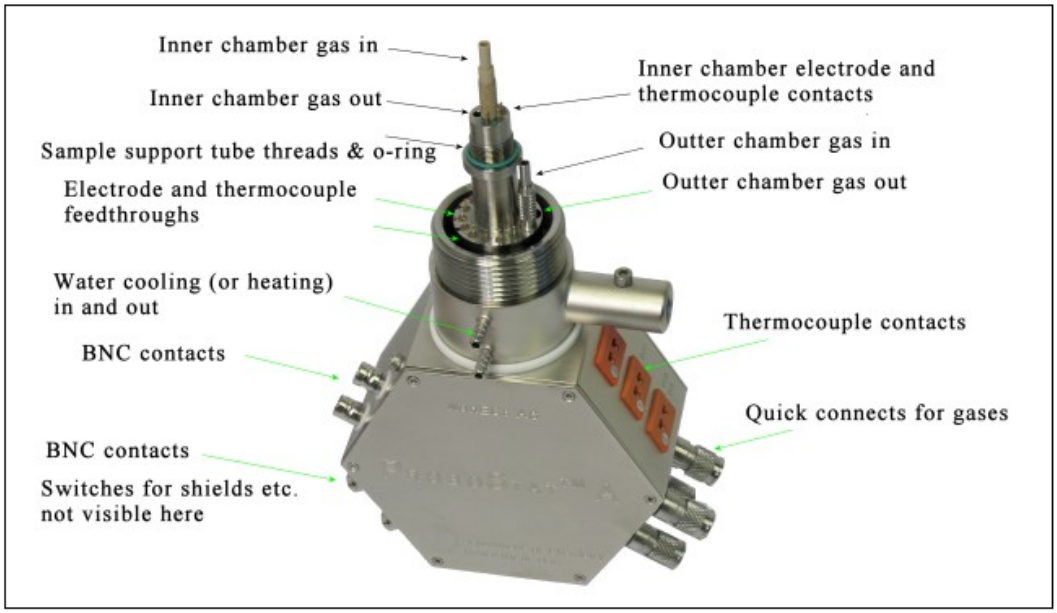

Figure 5.5 ProboStat base unit

5.1.2 The furnace system

For the furnace system, a custom-made 3kW vertical split tube furnace it was used, which was controlled by Eurotherm 2416 PID Controller. The tube geometry of the furnace helped to achieve thermal uniformity in the heating chamber which is important for the consistency of the testing. Furthermore, the splitting feature helped in the assembly of the experiment, since for every new experiment the ProboStat™ had to be removed, remounted and inserted back into the furnace. A photo of the furnace as well as the controlling system is shown below.

Figure 5.6 Furnace system

5.1.3 The flow valves

To control the gas flow in the anode and the cathode of the fuel cell, the Red-y™ gas flow controllers from Voegtlin were used. Red-y flow valves are mass flow sensors/controllers since mass flow measurements are mainly independent of temperature and pressure. However, they are calibrated according to the gas that will flow through them to convert their input data into the standard volumetric flow (e.g. ln/min). In our experiment, three Red-y valves were used to regulate the flow of hydrogen, oxygen, and argon.

Figure 5.7 Voegtlin Flow valves

5.1.4 The DC Load / Potentiostat

The DC load is the most essential tool for fuel cell testing. The DC load was used to draw constant current from the fuel cell and measure the degradation of the cell. It was also used for applying current steps and forming the characteristic V-I curve of the fuel cell. The DC load that was used was the RND 320 KEL102, a programmable 150W DC load with voltage range 0-120V and current range 0-30A.

Figure 5.8 RND DC load

Moreover, the potentiostat was replacing the DC load when more complicated measurement techniques, such as impedance spectroscopy measurement, were required. A potentiostat is an instrument with two, three, or four terminals (three in our case): the working electrode, the counter electrode and the reference electrode. The main function of the potentiostat is to control the working electrode's potential. Potentiostats are used for electrochemistry experiments because they are precise instruments, and they can operate complex measurement techniques. The potentiostat that was used was the SP-150 from Biologic company.

Figure 5.9 Biologic Potentiostat

5.1.5 Data acquisition unit

Last but not least, the Agilent 3497A DAQ unit combined with a 20 channel multiplexer was utilized in order to read and save the measurements of the temperature in the anode and the cathode side of the fuel cell, the voltage as well as the current that was drawn from the cell.

Figure 5.10 Agilent DAQ unit

5.2 Testing software

As was mentioned above the testing rig consist of five different instruments that control the experiment's parameters, read the sensors' values, and store them. Each of these instruments has its own software, which makes the whole experiment procedure complicated and prone to 'data saving' mistakes. For that reason, we decided to create an application that will control all the instruments and save the data in a predefined form. The application was created in LabVIEW® software because of LabVIEW's ability to create a user-friendly graphical environment.

The first step was to identify both the communication system of each measurement device and the connection type with the computer. The results are as follows:

Table 5.1 Connection system of measurement instruments

Instrument	Communication Protocol	Connection Type
Agilent DAQ	LabVIEW Library	GPIB
Eurotherm furnace	Modbus	RS232
Voegtlin Valves	Modbus	RS233
RND DC Load	SCPI commands	USB
Biologic Potentiostat	LabVIEW Library	USB

- LabVIEW Library: The LabVIEW Library is a library of commands that every company has developed for their instruments to communicate with the computer. With this communication protocol, the user has to install the LabVIEW driver of the instrument and then use the given commands from the library to create a program that can control the instrument
- Modbus protocol: Modbus is an open serial communication protocol developed by Modicon® in 1979. The protocol is based on the communication between the Modbus Master (the device that requests the information) and the Modbus Slaves (the devices that provide the information to the Master). Each Slave has its unique address with a maximum of 247 Slave Addresses. The Master can write information to the Slaves too.
- SCPI commands: SCPI commands are ASCII strings with a format determined by the company that provides the instrument. The commands are sent to the instrument over the physical communication layer and then the reply (if there is an available for this command) are sent back from the instrument to the computer. A famous example of SCPI commands is the command *IDN? which returns, usually, the device's identity.

Subsequently, having established the communication between the instruments and the computer we determined the goals of the application. The goals that were set are listed below:

1. To combine the control of all the instruments at the same application but in the same time every instrument to be independent
2. To present the measurements during the experiments in an informative way
3. To require from the user as few inputs as possible
4. To establish a data organizing and saving system
5. To prevent accidents from power outages, or electronic malfunctions that can come up
6. To inform the user via email for errors that can come up

Taking into consideration all the goals above the following app was created from scratch with the following functions.

5.2.1 Software's General Settings Tab

First of all, the measurement procedure does not start without the general tab filled. As it is shown in the picture below, in the first tab the user must fill all the essential information of the experiment. The details asked from the user are; the folder in which the data will be saved, the experiment's temperature, the fuel and if it is humidified, the date and time that the experiment starts, and the sample name of the tested fuel cell. Additionally, a field for a brief description of the experiment is available which is saved separately inside the main file in a text document form.

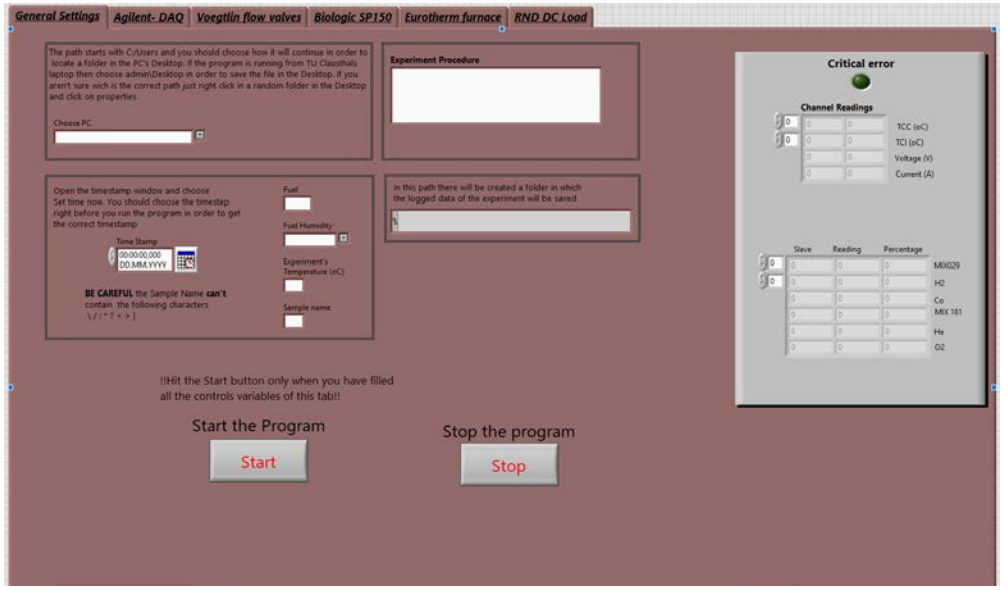

Figure 5.11 Application's first tab

After completing the general tab inputs, the user can hit the start button and proceed to the next tabs. When the start button is enabled, the saving directory is printed in the created path variable. Except for the general tab, there are five more tabs; each tab is assigned to one measurement device. To activate the communication with each instrument the user must enable the main Boolean switch of each tab.

5.2.2 Agilent DAQ System Tab

Continuing with the Agilent DAQ system tab, this tab consists of the start and stop communication button, the resource name of the connection, and two sub-tabs; one for the inputs and one for the outputs. In the input tab the user sets the connected channels, the sampling rate etch. These inputs are saved as preferred inputs so the user has to change them only if something changes in the hardware configuration. In the second tab, the collected data are presented in graphs in order to be visible for the user how the experiment evolves.

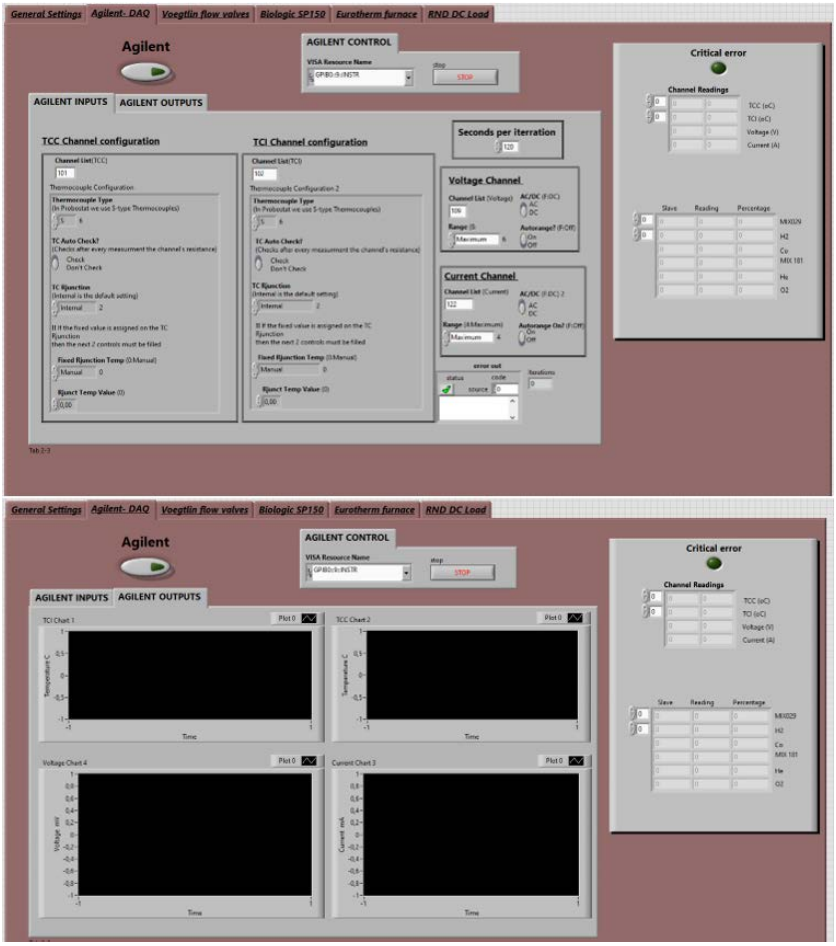

Figure 5.12 Agilent LabVIEW tab

5.2.2 Voegtlin flow valves Tab

The flow valves tab follows almost the same structure as the Agilent tab. It is divided into two sub-tabs, in the first tab all the details and readings from the valves are presented and in the second tab, the user can write the desired flow values. There is the option if the user wants to change the flow radically, to switch on the 'ramp with delay' button to smooth the transition. Moreover, there is the option of a warning email sent when there are differences between the user indicated and the actual reading values of flow.

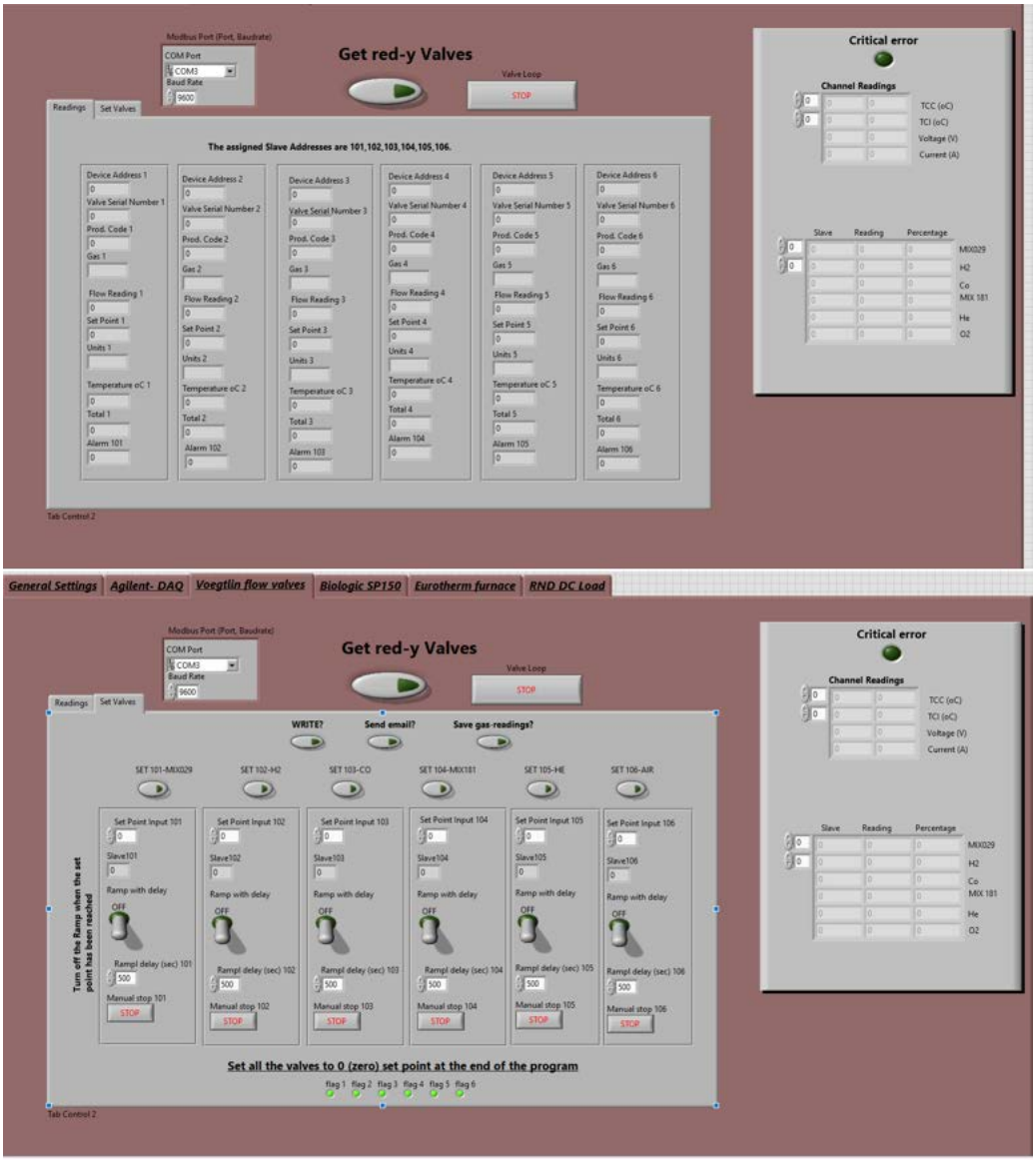

Figure 5.13 Flow Valves LabVIEW tab

5.2.3 Potentiostat Tab

The Potentiostat is used to perform precise and complicated measurements function. Thus, its structure is different from the previous instruments. The potentiostat tab is divided into 6 sub-tabs. Each sub-tab represents a testing function. The available functions are:

1. OCV (open circuit voltage). The Open Circuit Voltage consists of a period during which no current flows and no potential is applied to the working electrode. Therefore, the evolution of rest potential can be recorded.
2. V-I (current steps which create a V-I curve). V-I Characterization is intensively used to carry out investigations on Fuel cells. The principle of this technique is to apply small current steps and to measure the corresponding potential and power. The current steps are increasing till the potential drop under a crucial value. Some characteristic parameters of the cell such as maximum current, maximum potential, and maximum power can be determined.
3. PEIS (potentiostatic electrochemical impedance spectroscopy). PEIS technique performs impedance measurements into potentiostatic mode in applying a sine wave around a DC potential E that can be set to a fixed value or relative to the cell equilibrium potential.
4. GEIS (galvanostatic electrochemical impedance spectroscopy). GEIS technique works the same as the PEIS technique with the difference that the current is controlled instead of the potential.
5. CC (constant current). This technique is used in order to draw constant current from the fuel cell and observe its degradation through time. This technique replaces the use of a DC load.
6. CV (cyclic voltammetry). The CV technique consists in scanning the potential of a stationary working electrode using a triangular potential waveform. During the potential sweep, the potentiostat measures the current answer of the system. The cyclic voltammogram is a current response plotted as a function of the applied potential.

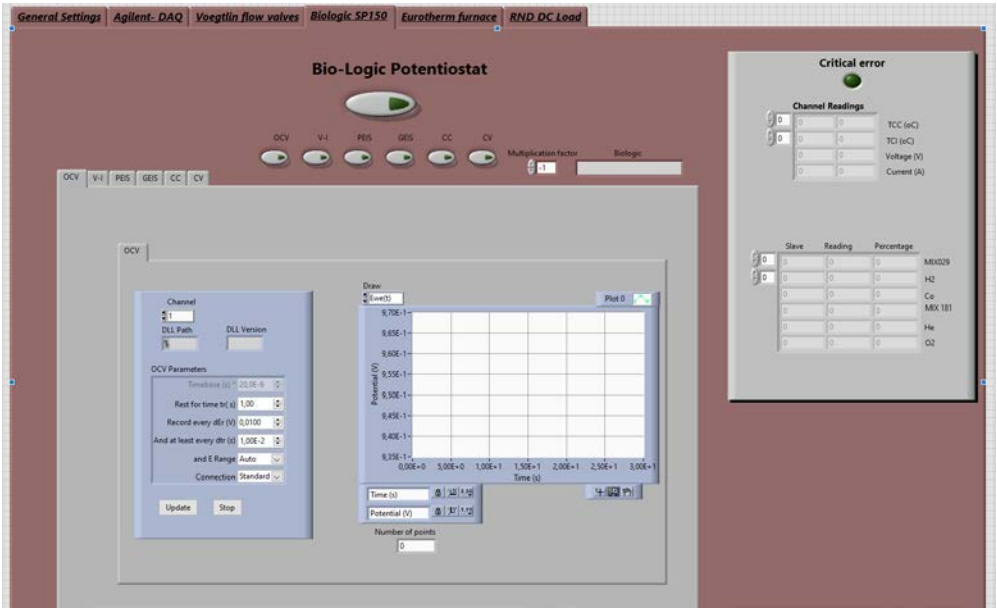

Figure 5.14 Potentiostat LabVIEW tab

5.2.4 Furnace Tab

This tab is used to control the PID controller for the furnace. It is divided into 4 techniques: ramp with rate, a ramp with time, and a dwell/ cool down, and program. The first three functions are used when the user wants to set just a simple process. On the other hand, the program function creates a profile of temperature that the furnace can achieve. The program mode has thirteen available segments. Furthermore, the user is able to put the furnace on hold and back in running mode. The process value that is indicated in the right of the tab is the actual value that the thermocouple reads and it is also indicated in the upper graph. In the lower graph, the profile temperature is presented.

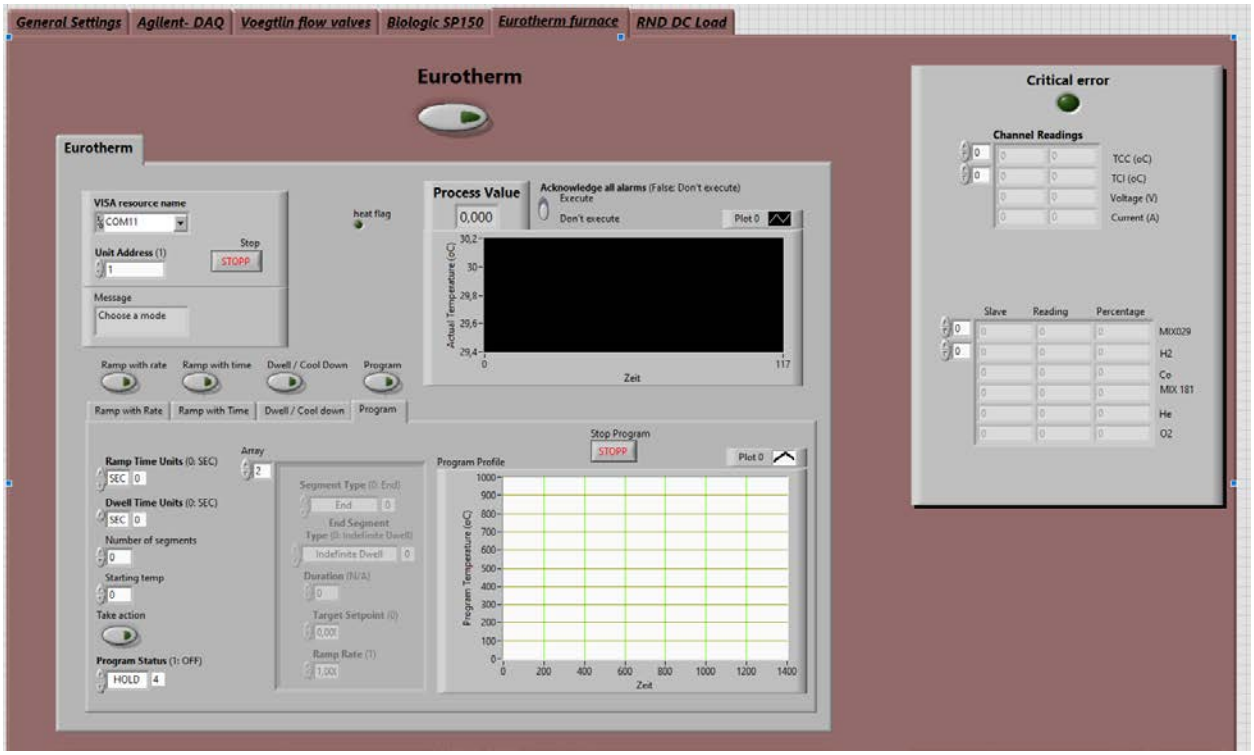

Figure 5.15 Furnace LabVIEW tab

5.2.5 DC Load Tab

The DC Load tab is used for two main functions: the constant current function and the V-I characterization function. These two functions are also available from the potentiostat. The V-I characterization function works exactly like in the potentiostat which is described above. The constant current function works differently in the DC load. The program starts with user's

indicated current steps to reach the desired voltage. Usually, the constant current is held at 0,6V. Moreover, the user defines the lowest value that the cell can operate under constant current (usually 0.56V). When this value is reached the technique stops and either it starts again with current steps to find the desired voltage or it stops until the user enables it again (depends on the user's choice in the termination technique Boolean control). The two graphs present the resulted voltage and current through time.

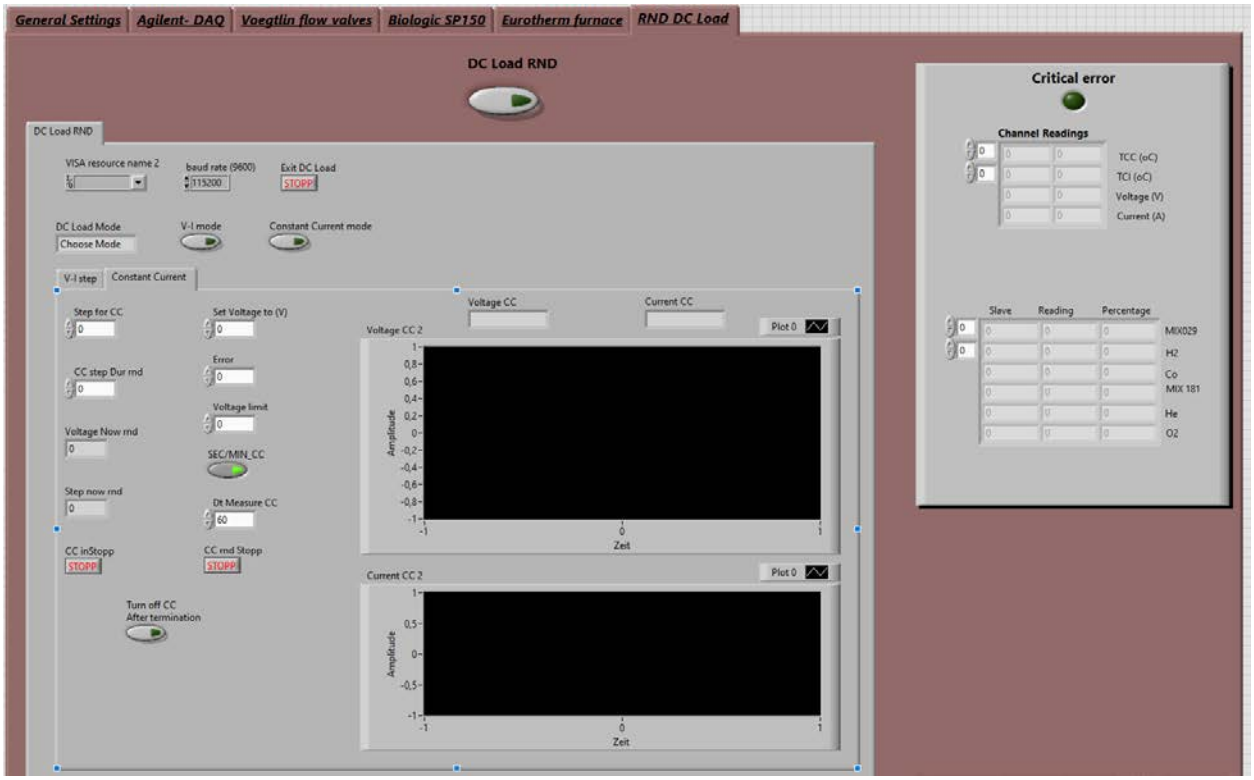

Figure 5.16 DC Load LabVIEW tab

5.2.6 Application's safety features

As shown in the pictures above, on every page there is a box on the left that contains the most useful information that should be visible despite the instrument that the user wants to control. This box contains the readings of anode and cathode temperature sensors, the voltage and the current of the fuel cell, the flow rate of every valve, and the caution light of critical error. A critical error is enabled whenever the gas readings are different from the user indicated value, when the temperature of the furnace is more than ten degrees off than the desired value, or for whatever reason there is hydrogen flow and the temperature of the furnace is below 500 °C. In that case, the application automatically turns off the flow of hydrogen and activates the flow of Argon in

the anode side. Moreover, the application turns off every other function that draws current from the cell. Another important aspect of the application is that, because the fuel cell experiment runs for many days, whenever an error or a critical error occurs the application sends automatically an email with the error's details to the user.

6. Fuel cell Fabrication

6.1 SOFC structure types

There are many different geometries and types of solid oxide fuel cells. As far as geometry is concerned, some of the most popular designs are planar (rectangular or button), tubular and monolithic.

- The planar design consists of two thin porous layers, the anode, and the cathode, which are separated by a thin and dense layer, the electrolyte. Planar fuel cells do not require special manufacturing techniques. They can limit ohmic resistance and consequently high performance.

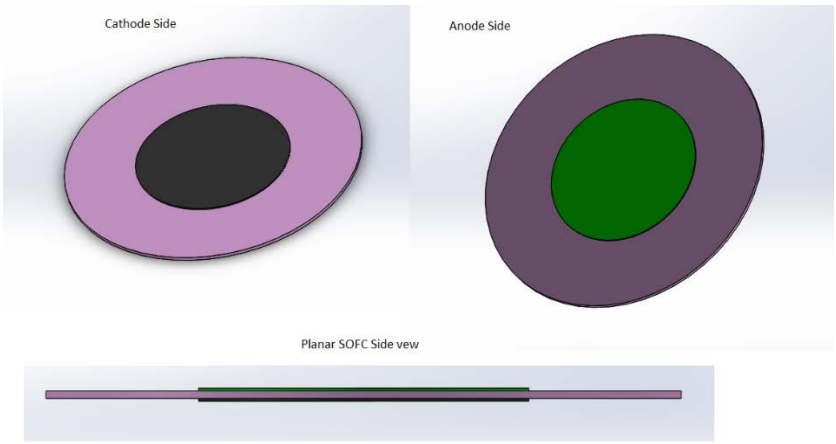

Figure 6.1 Planar SOFC

- In the tubular design, the anode, the electrolyte and the cathode have a cylindrical shape with the cathode being the inner cylinder and the anode the outer one. The oxygen flows inside the tubular cell and the hydrogen, or whichever fuel is used, flows in the outer environment of the tubular cell. With the tubular design, sealing can be achieved effortlessly. However, their manufacturing procedure is expensive and complicated and they also have high ohmic losses.

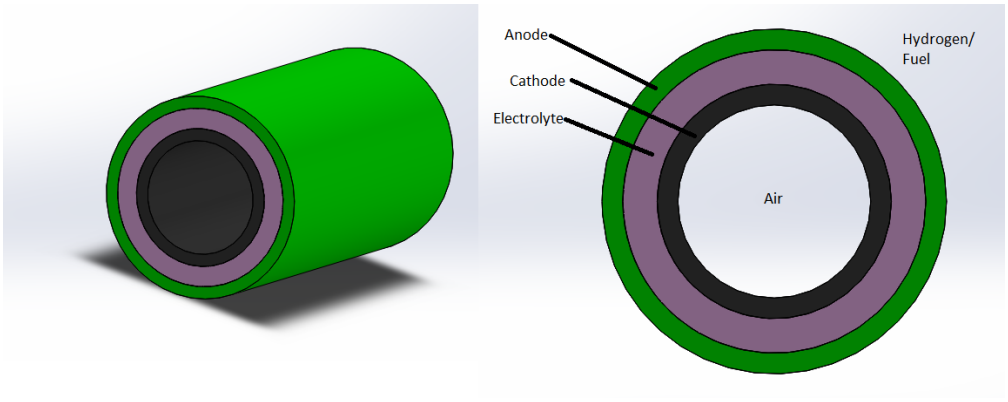

Figure 6.2 Tubular SOFC

- The monolithic design is mimicking the design of a cooler. The three-layer assembly forms a corrugated structure that creates flow channels. These channels can be either all facing the same direction (co-flow design) or placed in 90 degrees (cross-flow design) [35].This design combines both an easy sealing and a compact structure. However, it is a complicated design that requires high- end manufacturing techniques.

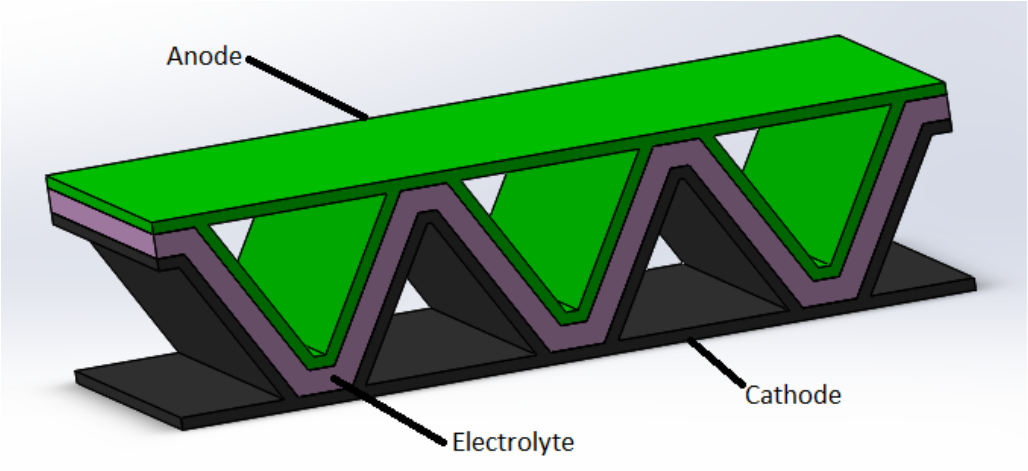

Figure 6.3 Monolithic SOFC

Analyzing further the planar geometry, as it is the geometry that was used for the experiments of this research, there are three types of planar fuel cells depending on which is the thickest/ sturdiest layer. Therefore, there are anode, cathode and electrolyte supported structures, with the thickness of each structure varying as is shown in the table below.

Table 6.1 SOFC planar structures

SOFC Planar Structure	Electrolyte Thickness	Anode Thickness	Cathode Thickness
Anode Supported	10-20 um	1-2 mm	0.1-0.2 mm
Cathode Supported	10-20 um	0.1-0.2 mm	1-2 mm
Electrolyte supported	0.1-0.5 mm	0.1-0.2 mm	0.1-0.2 mm

Each structure possesses different characteristics. The electrolyte-supported cells show the best mechanical properties as well as resistance to thermal shocks. However, because of their thick electrolyte layer, they have higher resistance and consequently the worst performance compared to the other two. Cathode-supported cells may present mechanical and delamination issues. Moreover, because of their thicker cathode layer, they show an increased oxygen mass transport resistance. Nonetheless, their overall resistance is lower than that of electrolyte-supported cells and as a result, they present better performance. Last but not least, anode-supported cells have the same mechanical weaknesses as the cathode supported, and they present higher fuel transport resistance. However, that seems not to be a restrictive problem since the fuel cell is supplied with 100% fuel when it utilizes only 21% of the air which is oxygen. Furthermore, the extra thickness of the anode proves to be an advantage when different fuels like hydrocarbons are used. That's because the extra anode thickness leads to an increase in the time that the fuel crosses the anode layer, and therefore there is a higher conversion percent of the fuel to hydrogen. In the context of this research there were available electrolyte substrates in the lab. Thus the structure of the cells that were tested was electrolyte-supported.

6.2 SOFC Fabrication methods

There are many fabrication methods for producing solid oxide fuel cells. Some of the most popular are dry pressing, screen printing, and tape casting. These methods can also be combined to produce a fuel cell. For example, the electrolyte layer can be manufactured with the dry pressing method and the anode and cathode layer to be added with the screen printing method. Dry pressing is the procedure in which loosely granulated ceramic powders are compressed within a die-punch arrangement [36] and then sintered at high temperatures. Dry pressing is an economical and simple constructing method. Screen printing is the method that is usually combined with dry pressing or tape casting. In the screen printing method, the raw materials are

in a paste form (powders combined with a binder). A screening mesh is placed onto an applying bed via a thin spacer. This spacer can be as thin as a few micrometers. When the paste is applied to the screen, the thickness of the final layer that is created in the bed equals the thickness of the spacer. In this way, a thin layer of paste is produced and then it is sintered to harden and get the desired porosity. Screen printing is a simple way of producing electrode layers with great accuracy. Last but not least, the tape casting method is a method similar to screen printing. The desirable powder is in a slurry form which is dispensed into a moving carrier [37]. The thickness of the layer depends on the height of the forming knife which compresses the slurry as it moves forward. After that, the thin slurry is either sintered or just dried. Tape casting is a precise method of manufacturing that is employed for larger-scale productions.

6.3 Fabrication of the tested cells

For this research, the screen printing method was used to fabricate the anode and cathode layer onto a bought electrolyte substrate. To be more specific, electrolyte disc substrates from fuelcellmaterials.com were bought. The details of the electrolyte discs are shown below:

Table 6.1 YSZ-8 Electrolyte substrate

Material	YSZ-8
Diameter	25 mm
Thickness	0.3 mm

The substrate was placed in the screen printing jig and held in place with a vacuum table.

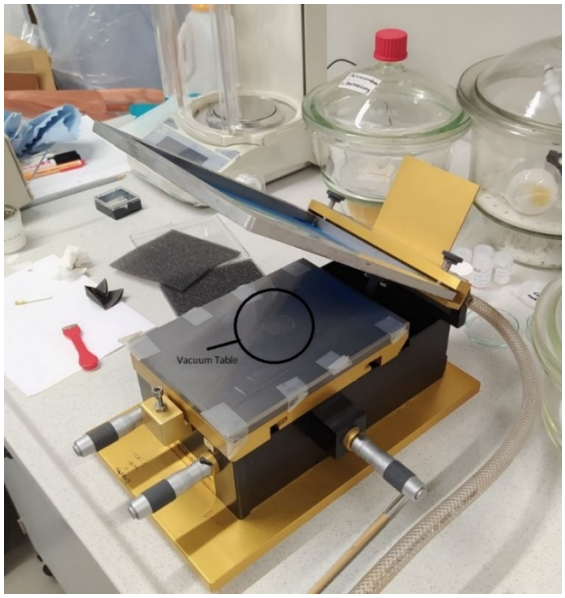

Figure 6.4 Screen Printing Jig

Then a small amount of the ink material was placed onto the screening mesh (100 um spacer) and applied to the electrolyte substrate with a spatula.

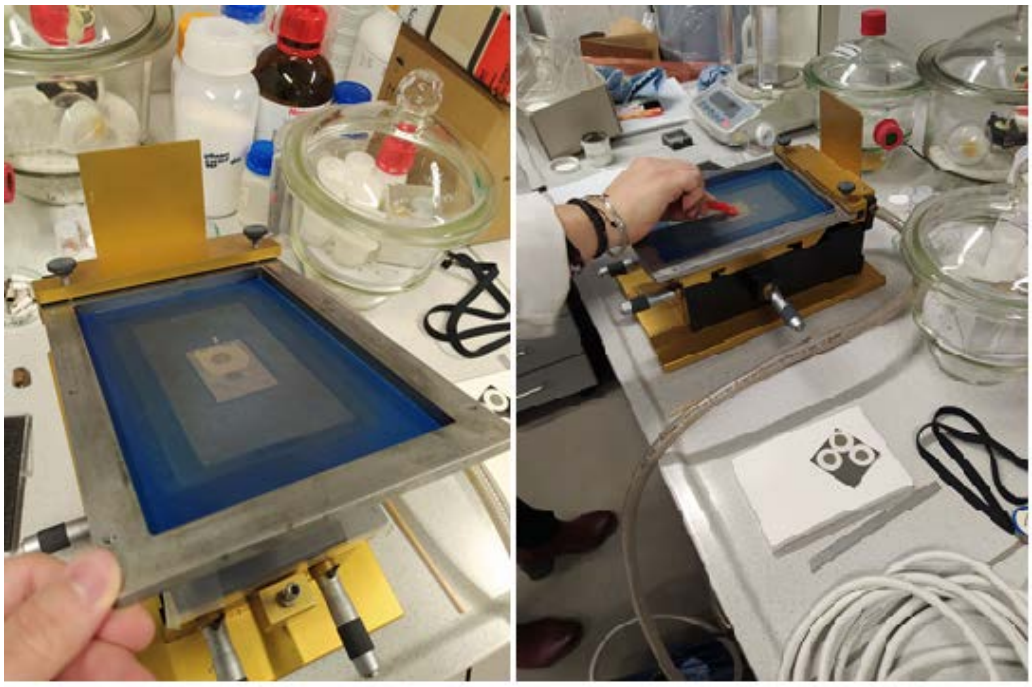

Figure 6.5 Screening Mesh

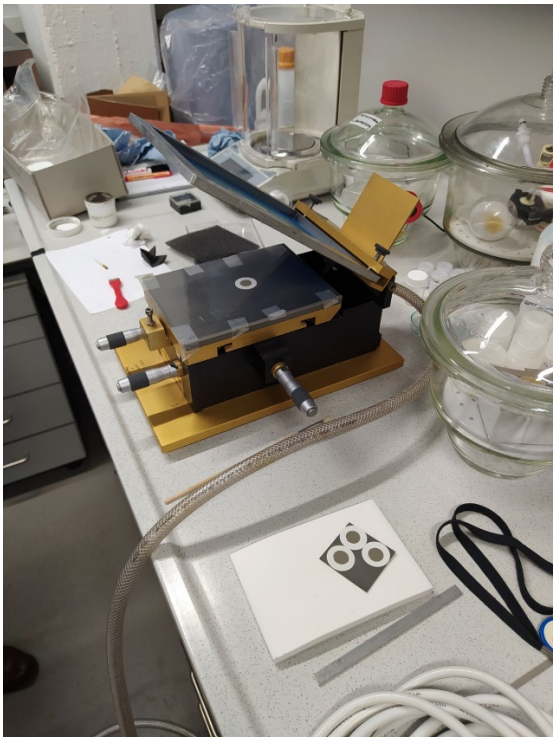

Figure 6.6 Anode Screen Printing

After that, the anode was screen printed onto the electrolyte. Then the electrolyte was sintered at 1250^{o}C. The same procedure was followed to screen print the cathode layer on the other side. The anode layer was constructed first because it was sintered at a higher temperature.

Figure 6.7 Fuel Cell Sintering

The furnace profiles of the anode and the cathode layer are shown below:

Table 6.2 Anode and Cathode Furnace profiles

Anode Furnace Profile				
Step	Process	Target	Rate (deg/min)	Duration (min)
1	Ramp	200	1	
2	Dwell	200		30
3	Ramp	1250	2	
4	Dwell	1250		180
5	Ramp	25	2	
Cathode Furnace Profile				
Step	Process	Target	Rate (deg/min)	Duration (min)
1	Ramp	200	1	
2	Dwell	200		30
2	Ramp	1100	2	
3	Dwell	1100		120
4	Ramp	25	2	

The first ramp till 200 ^{o}C was used to dry the anode/cathode paste. After that, a smooth ramp was used to reach the sintering temperature. The dwell time at the high temperatures was decided from previous experiments that have been conducted in the lab. Generally, the dwell time of the furnace affects the porosity of the layer. Finally, after the dwell time at the high temperature, there was a smooth transition to the environmental temperature.

Several fuel cells were constructed for this research. The ink pastes that were used for the anode and the cathode layers were purchased from NexTech Materials Ltd. (which is now NexCeris LLC.http://www.nexceris.com/).The specifications of each sample are shown in the table below:

Table 6.3 IS1 SOFC Sample

Sample IS1			
	Material	Thickness (mm)	Diameter (mm)
Anode	NiO-GDC	0.2	13
Cathode	LCSF	0.1	13
Electrolyte	YSZ8	0.3	25

Table 6.4 IS2 SOFC Sample

Sample IS2			
	Material	Thickness (mm)	Diameter (mm)
Anode	NiO-GDC	0.1	13
Cathode	LSM	0.1	13
Electrolyte	YSZ8	0.3	25

Table 6.5 IS3 SOFC Sample

Sample IS3			
	Material	Thickness (mm)	Diameter (mm)
Anode	NiO-YSZ	0.1	13
Cathode	LSM	0.1	13
Electrolyte	YSZ8	0.3	25

7. Experimental procedure

The experimental procedure starts by fixing the fuel cell in the ProboStat. The main goal at this step is to achieve a stable connection between the electrodes of the cell and the platinum electrical connectors of the ProboStat device. The cell is placed between a gold gasket, the cathode's electrical connector, and a spring-loaded component that helps with the sealing of the anode and the cathode. After that, the fuel feed lines are placed and the cell is ready for testing. The steps that have been described are shown in the figures below.

Figure 7.1 ProboStat fuel cell fixture

After placing the fuel cell in the ProboStat, the sealing procedure start. The sealing of the anode side is accomplished with the gold gasket. To make sealing fit every imperfection of the ceramic tube, the ProboStat fixture is warmed till 940 ^{o}C with a 2 deg C per minute ramp and stays at this temperature for 7 hours. The gold is getting softer in that temperatures and because of the springs' tension, the gasket takes exactly the form of the electrolyte and the ceramic tube. Thus, perfect sealing is achieved. During the whole procedure, Argon flows to the anode side and oxygen to the cathode to help with the heat dissipation. After that, the fixture assembly cools down to 600 ^{o}C, the gasket hardens again and then the reduction of the anode side begins. The reduction procedure takes place at a slowly elevating temperature till the final temperature with argon is replaced gradually by hydrogen. At the final temperature (850 ^{o}C for this thesis experiments) only hydrogen flows at the cathode side and the Constant Current, plus every other characterization test, is started. The temperature profile is shown in the figure below.

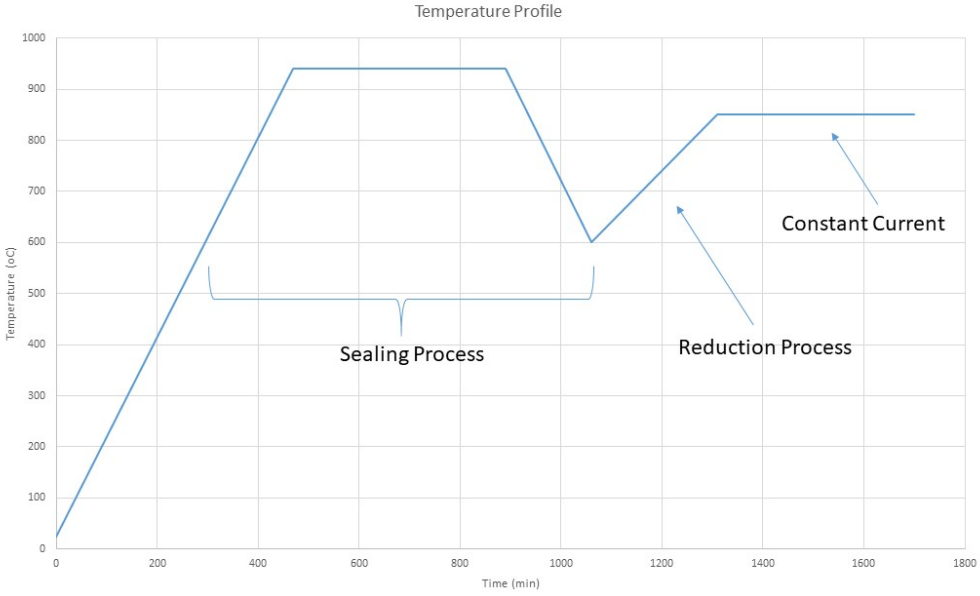

Figure 7.2 Temperature profile of fuel cell testing

8. Results

As it was mentioned in *chapter 6,* three fuel cells were fabricated for testing (IS1, IS2, IS3 are the names of each fuel cell respectively). IS2 was the sole fuel cell that attained the full experimental procedure and gave fruitful results, as Is1 and Is3 suffered from early failure. Let's analyze the results of each fuel cell.

1.1 8.1 IS1 fuel cell results

For the IS1 fuel cell, the reduction process escalated as shown in the table.

Table 8.1 Reduction process of IS1

IS1 Reduction				
Temperature (oC)	Voltage (V)	Ar (ml/min)	H2 (ml/min)	O2 (ml/min)
600	0.02	22	3	20
660	0.93	20	5	20
720	0.93	15	40	20
780	0.99	5	20	20
810	1.01	0	25	20
850	1.01	0	25	20

However, when the constant current process started, only 14 mA resulted in a voltage drop to 0.6 V (from 1.01). This poor performance indicated that the cell didn't work correctly and thus the testing stopped and the fuel cell was cooled down. Examining, the fuel cell in the microscopy it was observed that there was delamination in the cathode side and that was the reason why it didn't work. The figures below show the microscopy's results.

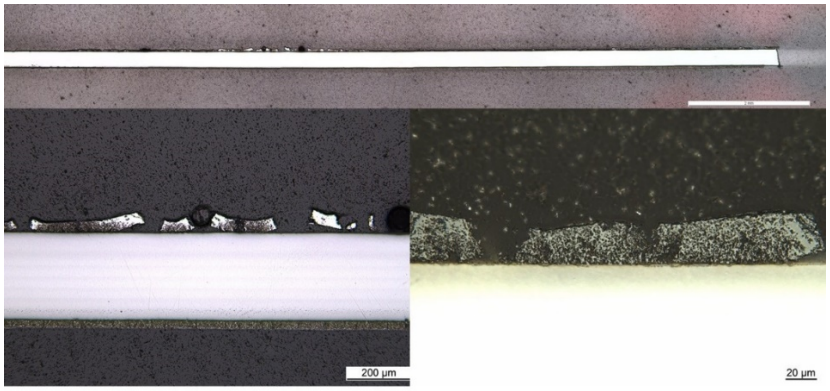

Figure 8.1 Microscopy images of IS1 fuel cell

The fuel cell was also prepared and scanned in a scanning electron microscope (SEM). For the preparation of the scanning, the cell was cut in half and dipped in epoxy resin with the cut section of the cell facing up. After that, the surface is polished and then a copper film is added to the surface to enhance the conductivity of the sample. Below, it is shown a picture of a fuel cell prepared for scanning.

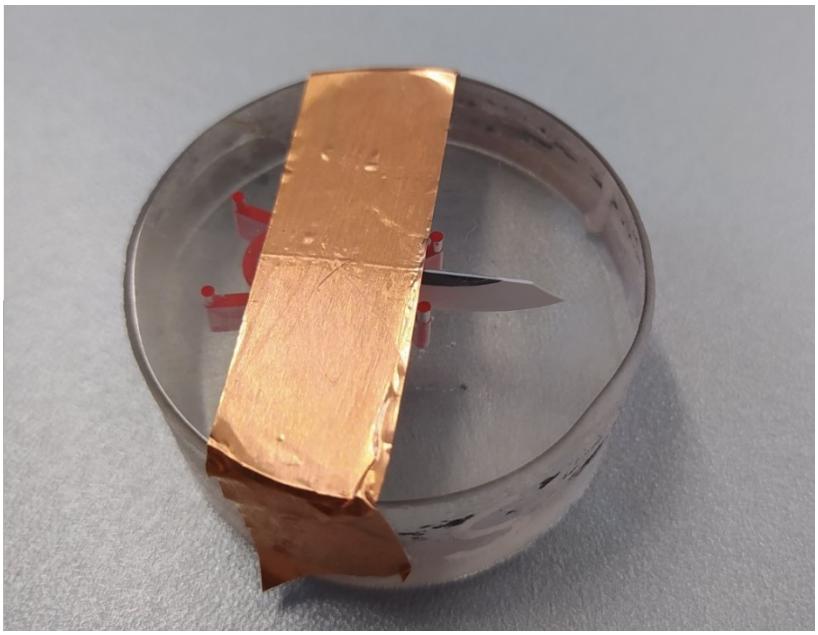

Figure 8.2 IS1 Sample prepared for SEM

In the scanning electron microscope except for the information for the morphology of the sample in nanoscale, EDX (energy dispersive X-ray) analysis took place too. With the EDX analysis information about the chemical elements contained in the fuel cell in different points was collected. The results are presented in the following table.

Table 8.2 IS1 EDX analysis of the anode side

Chemical Elements	**Anode**						
	EDX1	EDX2	EDX3	EDX4	EDX5	EDX6	EDX7
Ni	74.58	84.28	68.47	68.47	72.22	1.65	1.65
Ce	25.42	15.35	31.53	31.53	27.03	0	0
Zr	0	0.37	0	0	0.75	98.35	98.35

As it is shown in the table above point 7 is closer to the electrolyte and point 1 is in the outer perimeter of the cell. The points where its measurement was taken are shown in the figure below. From the EDX measurements, the percentage of the nickel mix with GDC is confirmed. Theoretically, the mixture that was used had 75% Ni and 25% GDC which is close to the measurement that was taken in the outer perimeter. In the figure below the SEM generated image is presented containing the points that each EDX measurement was taken.

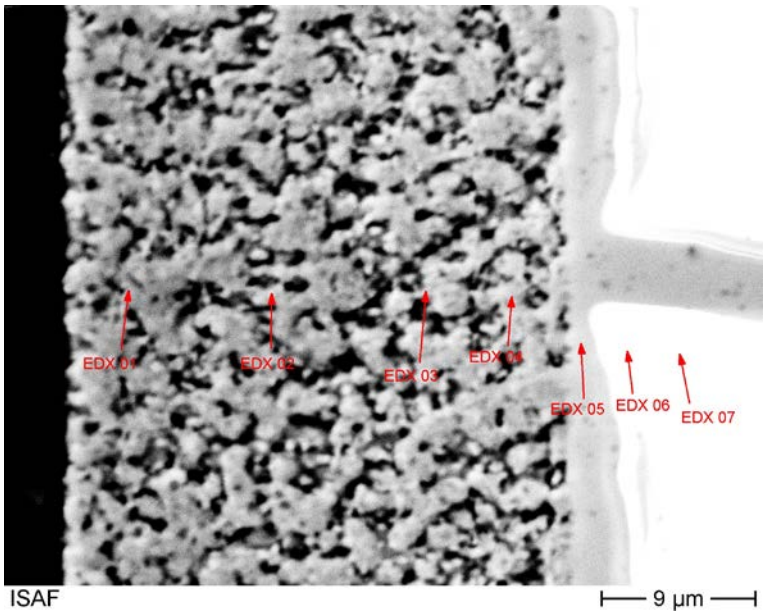

Figure 8.3 IS1anode SEM image

Accordingly, the same procedure was repeated for the cathode side, with the results presented below.

Table 8.3 IS1 EDX analysis of the cathode side

Chemical Elements	**Cathode**						
	EDX1	EDX2	EDX3	EDX4	EDX5	EDX6	EDX7
Zr	100	99.17	47.2	5.24	2.11	1.79	1.58
La	0	0.83	14.38	73.28	77.81	79.53	78.48
Sr	0	0	37.02	18.85	17.78	16.63	17.68
Ce	0	0	1.4	2.32	2.3	2.05	2.26
Ga	0	0	0	0.31	0	0	0

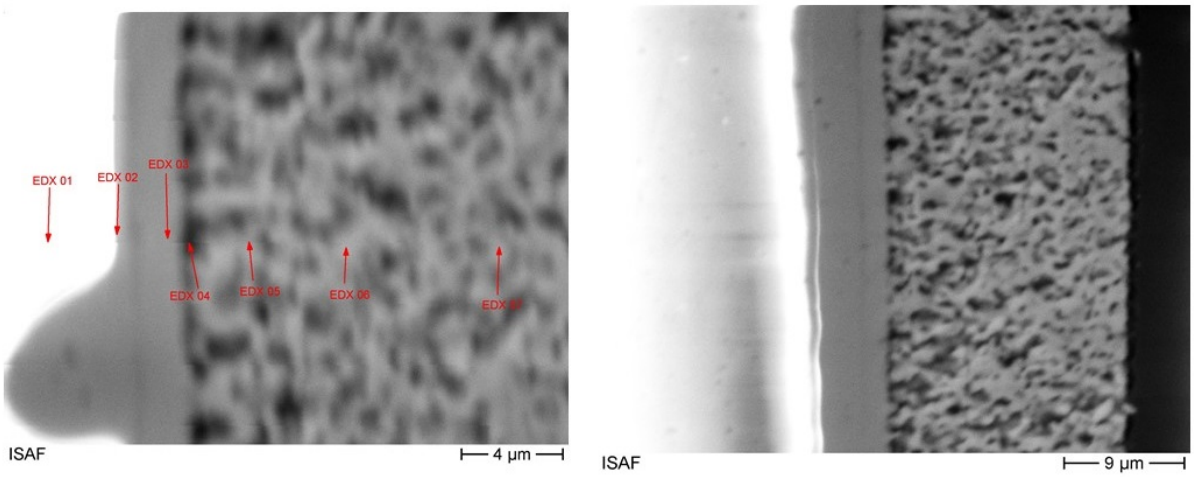

Figure 8.4 IS1cathode SEM image

8.2 IS2 fuel cell results

In order to avoid the delamination issues that occurred in the first cell, better preparation of the electrolyte substrate was made. The electrolyte's surface was ground with 120p sandpaper and then cleaned thoroughly. Indeed, the IS2 fuel cell was a successful cell that was tested for 200h. Unfortunately, due to the bad weather on the testing days, 2 power outages occur during the test. The degradation in the performance of the cell after the 2 power outages is obvious in the results. However, it was an opportunity for all the safety features of the software that was developed to be checked. The reduction process of the IS2 fuel cell is presented in the following table.

Table 8.4 Reduction process of IS2

IS2 Reduction				
Temperature (oC)	Voltage (V)	Ar (ml/min)	H2 (ml/min)	O2 (ml/min)
600	0.04	22	3	20
660	0.94	20	5	20
720	0.94	15	40	20
780	0.99	5	20	20
810	1.02	0	25	20

850	1.01	0	25	20

With the reduction process complete a PEIS test was conducted. The results are displayed in the following graph.

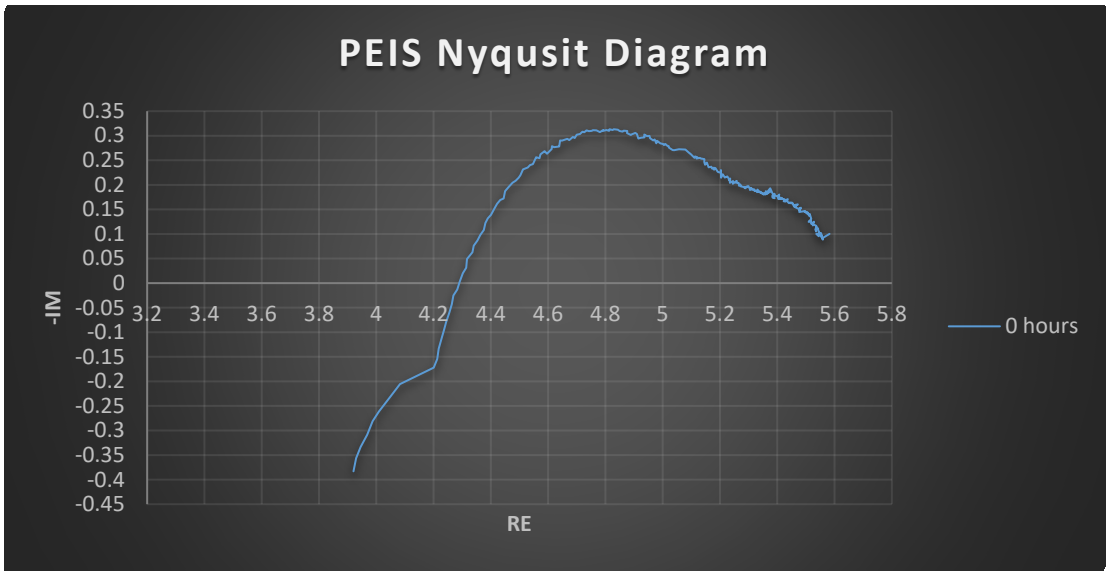

Figure 8.5 IS2 First PEIS test

From the PEIS test, the ohmic resistance of the fuel cell can be found as well as the two semicircles that are indicating the anode and cathode activation losses. The fuel cell seems to have a high ohmic resistance, but that was expected to happen since the fuel cell is electrolyte supported, consequently, the electrolyte is thick. Moreover, a j-V measurement was taken. The resulted j-V graph is shown below.

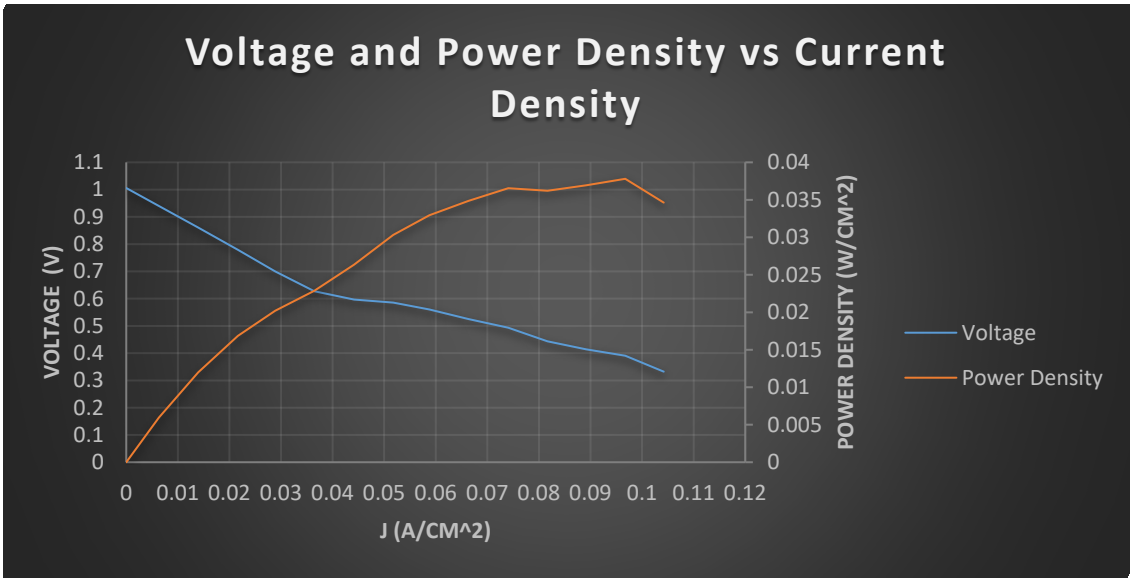

Figure 8.6 IS2 j-V graph

From the j-V graph, the three distinct areas of activation, ohmic, and concentration losses are shown. Moreover, the power density versus the current density is presented. After completing the first characterization tests, the constant current measurement starts. The constant current is interrupted every 25h for a PEIS measurement in order to observe the degradation of the cell through time. As it was mentioned above, the first two 25 hour measurements were interrupted by a power outage. The first constant current started at 78 mA, aiming to achieve a voltage drop to 0.6V. The CC measurement is presented below.

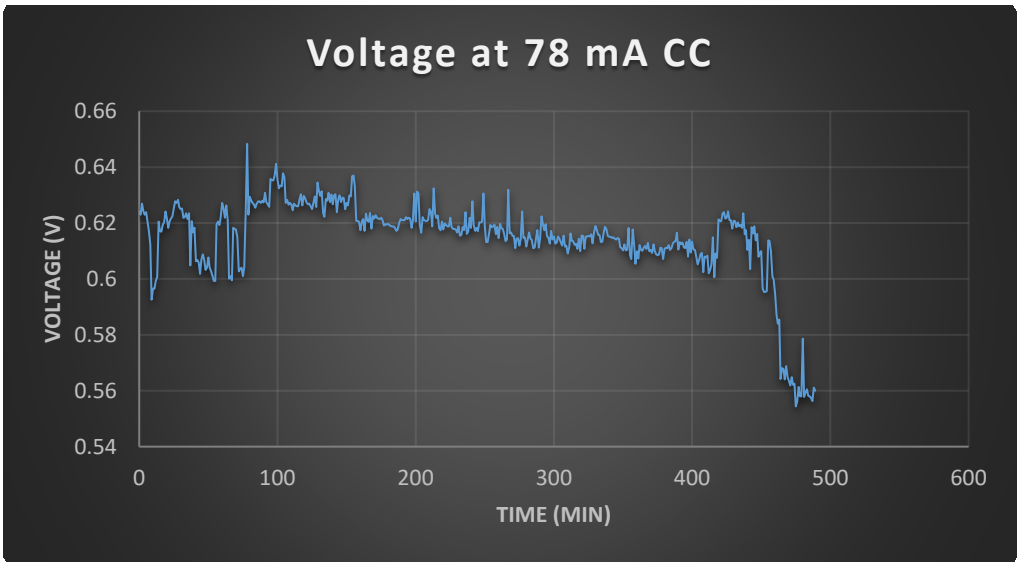

Figure 8.7 IS2 First CC graph

After recovering from the power outage another PEIS measurement was made. The PEIS graph is presented below.

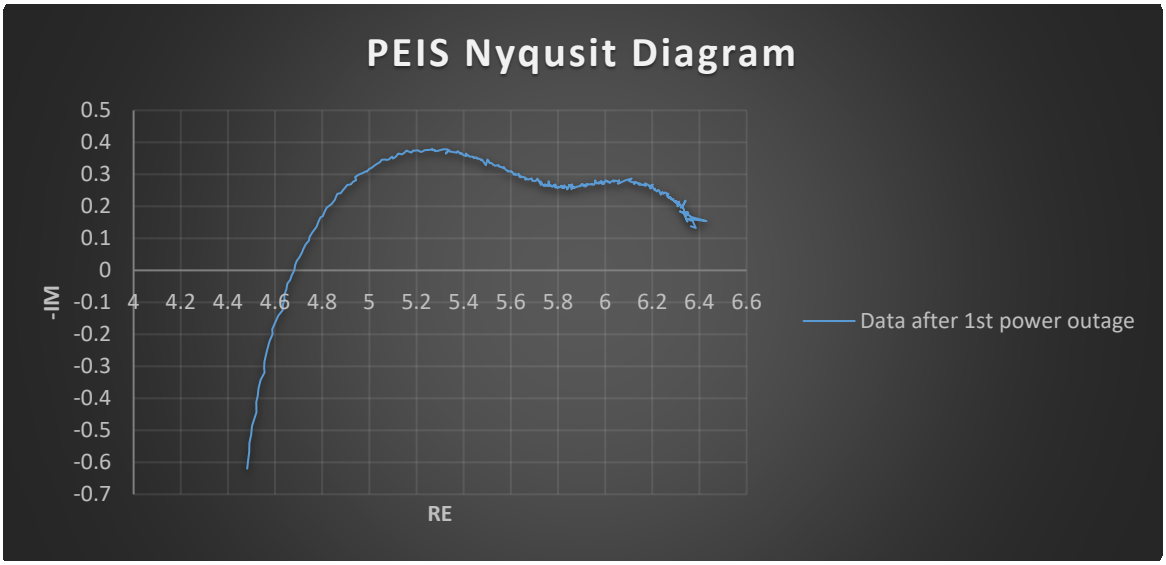

Figure 8.8 IS2 PEIS graph after 1st power outage

Comparing the two graphs it is observed how the electrolyte's ohmic resistance, as well as the cathode's activation loss, increased after the power outage. However, since the cell was not ruined a constant current measurement started again. This time in order to achieve a voltage drop to 0.6V only 65 mA were drawn (compared to 78 before). The resulted graph is presented below.

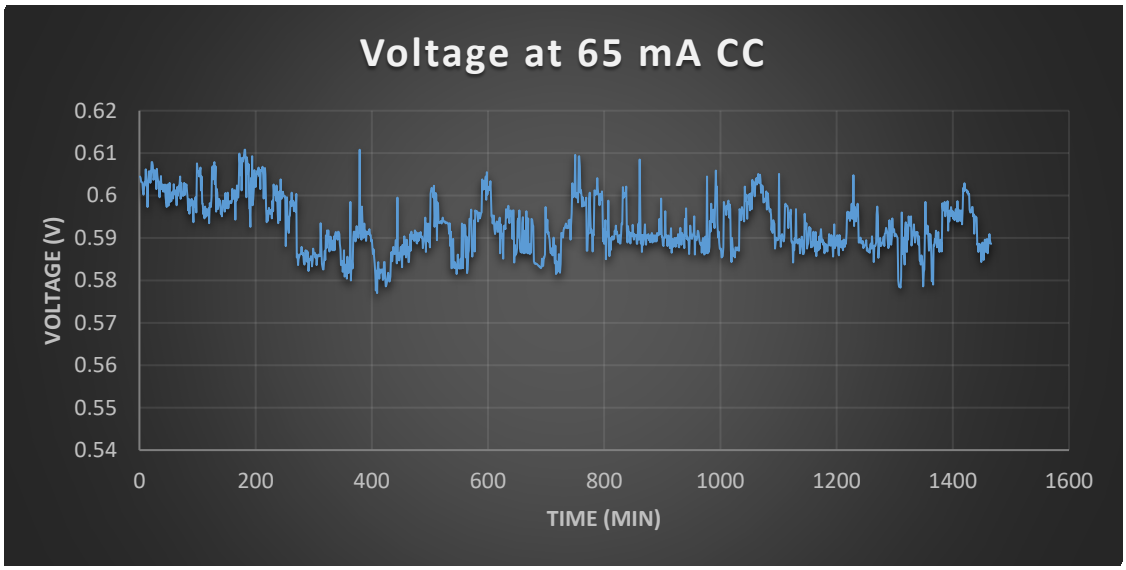

Figure 8.9 IS2 CC graph after 1st power outage

Another power outage interrupted the second CC measurement, however, the fuel cell recovered without any damages. From this moment the 200h CC measurement begins with interrupts every 25 hours for PEIS measurements. The collected data are presented in the graphs below.

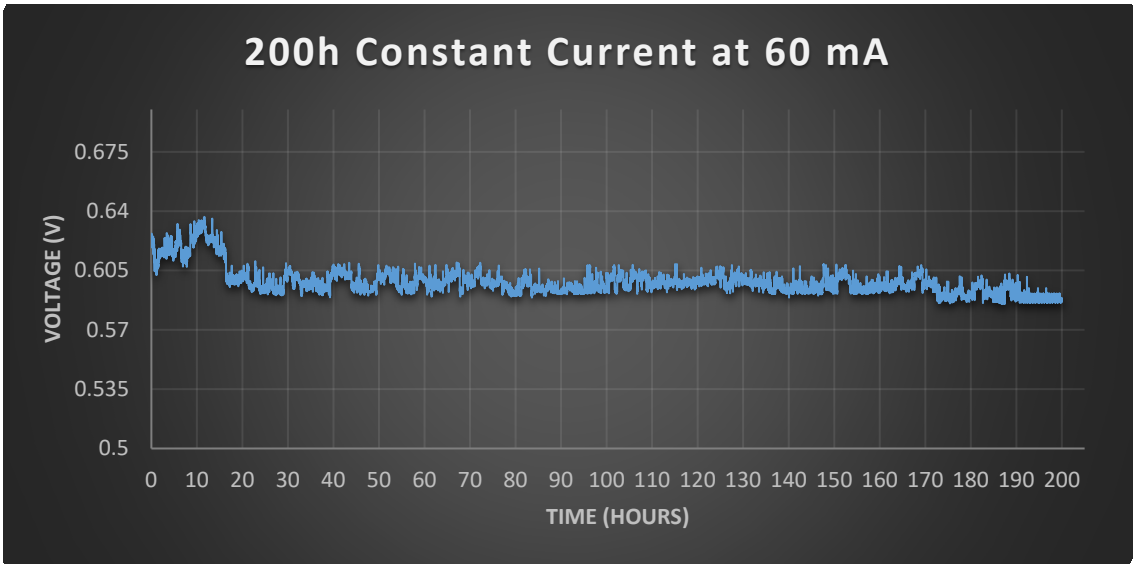

Figure 8.10 IS2 CC graph after 2nd power outage

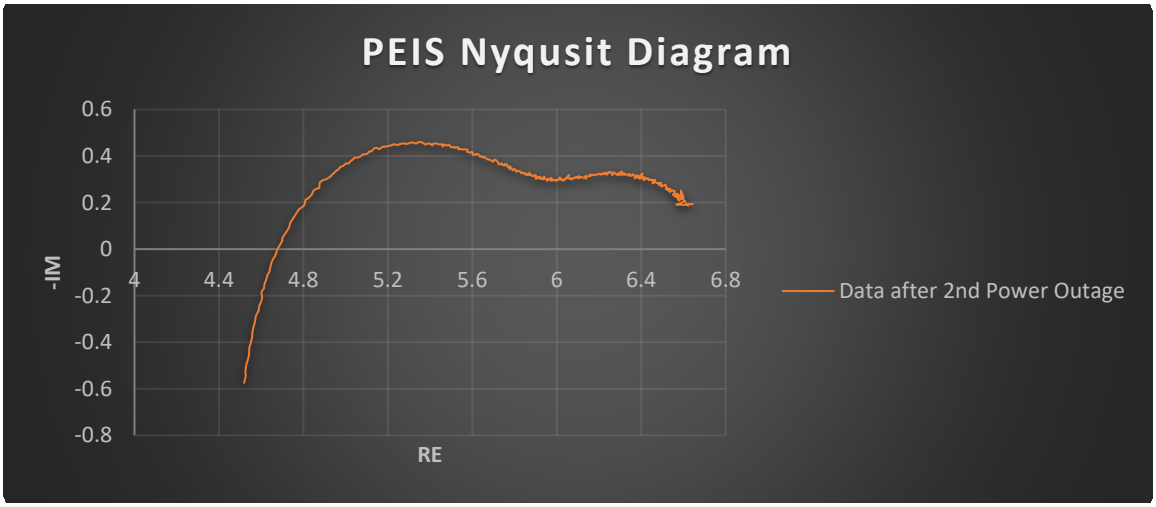

Figure 8.11 IS2 PEIS graph after 2nd power outage

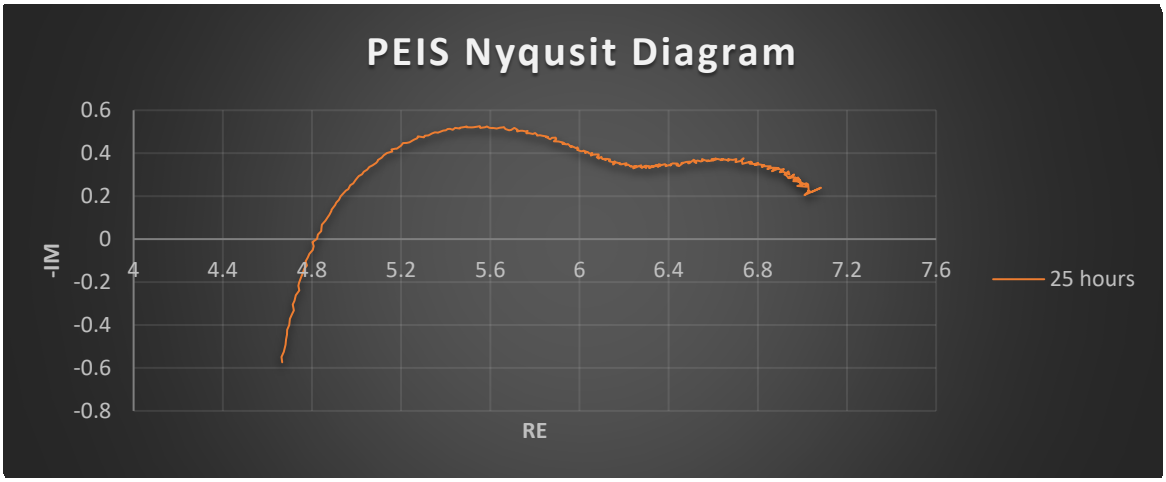

Figure 8.12 IS2 PEIS at 25 hours

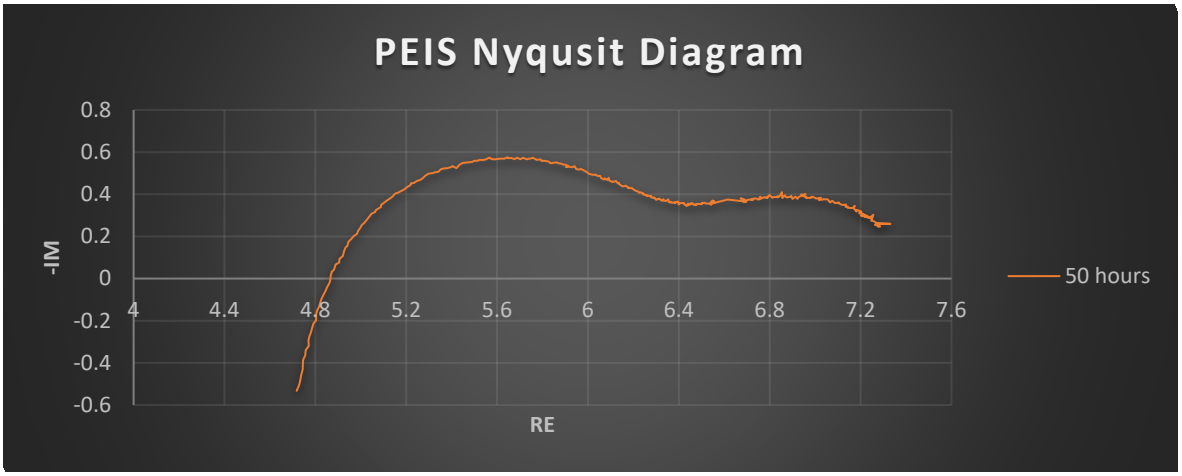

Figure 8.13 IS2 PEIS at 50 hours

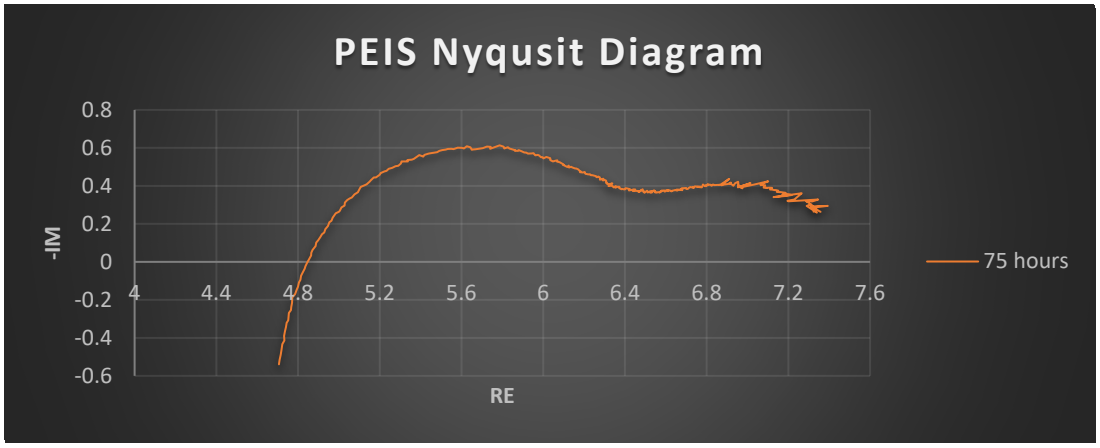

Figure 8.14 IS2 PEIS at 75 hours

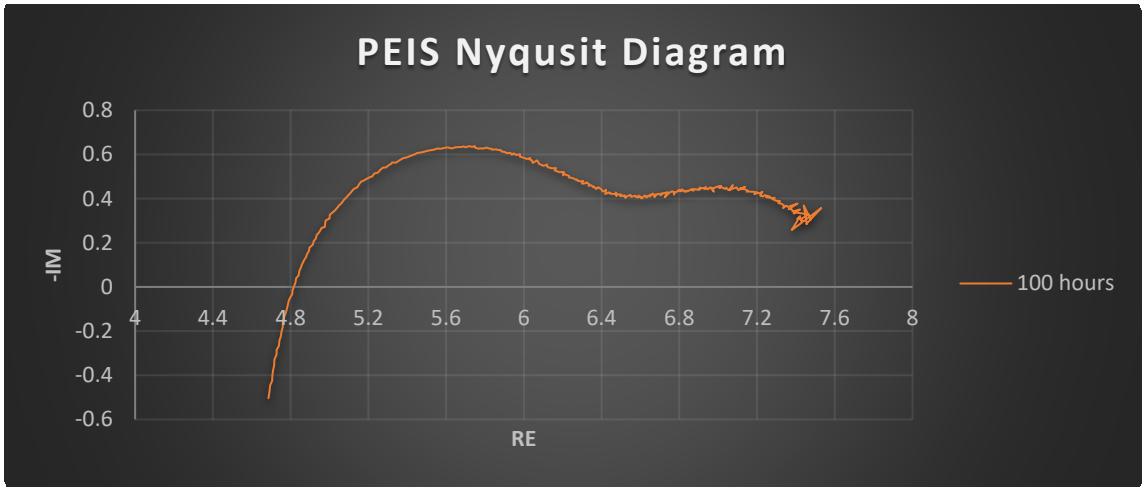

Figure 8.15 IS2 PEIS at 100 hours

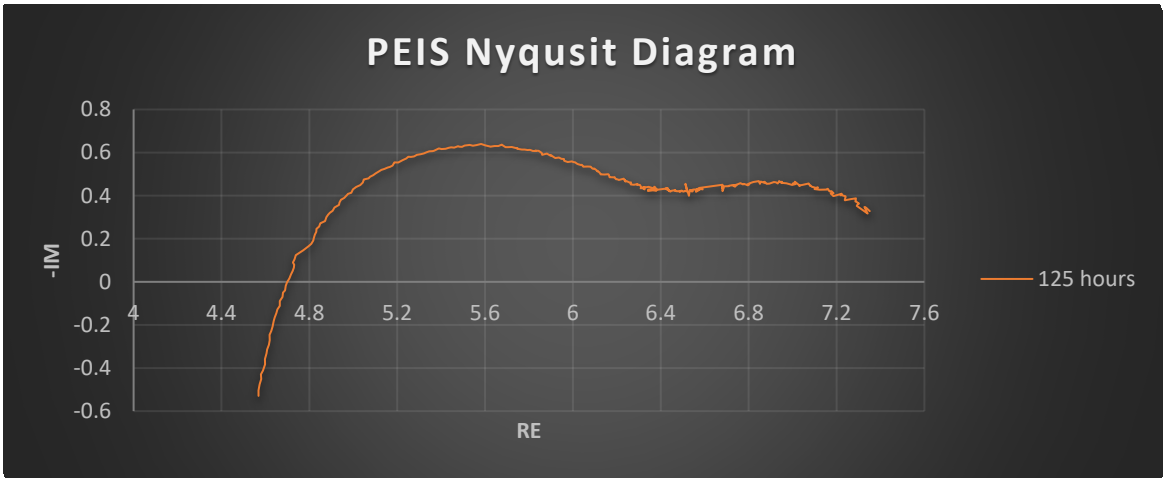

Figure 8.16 IS2 PEIS at 125 hours

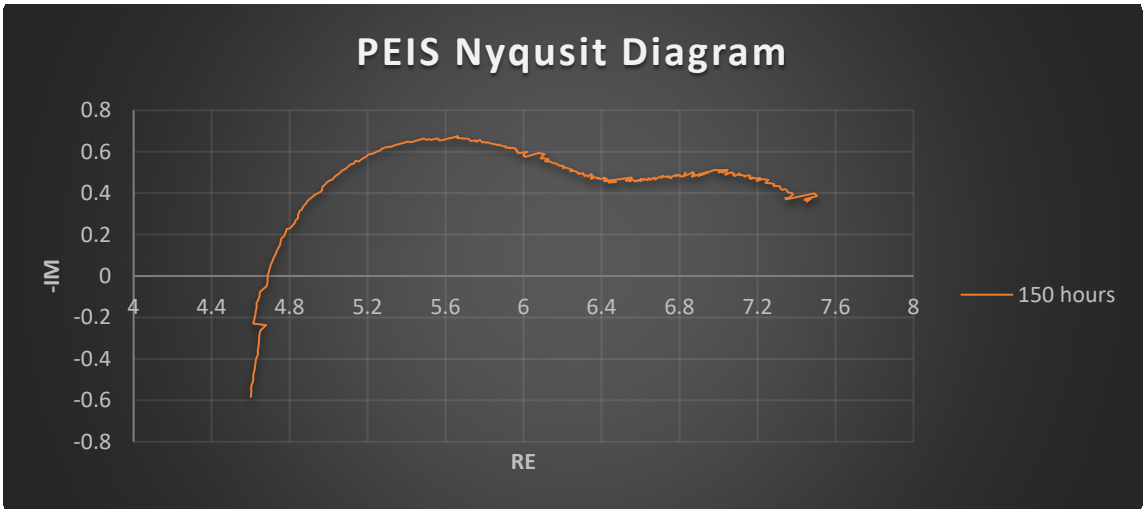

Figure 8.17 IS2 PEIS at 150 hours

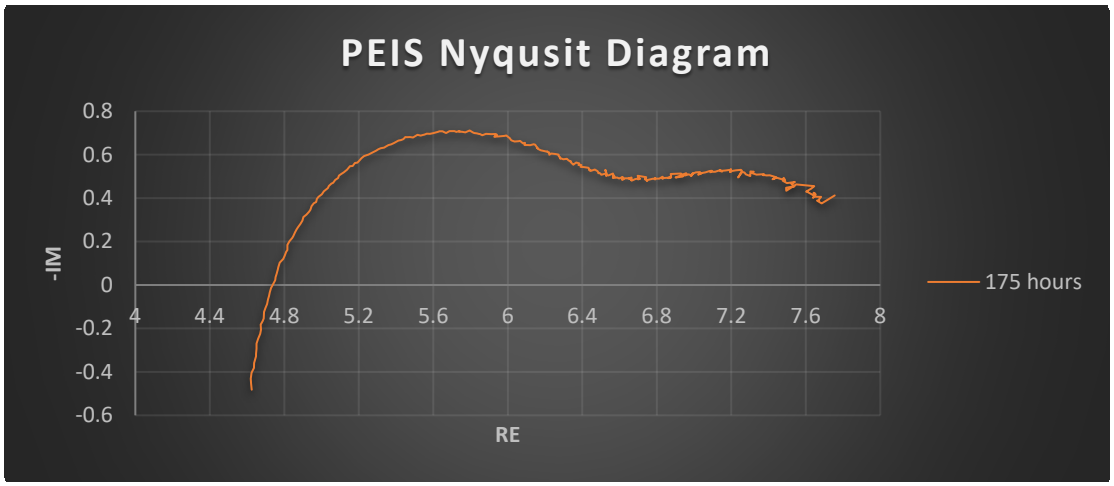

Figure 8.18 IS2 PEIS at 175 hours

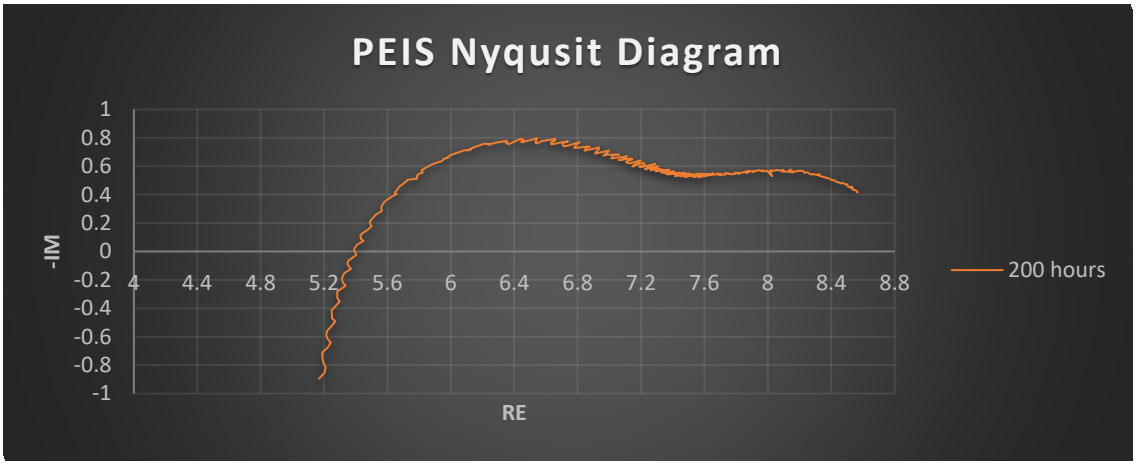

Figure 8.19 IS2 PEIS at 200 hours

To begin with, comparing the first results of the cell with the results after two power outages it is apparent that there is a significant drop in the performance of the cell. Just from the constant current test, in the first place, the 0.6V voltage drop resulted from a 78 mA current draw, while after the power outages just a 60 mA current draw resulted in the same voltage drop to 0.6V. That was reasonable to happen as the fuel cells are not able to handle abrupt transition phenomena. As far as the stable testing of the cell is concerned (the last 200h of testing), the degradation in the performance of the fuel cell is shown from the constant current graph, where in the last 30 hours the drop voltage starts to increase. Furthermore, from the PEIS graphs the semicircles, that represent the activation losses of the anode and the cathode, constantly expanded indicating that the anode and cathode materials are losing their catalytic effectiveness.

The fuel cell was also prepared for SEM and EDX measurements after the 200h of testing. The SEM image of the anode with the EDX measurements are presented below:

Table 8.5 IS2 anode EDX measurements

Chemical Elements	**Anode**			
	EDX1	EDX2	EDX3	EDX4
Ni	74.37	71.1	20.04	0
Ce	25.63	28.9	20.22	0
Zr	0	0	59.74	100

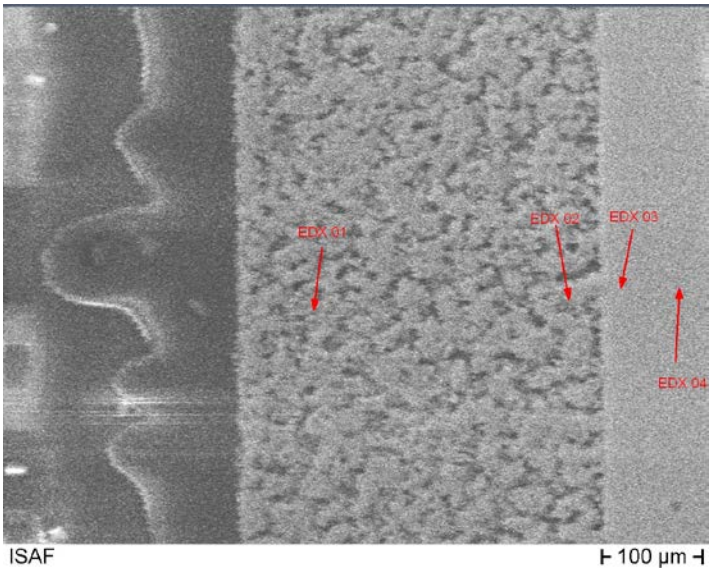

Figure 8.20 IS2 Anode SEM image

Respectively, for the cathode:

Table 8.6 IS2 cathode EDX measurements

Chemical Elements	Cathode						
	EDX1	EDX2	EDX3	EDX4	EDX5	EDX6	EDX7
Zr	100	71.1	1.41	10.63	1.61	1.02	0.97
La	0	28.9	95.95	32.75	39.09	38.53	39.22
Mn	0	0	2.64	55.54	58.38	59.42	58.84
Sr	0	0	0	1.08	0.92	1.03	0.97

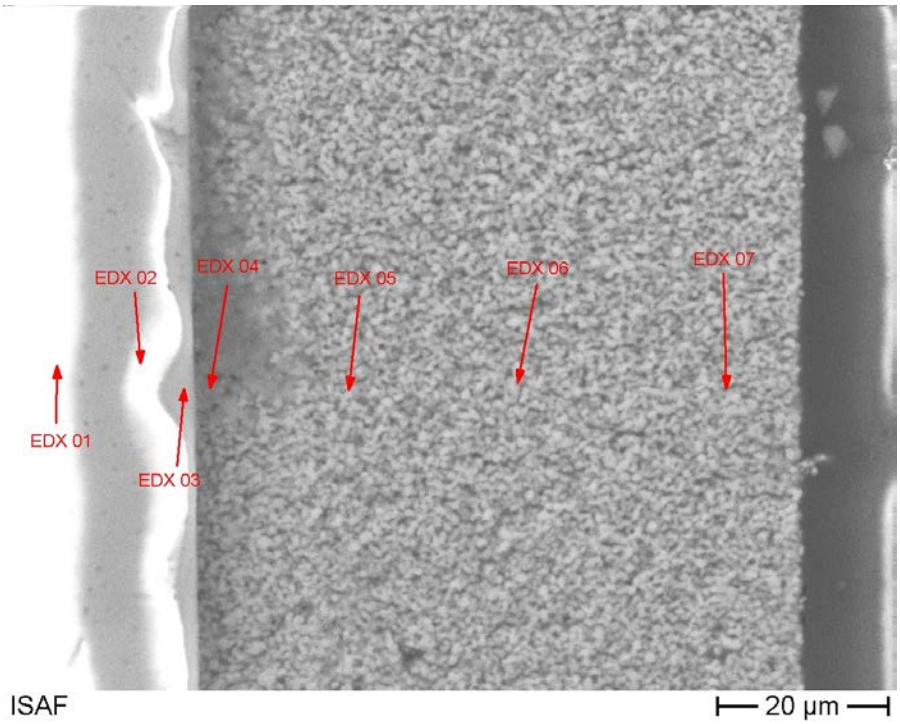

Figure 8.21 IS2 Cathode SEM image

Comparing the results of IS1 EDX measurements with the IS2 one, the diffusion of the materials can be observed after 200h of testing.

8.3 IS3 fuel cell results

The IS3 was fabricated with NiO-YSZ anode instead of NiO-GDC cermet. The reduction process of the cell started with the following results measured.

Table 8.7 Reduction Process of IS3

IS3 Reduction				
Temperature (oC)	Voltage (V)	Ar (ml/min)	H2 (ml/min)	O2 (ml/min)
600	0.01	22	3	20
660	0.97	20	5	20
720	1.02	15	40	20
780	1.03	5	20	20
810	1.04	0	25	20
850	0.8	0	25	20

Unfortunately, the fuel cell broke at some point from 810 ^{o}C to 850^{o}C and lost its sealing. For that reason, no further results were obtained from this cell.

9. Discussion and Conclusions

The subject of this thesis was to develop a solid testing rig and a user-friendly software in order to ease and accelerate the SOFC testing procedure. For the sake of evaluating the proper function of the testing rig and the software fuel cells were fabricated and tested. In the meantime, a holistic view of all the aspects of solid oxide cells (modeling, characterization, fabrication, and testing) was obtained

More specifically, a LabView application was developed to control and monitor the full experimental procedure when testing new SOFCs. The electrochemical techniques used to evaluate the performance of SOFCs were V-I characterization, Potentiostatic Impedance Spectroscopy and Constant Current draw. In order to verify the effectiveness of the program three SOFCs were constructed and put into continuous testing. Laboratory testing of homemade SOFCs proved to be a challenging procedure. Electrochemical techniques when combined with surface characterization techniques (microscopy) revealed what was already expected: the performance of the cell is dependent to many factors which include not only the catalytic activity of electrode materials but also the in-situ solid construction of a new cell. The SOFCs abbreviated as IS1 and IS3 met unfortunately early failure. IS1 faded early due to delamination in the cathode which was probably provoked by poor electrolyte surface preparation for adhesion. On the other side IS3 broke in the middle of the experiment at high temperature. This phenomenon can be attributed to the fact that the electrolyte substrate was fitted tightly in the experimental fixture and a slight misalignment cause the fuel cell to brake.

Fortunately, the experimental procedure was successfully completed when tested the SOFC IS2. This SOFC attained more than 200 hours at 70mA current draw and delivered a maximum power density at 37mW/cm^2. However, a brief literature review can reveal that these metrics cannot constitute promising results for now. In Table9.1 some of the recent results of similar studies can be found [38] [39] [40] [41] .

Table 9.1 Literature comparative table

Sample	Anode	Cathode	Electrolyte	Max Power Density (W/cm2)
IS2	NiO-GDC	LSM	YSZ8	0.037
ChangjingFu et.al.	NiO-GDC	LSCF	GDC	0.9
Seung Young Park et. al.	NiO-GDC	LSCF	YSZ	0.3
Jae-Ha Myung et. al.	NiO-GDC	LSCF	GDC	0.36
Kazuhiro Yamamoto et. al.	NiO-GDC	LSCF	GDC	0.08

All in all, simultaneously trying to balance affective fabrication of electrodes and whole cells while decreasing intrinsic reaction overpotentials remains a challenging subject when developing SOFCs. There are plenty sources which appear to deteriorate the performance of a cell, for instance the thick commercial electrolyte substrates which led to a high ohmic resistance, and the screen-printing fabrication method of commercial inks for the electrode's layers.

This thesis was conducted with the hope that further studies can be evolved in the testing rig that was constructed, researching several electrode and electrolyte materials. Moreover, testing with alternative fuels such as NH3 (ammonia) and comparative studies with H2 fuel would be of great interest. Solid oxide fuel cells are a rapidly growing research field, as they meet certain critical demands considering next generation energy storage and conversion systems. It is anticipated that during the next few years they will fulfill their potential of establishing a sustainable green economy.

List of Figures

List of Tables

References

[1] Ryan O'Hayre, Suk-Won Cha, Whitney Colella, Fritz B. Prinz, Fuel Cell Fundamentals, Wiley, 2016.

[2] J. W. Fergus, "Electrolytes for solid oxide fuel cells," *Journal of Power sources,* p. 11, 21 June 2006.

[3] D.W. Strickler, W.G. Carlson, "Electrical Conductivity in the ZrO2-Rich Region of Several M2O3-ZrO2 Systems," *Journal of the American Ceramic Society,* vol. 48, no. 6, pp. 286-289, 1965.

[4] J.M. Dixon, L.D. LaGrange, U. Mergen, C.F. Miller, J.T. Porter, "Electrical Resistivity of Stabilized Zirconia at Elevated Temperatures," *Journal of the Electrochemical Society,* vol. 110, pp. 276-280, 1963.

[5] S. P. F. Badwal, "The Ionic Conductivity of Yttria-Zirconia Compositions," *Key Engineering Materials,* vol. 53, pp. 235-240, 1991.

[6] K. Nomura, Y. Mizutani, M. Kawai, Y. Nakamura, O. Yamamoto, "Aging and Raman scattering study of scandia and yttria doped zirconia," *Solid State Ionics,* vol. 132, pp. 235-239, 2000.

[7] V.V. Kharton, F.M.B. Marques, A. Atkinson, "Transport properties of solid oxide electrolyte ceramics: a brief review," *Solid State Ionics,* vol. 174, no. 1-4, pp. 135-149, 2004.

[8] M. Weller, F. Khelfaoui, M. Kilo, M.A. Taylor, C. Argirusis, G. Borchardt, "Defects and phase transitions in yttria- and scandia-doped zirconia," *Solid State Ionics,* vol. 175, no. 1-4, pp. 329-333, 2004.

[9] B. M.M., "Some structural aspects of ionic conductivity in zirconia stabilised by yttria and calcia," *Materials Science Poland,* vol. 24, pp. 39-44, 2006.

[10] Bjarke Dalslet, Peter Blennow, Peter Vang Hendriksen, Nikolaos Bonanos, Dorthe Lybye & Mogens Mogensen, "Assessment of doped ceria as electrolyte," *Journal of Solid State Electrochemistry,* vol. 10, no. 8, pp. 547-561, 2006.

[11] Hidenori Yahiro, Koichi Eguchi, Hiromichi Arai, "Electrical properties and reducibilities of ceria-rare earth oxide systems and their application to solid oxide fuel cell," *Solid State Ionics,* vol. 36, no. 1-2, pp. 71-75, 1989.

[12] David A. Andersson, Sergei I. Simak, Natalia V. Skorodumova, Igor A. Abrikosov, Börje Johansson, "Optimization of ionic conductivity in doped ceria," *Proceedings of the National Academy of Sciences,* vol. 103, no. 10, pp. 3518-3521, 2006.

[13] K. Schwarz, "Materials design of solid electrolytes," *Proceedings of the National Academy of Sciences,* vol. 103, no. 10, p. 3497, 2006.

[14] Rajalekshmi Chockalingam,Ashok K. Ganguli, Suddhasatwa Basu, "Praseodymium and gadolinium doped ceria as a cathode material for low temperature solid oxide fuel cells," *Journal of Power Sources,* vol. 250, pp. 80-89, 2014.

[15] Rajalekshmi Chockalingam, Snehil Jain, Suddhasatwa Basu, "Studies on Conductivity of Composite GdCeO2-Carbonate Electrolytes for Low Temperature Solid Oxide Fuel Cells," *Integrated Ferroelectrics,* vol. 116, no. 1, pp. 23-34, 2010.

[16] L. Qiu, T. Ichikawa, A. Hirano, N. Imanishi, Y. Takeda, "Ln1−xSrxCo1−yFeyO3−δ (Ln=Pr, Nd, Gd; x=0.2, 0.3) for the electrodes of solid oxide fuel cells," *Solid State Ionics,* vol. 158, no. 1-2, pp. 55-65, 2003.

[17] J. M. Ralph, A. C. Schoeler, M. Krumpelt , "Materials for lower temperature solid oxide fuel cells," *Journal of Materials Science,* vol. 36, pp. 1161-1172, 2001.

[18] Xingyan Xu, Changrong Xia, Guoliang Xiao, Dingkun Peng, "Fabrication and performance of functionally graded cathodes for IT-SOFCs based on doped ceria electrolytes," *Solid State Ionics,* vol. 176, no. 17-18, pp. 1513-1520, 2005.

[19] E. D. Wachsman, P. Jayaweera, N. Jiang, D. M. Lowe, B. G. Pound, "Stable High Conductivity Ceria/Bismuth Oxide Bilayered Electrolytes," *Journal of The Electrochemical Society,* vol. 144, 1997.

[20] Yichuan Chen, Linrui Zhang, Yongzhe Zhang, Honli Gao, Hui YanHui Yan, "Large-area perovskite solar cells – a review of recent progress and issues," *RSC Advances,* vol. 8, no. 19, pp. 10489-10508, 2018.

[21] S. M. Haile, "Fuel cell materials and components," *Acta Materialia,* vol. 51, no. 19, pp. 5981-6000, 2003.

[22] Lei Bia, Eman Husni Da'as, Shahid P. Shafi, "Proton-conducting solid oxide fuel cell (SOFC) with Y-doped BaZrO3," *Electrochemistry Communications,* vol. 80, pp. 20-23, 2017.

[23] P. Holtappels, C. Sorof,M. C. Verbraeken, S. Rambert, U.Vogt, "Preparation of Porosity–Graded SOFC," *Fuel Cells,* vol. 6, no. 2, pp. 113-116, 2006.

[24] J. W. Fergus, "Oxide anode materials for solid oxide fuel cells," *Solid State Ionics,* vol. 177, pp. 1529-1541, 2006.

[25] Swadesh K. Pratihar, A. Dassharma, H. S. Maiti , "Properties of Ni/YSZ porous cermets prepared by electroless coating technique for SOFC anode application," *Journal of Materials Science,* vol. 42, p. 7220–7226, 2007.

[26] Yun-Hui Huang, Ronald I. Dass, Zheng Liang Xing, John B. Goodenough, "Double Perovskites as Anode Materials for Solid-Oxide Fuel Cells," *Science,* vol. 312, no. 5771, pp. 254-257, 2006.

[27] Chunwen Sun, Ulrich Stimming,, "Recent anode advances in solid oxide fuel cells," *Journal of Power Sources,* vol. 171, no. 2, pp. 247-260, 2007.

[28] W. L. Worell, "Electrical properties of mixed-conducting oxides having high oxygen-ion conductivity," *Solid State Ionics,* vol. 52, no. 1-3, pp. 147-151, 1992.

[29] Harumi Yokokawa,Natsuko Sakai,Teruhisa Horita,Katsuhiko Yamaji, "Recent Developments in Solid Oxide Fuel Cell Materials," *Fuel Cells,* vol. 1, no. 2, pp. 117-131, 2001.

[30] Rong-Tsu Wang,Horng-Yi Chang, Jung-Chang Wang , "An Overview on the Novel Core-Shell Electrodes for Solid Oxide Fuel Cell (SOFC) Using Polymeric Methodology," *Polymers,* vol. 13, pp. 2774-2796, 2021.

[31] Emmanuel Balogun, Paul Barendse, Jessica Chamier, "Effect of Anode and Cathode Relative Humidity Variance and Pressure Gradient on Single Cell PEMFC Performance," in *IEEE ENERGY CONVERSION CONGRESS & EXPO*, Portlanf, Oregon, 2018.

[32] Shuab Khan, S M Aijaz Rizvi, Shabana Urooj, "Equivalent Circuit Modelling using Electrochemical Impedance Spectroscopy for Different Materials of SOFC," in *INDIACom 2016*, New Delhi, 2016.

[33] Tien Quang Nguyen, Co Breitkopf, "Determination of Diffusion Coefficients Using Impedance Spectroscopy Data," *Journal of The Electrochemical Society,* vol. 165, no. 14, pp. 826-831, 2018.

[34] Sung-Kwan Ryu, Young-Woo Choi, Chang-Soo Kim, T. H. Yang, Han-Sung Kim, Jin-Soo Park, "Preparation and Characterization of Ionic Liquid-based Electrodes for High Temperature Fuel Cells Using Cyclic Voltammetry," *Journal of the Korean Electrochemical Society,* vol. 16, no. 1, pp. 30-38, 2013.

[35] Abdalla M. Abdalla, Shahzad Hossain, Pg MohdIskandr Petra, Mostafa Ghasemi Abul K. Azad, "Achievements and trends of solid oxide fuel ells in clean energy field: a perspective review," *Front. Energy 14,* 2020.

[36] Lewis, Jr., WA, "Dry pressing technicall ceramics," 01 04 1996.

[37] Nurul Akidah Baharuddin, Nurul Fahrara Abdul Rahman, Hamimah Abd. Rahman, Mahendra Rao Somalu, Mohd Azham Azmi, Jarot Raharjo, "Fabrication of high quality electrode films for solid oxide fuel cell by screen printing: A review on important processing parameters," *Energy Research,* 25 05 2020.

[38] Changjing Fu, Siew Hwa Chan, Qinglin Liu, Xiaoming Ge, G. Pasciak, "abrication and evaluation of Ni-GDC composite anode prepared by aqueous-based tape casting method for low-temperature solid oxide fuel cell," *International Journal of Hydrogen Energy,* vol. 35, no. 1, pp. 301-307, 2010.

[39] Seung-Young Park, Chan Woong Na, Jee Hyun Ahn, Rak-Hyun Song, Jong-Heun Lee, "Preparation of highly porous NiO–gadolinium-doped ceria nano-composite powders by one-pot glycine nitrate process for anode-supported tubular solid oxide fuel cells," *Journal of Asian Ceramic Societies,* vol. 2, no. 4, pp. 339-346, 2014.

[40] Jae-ha Myung, Hyun-Jun Ko, Jong-Jin Lee, Ji-Hwan Lee, Sang-Hoon Hyun, "Synthesis and characterization of NiO/GDC–GDC dual nano-composite powders for high-performance methane fueled solid oxide fuel cells," *International Journal of Hydrogen Energy,* vol. 37, no. 15, p. 11351–11359, 2012.

[41] Kazuhiro Yamamoto, Nan Qiu, Satoshi Ohara, "In situ fabrication of high-performance Ni-GDC-nanocube core-shell anode for low-temperature solid-oxide fuel cells," *Scientific Reports,* vol. 5, pp. 1-6, 2015.

Appendix

SOFC-Experiment (V5) Program's Manual

1.2 Fundamental LabVIEW elements

In the user's interface of the LabVIEW, there are two main elements: controls and indicators. The controls are tabs that should be filled by the user to control the variables of the program (there are also Boolean controls that are represented by buttons or switches). Controls are tabs with a white background. On the other hand, indicators are tabs that get values calculated from the program. Indicators have a grey background as is shown in the picture below.

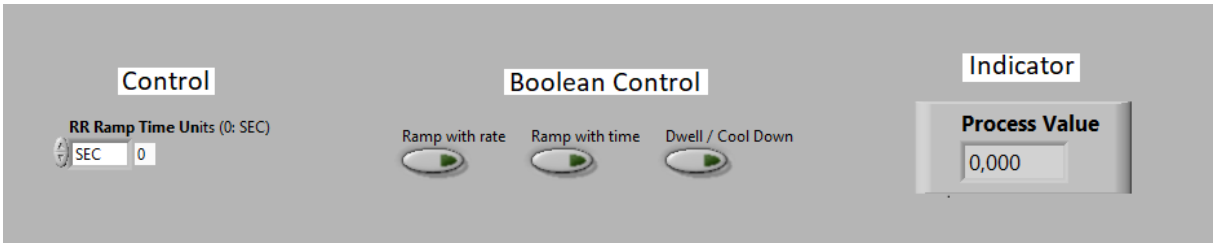

Figure A1 LabVIEW basic elements

1.3 2D array and how to index a 2D-array

There are occasions in the program that you have to index a 2D array. The 2D array is like a matrix and it is represented usually as a tab that consists of a number, at the left, which indicates the current column, and the existing rows at the right. For more clarity, an example is shown below in the picture.

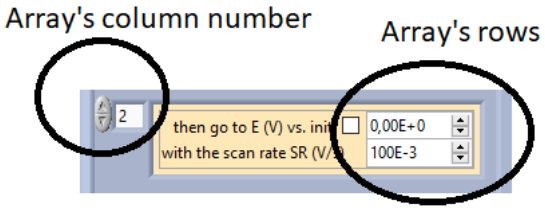

Figure A2 LabVIEW array

1.4 General instructions for using SOFC experiment program

First of all, it is extremely important to open the LabVIEW program from the folder that is saved as shown in the path below the title. If the program and the SubVIs transferred to another folder the program will not work properly.

The program is divided into 5 tabs. Every tab controls an instrument and the first tab is the tab with the general settings of the whole program. To run the program correctly, you have to fill in the data of every control in the first tab and then hit the start button. In the "*choose pc*" control, you define the path of the folder that the data will be saved. In this control, there are 2 default options. If the program is running on the University's laptop, then the admin/… is the correct option. However, if the program is running on another PC you can write manually the path of the folder that you prefer to save the data. You can find the folder's path by right-clicking in the desirable folder and then choosing properties. In the properties tab, the folder's path is shown. Be careful the C:\Users part of the path **exists already** in the program so you have to write the rest of the path.

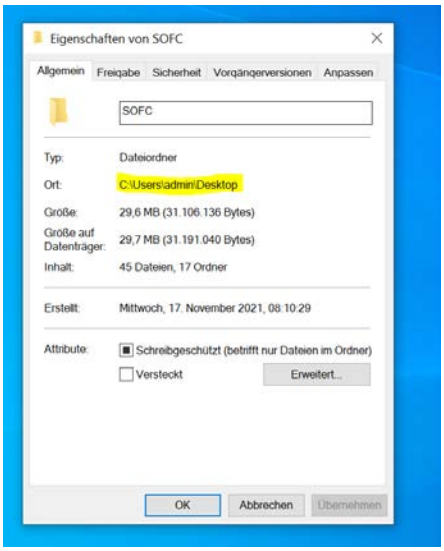

Figure A3 LabVIEW log file path

In the timestamp control, you have to click on the square button and select "*get the current time*". Then fill in the fuel type, the fuel's humidity, and the temperature of the experiment, and then click on the start button. The "created path" is an indicator that shows the path where the data will be saved. Last but not least, the "*stop the program*" button stops the whole program but to work properly, every instrument has to be stopped individually from its tab and then stop the whole program.

1.5 Assigning COM Ports

Most of the instruments that are used in the experiment are connected via serial RS232 connection. That means that when they are connected to the PC they are assigned in COM ports. In the program, it is very important to match the correct COM port to each instrument.

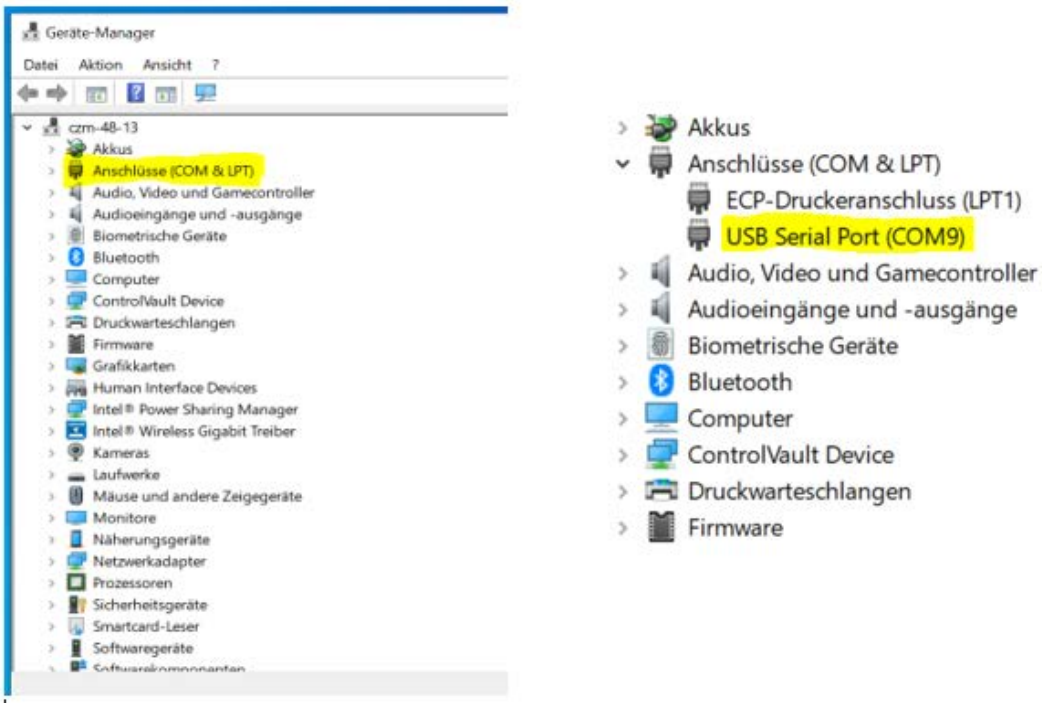

Figure A4 LabVIEW COM port assignment

(BioLogic and Agilent are connected with USB and GPIB respectively so it is pretty obvious how they will be assigned in the program). This can be found in the device manager in the COM Ports option. It is important to have already the device manager opened and see the moment you plug the instrument in the PC which is the new imported COM because three devices are connected via COM Ports (Flow valves, DC load, Eurotherm PID controller) and you should assign the correct port to the correct instrument.

1.6 The running file of program

As far as the original program is concerned which is running via the LabView program it is very important to not change the path that it runs. It is saved in the C – disk in the following path *C:\SOFC Labview program\Final-Labview programs* and it is saved in this folder with all the subprograms and libraries that are required. In case of moving the program to another place on the PC, it will probably not run correctly (the problem occurs in the EC Lab libraries which they have their path saved manually. If the program is saved and run in another PC, then the EC lab libraries path should be saved correctly. Be careful the path insertion exists in almost every EC lab command). If an independent app is used then it is free to be saved and run without any problem.

1.7 Instrument Tabs

1.7.1 Agilent tab

The Agilent tab is divided into two tabs. In the first tab, the settings of each channel are defined and in the second tab, the collected data are presented in graphs.

In the first tab (Agilent inputs), the general settings should be filled.

Visa Resource Name:

Since the Agilent is connected with a GPIB device (in the address 9) GPIB0::9::INSTR should be the resource name of the instrument.

The channel configuration is pretty straightforward. First of all, the assigned channel addresses from the Agilent should be filled in. TCC Then for the thermocouples:

Type of thermocouple:

is the only important tab of temperature channels (which is J type for the Probostat configuration)

TC Auto Check

Set to "*Don't check*" this function checks at every measurement the resistance of the thermocouple in the instrument's connection to determine if the connection is correct.

TC Rjunction

Set to "*Internal*". Thermocouple measurements require a reference junction temperature. For the reference junction temperature, you can use an internal measurement on the

module, an external thermistor or RTD measurement, or a known fixed junction temperature.

Fixed Rjunction Temp

Set to "*Manual*"

Rjunct Temp Value

Set to "*0,00*"

Seconds per iteration

is a very important control to be filled because in every iteration one set of data is collected. So, the seconds per iteration define the data collection rate.

In the voltage and current configuration, the control tabs that should be filled in are determine if the voltage and the current are AC or DC and the range of the collected data.

Agilent outputs tab

In the "*Agilent outputs*" tab, there is nothing to fill only graphs with the collected data.

It is crucial to communicate correctly with the Agilent data logger first you have to connect the sensors/ the circuit in the multiplexer's channels. Then configure each channel's setting in the Agilent MUX settings manually from Agilent's screen and then insert the same settings in the program. But first of all, they should be defined manually in the instrument.

1.7.2 Voegtlin flow valves tab

This tab controls the flow valves and is divided into three tabs. First of all, the correct COM port should be assigned.

The baud rate is set to 9600 (you should not change this value). The assigned addresses of every valve can be found in the Get Red-y app. In the program, slave values 101 to 106 have been assigned to the flow valves.

Readings tab

The "*Readings*" tab represents all the useful information for all the valves there is nothing to be set in this tab.

Set valves tab

The "*Set valves*" tab is used to define the desirable flow of each valve. If you want to set a value you have to enable the write, enable the valve that you want to control, and write the

desirable value. If you want a smooth transition from the current value to the value that you will set, you have to enable the "*ramp with delay*" and set the seconds of delay. For example, if you set 500 ml/sec transition with a 500-sec delay there will be a 1 ml/sec increase till the 500 ml/sec will be reached. If you want to receive an email in the SOFC lab email for an error you have to enable the send email control. The third tab is used only to represent the percentages and the readings of the flow valves.

1.7.3 Biologic SP150 tab

This tab is used for the potentiostat and it is divided into 6 tabs. Every tab is a potentiostat's different function. To use a function, you have to fill in all the information first and then enable it from the Boolean controllers at the top of the tab. Be careful, **you can't enable more than one function at the same time.**

1.7.4 OCV: Open Circuit Voltage

The Open Circuit Voltage (OCV) consists of a period during which no current can flow and no potential can be applied to the working electrode. The cell is disconnected from the power amplifier. On the cell, the potential measurement is available. Therefore, the evolution of rest potential can be recorded. This period is commonly used as preconditioning time or for the system to reach thermodynamic equilibrium.

Rest for tR (s)

sets a defined duration tR for the recording of the rest potential.

or until |dEwe/dt| < |dER/dt| = ... mV/h

stops the rest sequence when the slope of the open circuit potential with time, |dER/dt| becomes lower than the set value (value 0 invalidates the condition).

Record Ewe every dER = ... mV resolution and at least every dtR = ... s

allows the user to record the working electrode potential whenever the change in the potential is dER with a minimum recording period in time dtR.

Data recording with dER resolution can reduce the number of experimental points without losing any "interesting" changes in potential. When there is no potential change, only points

ac-cording to the dtR value are recorded but if there is a sharp peak in potential, the rate of recording increases.

E Range = …

enables the user to select the potential range and to adjust the potential resolution according to the experiment (See EC-Lab Software User's Manual for more details on the potential resolution adjustment).

1.7.5 V-I Characterization

V-I Characterization is intensively used to carry out investigations on Fuel cells. The principle of this technique is to apply small current steps and to measure the corresponding potential and power. The current steps are increasing till the potential drop under a crucial value. Some characteristic parameters of the cell such as maximum current, maximum potential, and maximum power can be determined.

Current V-I step:

defines the current step that it will be applied

Number of steps:

Defines the number of steps that will be made. It is recommended the number of steps to set very high (calculate the number of steps that are required to have a sum of about 1.2 A). That's because we don't want the program to stop due to the number of steps but due to the number of the Voltage lowest value.

Duration step:

Defines the duration of each current step. It is the time that it is given to the cell till an equilibrium is reached in each current step.

Voltage Lowest Value:

defines the value of voltage that when it is reached the current stops to increase.

Repeat N times:

Defines the times that you want to repeat the current step process.

Record Ewe every dER = ... mV resolution and at least every dtR = ... s

allows the user to record the working electrode potential whenever the change in the potential is dER with a minimum recording period in time dtR.

Data recording with dER resolution can reduce the number of experimental points without losing any "interesting" changes in potential. When there is no potential change, only points ac-cording to the dtR value are recorded but if there is a sharp peak in potential, the rate of recording increases.

E Range = …

enables the user to select the potential range and to adjust the potential resolution according to the experiment. (See EC-Lab Software User's Manual for more details on the potential resolution adjustment)

I Range = … Bandwidth = …

enables the user to select the current range and the bandwidth (damping factor) of the potentiostat regulation.

1.7.6 PEIS: Potentiostatic Electrochemical Impedance Spectroscopy

The Potentio Electrochemical Impedance Spectroscopy (PEIS) technique performs impedance measurements into potentiostatic mode in applying a sine wave around a DC potential E that can be set to a fixed value or relative to the cell equilibrium potential. For very capacitive or low impedance electrochemical systems, the potential amplitude can lead to a current overflow that can stop the experiment to protect the unit from overheating. Using GEIS instead of PEIS can avoid this inconvenient situation. Moreover, during corrosion experiments, a potential shift of the electrochemical system can occur. PEIS technique can lead to impedance measurements far from the corrosion potential while GEIS can be performed at a zero current.

The potential of the working electrode follows the equation:

$Ewe=E+Va \sin(2\pi f t)$

Set Ewe to E = … V *vs.* Previous

sets the fixed potential *vs.* the previous:

for a ts = …

sets tE large enough to wait for the cell current stabilization, in the case where the applied potential is different from the open circuit potential. During this period, no impedance measurement is done.

Record every dI = … pA/nA/µA/mA/A and dt = … s

offers the possibility to record Ewe and I during the DC period before the AC simulation with two conditions on the current variation dI and/or on time variation dt.

Impedance scan

Scan from fi = … MHz/ ... /µHz to ff = … MHz/... /µHz

defines the initial (fi) and final (ff) frequencies of the scan. To have the first measured point more rapidly, it is recommended to scan from the highest frequencies to the lowest ones, but it is possible to reverse the frequencies scan order.

with Nf = … points per decade

defines the frequencies distribution between the scan boundaries f_i and f_f. It is possible to select the number of points per decade $N_{(d)}$ or the total number of points $N_{(t)}$, in linear or logarithm spacing.

For example, a scan from f_i = 100 kHz to f_f = 1 kHz with N_d = 5 points per decade in logarithm spacing, will perform measures at the following frequencies (in kHz):
100, 63.1, 39.8, 25.1, 15.8, 10, 6.31, 3.98, 2.51, 1.58, 1
and a scan from f_i = 100 kHz to f_f = 1 kHz with N_t = 11 total number of points in linear spacing, will make measures at these following frequencies (Hz):
100, 90, 80, 70, 60, 50, 40, 30, 20, 10, 1

sinus amplitude V_a = … mV

sets the sinus amplitude to V_a. Equivalence with V_{RMS} is also given.
Note the following relationships between V_a, V_{pp}, and V_{RMS} $V_a = V_{pp/2}$ and $V_{RMS} = V_{pp}/(2\ ).\ 2$

Wait for p_w = … period before each frequency measurement

offers the possibility to add a delay before the measurement at each frequency. This delay is defined as a part of the period. Of course, for low frequencies, the delay may be longer.

average N_a = … measure(s) per frequency

Repeat N_a measure(s) and average the values for each frequency.

Drift correction

corrects the drift of the system. It needs to be used when the system has not reached its steady-state regime. This feature is more specifically dedicated to low frequencies at which the impedance measurement can be pretty lengthy and for which the effect of the drift can be seen.

E Range = …

enables the user to select the potential range and to adjust the potential resolution according to the experiment. (See EC-Lab Software User's Manual for more details on the potential resolution adjustment)

I Range = … Bandwidth = …

enables the user to select the current range and the bandwidth (damping factor) of the potentiostat regulation.

1.7.7 GEIS: Galvanostatic Electrochemical Impedance Spectroscopy

This technique is very close to the Potentiostatic Impedance technique (PEIS), except that the current is controlled instead of the potential. Please refer to the PEIS for more details.

1.7.8 CC: Constant Current Load

This technique is used in order to draw constant current from the fuel cell and observe its degradation through time. This technique replaces the use of a DC load. It is divided into two steps. In the first step, the user defines a starting potential that wants to be reached (for example 0.7V). In the first step, small current steps are applied to achieve the desired potential. When the desired potential has been reached then the current is maintained at this level and it remains constant for a defined duration.

Current Step to find V:

Defines the step that is initially applied in order to find the desirable Voltage. It can be defined as high as possible since as the program progresses the step is decreasing in order to catch the desiring voltage with accuracy.

Set Voltage at:

Defined the Voltage in which the user wants to start from the constant load technique

Duration step to finding V:

Defined the duration of each step in the process of finding the desiring voltage. This variable is crucial because in every step the equilibrium must be reached.

Voltage error:

Defines the acceptable error in the final voltage that will be reached. For example, if we set a desiring voltage of 0.7 Volt with an error of 0.005 Volt then values like 0.696V or 0,704V are accepted.

Con curr Duration:

Defines the duration of the constant current technique.

Duration Unit:

Defines the unit of the duration.

Record Ewe every dER = ... mV resolution and at least every dtR = ... s

allows the user to record the working electrode potential whenever the change in the potential is dER with a minimum recording period in time dtR.

Data recording with dER resolution can reduce the number of experimental points without losing any "interesting" changes in potential. When there is no potential change, only points ac-cording to the dtR value are recorded but if there is a sharp peak in potential, the rate of recording increases.

E Range = …

enables the user to select the potential range and to adjust the potential resolution according to the experiment. (See EC-Lab Software User's Manual for more details on the potential resolution adjustment)

I Range = … Bandwidth = …

enables the user to select the current range and the bandwidth (damping factor) of the potentiostat regulation.

1.7.9 CV: Cyclic Voltammetry

The CV technique consists in scanning the potential of a stationary working electrode using a triangular potential waveform. During the potential sweep, the potentiostat measures the current answer of the system. The cyclic voltammogram is a current response plotted as a function of the applied potential.

Traditionally, this technique is performed using an analog ramp. Due to the digital nature of the potentiostat, the applied ramp consists of a series of small potential steps that approximate the targeted linear ramp.

Start from E (V) vs init:

Starts the scan from the defined E and every step that is defined on the array is calculated either from the initial potential or the previous potential.

Scans:

In this array, in the first-row tab, the potential step is defined either from the initial potential or from the previous. And in the second tab, the rate of the scan is defined. Careful, in the left foremost tab, the number of the row is indicated which starts from 0.

Stop after scan number:

Defines the number of the last step. For example, if you want to define 2 steps you will assign values to the rows from columns 0 and 1 and in the "stop after scan number" you will assign number 1.

Measure I from … to:

In these two tabs, a percentage is assigned to determine from which point of the step you want to measure the current. The values should be from 0 to 1.

E Range = …

enables the user to select the potential range and to adjust the potential resolution according to the experiment. (See EC-Lab Software User's Manual for more details on the potential resolution adjustment)

I Range = … Bandwidth = …

enables the user to select the current range and the bandwidth (damping factor) of the potentiostat regulation.

1.8 Eurotherm tab

This tab is used to control the PID controller for the oven. It is divided into 4 techniques: ramp with rate, a ramp with time, and a dwell/ cool down, and program. The process value that is indicated in the right of the tab is the actual value that the thermocouple reads and it is also indicated in the graph.

First of all, the most important value to be assigned is the correct COM port. After that, the unit address is assigned as 1 (all these values can be cross-checked before the connection of the Eurotherm controller in the build-in menu and graphical environment of the controller or in the itools app). If any error is created in the process then the temperature is maintained despite the error. The user can erase the error from the Boolean control "*Acknowledge all alarms*". All the techniques are ended with indefinite dwell. That means that when the ramp will end the temperature will remain for an indefinite time at the target point. If a cool down is required, then the cooldown technique must be turned on.

1.8.1 Ramp with rate

In this technique, a ramp is defined till a target temperature with the desired ramp rate.

RR Ramp Time Units:

Defines the units of time that will be used in the ramp (per sec/min/hours)

RR Dwell Time Units:

Defines the units of time that will be used in the dwell (sec/min/hours)

Ramp Rate:

Defines the rate in degrees of Celsius per ramp time units

RR Target setpoint:

Defines the target temperature that will be reached at the end of the ramp

1.8.2 Ramp with time

In this technique, a ramp is defined as a target temperature with the desired duration time.

RT Ramp Time Units:

Defines the units of time that will be used in the ramp (per sec/min/hours).

RT Dwell Time Units:

Defines the units of time that will be used in the dwell (sec/min/hours).

RT duration:

Defines the duration that the ramp will last in dwell time units.

RT Target setpoint:

Defines the target temperature that will be reached at the end of the ramp.

1.8.3 Dwell/Cool down

This tab has two functions both dwell and cool down. After a ramp at a certain temperature, a dwell or a cool down may follow. When the Dwell/Cool down is activated, the default function is the dwell function at an independent dwell target Setpoint. However, a cool down can be activated from its Boolean control. For the cool down, a target temperature must be assigned after which a dwell will start. The dwell can start either at the cool down temperature or in a new independent value (for dwell at the same target point of the cool down the corresponding Boolean must be activated).

Cooldown to:

Defines the temperature that the cooldown will stop and start the dwell.

Independent Dwell Target Setpoint:

Defines the target setpoint of the dwell.

D Ramp Time Units:

Defines the units of time that will be used in the ramp (per sec/min/hours).

D Dwell Time Units:

Defines the units of time that will be used in the dwell (sec/min/hours).

Dwell duration:

Defines the duration that the ramp will last in dwell time units.

Dwell Target setpoint:

Defines the target temperature that will be reached at the end of the ramp.

1.8.4 Program

The program works exactly like the program section in the PID controller. A max 16-segment program can be defined via the array (the indexing process of an array is explained in the first paragraph of this document). In the array, every value mentioned above can be defined in order for the whole program to be set. Furthermore, with the 'take action' Boolean the user can hold/run or stop the program manually.

Ramp Time Units:

In this control, the user indicates the units of the ramp segment, whether it will be degrees per second, or minute, or hour. The default is degrees per minute.

Dwell Time Units:

In this control, the user indicates the units of the dwell segment. Again the default value is minutes.

Number of Segments:

It is a crucial control and indicates from how many segments the heating program consists of. Be careful, the array indexing starts from 0 so if the last segment that we will import is for example 3, then the number of segments is 4.

Starting Temp:

This control indicates the temperature that the program is started and it is used only to create the program's graph.

Take Action:

This is a Boolean control. When it is true (led turned on) the user can import a Program Status, when it is false (led turned off) then the Program Status control is not taken into consideration.

Program Status:

It is activated only when the Take Action Boolean control is turned on and it indicates the status of the program. The user can decide whether the program will be RUN (running), HOLD (on pause), or OFF (turned off).

Program Array:

The program array is indexed separately for each segment by setting the counter control in 0,1…etch.

Segment Type:

This control indicates the selected segment. There are 6 available segment types:

1. The end, segment that indicates the termination of the program
2. The ramp rate, that indicates a temperature ramp controlled by a specific imported rate
3. The ramp time to target, that indicates a temperature ramp in which the total duration is imported and the rate is calculated automatically
4. The dwell, that indicates the duration that the furnace will stay at a certain temperature
5. The step that indicates a temperature target and the controller tries to reach this temperature with the fastest rate possible (it is not recommended)
6. The call which is not actually a type of segment, it is a function that calls a defined subprogram. In this program, the call function doesn't work

End Segment Type:

When the type of the selected segment is "end", then the type of end segment should be indicated. There are two available options for this program. Either "Indefinite Dwell" which means that the furnace stays for an indefinite time in the reached temperature, or "Reset" which means that the furnaces shut down its resistances after the program ends.

Duration:

This control is used only in the dwell and the time target rate and indicates the duration of the segment.

Target Setpoint:

This control set the desired temperature that should be reached from each segment

Ramp Rate:

This control indicates the rate of the temperature ramp.

1.9 RND DC load tab

This tab controls the DC Load and it is divided into two sub-tabs: V-I step and Constant Current. At the top of this tab, the Visa resource name should be imported. The baud rate is set to 115200. After that, the two Boolean controls are used in order to activate either the V-I step or the Constant current function. As it has been mentioned above in the Potentiostat the V-I step function is a function with current steps that determines the maximum power that the cell can produce. The constant current function draws constant current from the cell to a threshold the user indicates.

1.9.1 V-I Step

Step(A):

The user defines the current step (in Amperes) of the procedure

Voltage Lowest Value:

The user defines the lowest voltage value that when it is reached the function stops (or starts again from 0).

Step Duration:

The user defines the duration of each step. The duration can be either in seconds, or minutes depending on the position of the Boolean control.

Measure every:

The user defines the sampling rate. The measurement rate can be either in seconds or minutes depending on the position of the Boolean control.

Turn off VI after termination:

The user can select to end the V-I procedure after reaching the Voltage Lowest Value (true) or to repeat the process (false).

1.9.2 Constant Current

The constant current function does not start immediately. Firstly, the user indicates the desired voltage at which the constant current must take place. After that, the desired voltage is reached with small current steps. And finally, the constant current begins.

Step for CC:

The user defines the step with which the desired Voltage value will be reached.

Set Voltage to:

The user defines the desired Voltage value in which the constant current will take place.

Error:

The user defines the error that is allowed in the approach of the "set voltage to" value. For example, for a set voltage value to 0.6V and an error of 0.01, the values from 0,59 to 0,61 are considered correct.

Voltage limit:

The user defines the limit value of voltage that when it is reached the procedure stops or starts again from 0.

CC step Dur:

The user defines the duration of each step in the procedure of finding the desired voltage value.

Voltage Now:

It is an indicator that shows the measured voltage value.

Step Now:

It is an indicator that shows the current step.

Dt Measure CC:

The user defines the sampling rate in the constant current mode. The measurement rate can be either in seconds or minutes depending on the position of the Boolean control.

Turn off CC after termination:

The user can select to end the CC procedure after reaching the Voltage Limit Value (true) or to repeat the process (false).

The diagrams on the right show the measured voltage and current. The diagrams in the constant current mode start to record the values of the voltage and the current when the Voltage desired value has been reached.

The timer under the constant current control variables can be used to help the user count the elapsed time of constant current. The timer can be reset every time that the procedure starts and stops. For every reset of the timer, the previous time is saved in the indicator cluster. The timer's data are used only to help the user to keep track of the elapsed times of the experiment, its data are not saved. (The elapsed data for each measurement can be calculated from the timer data of its instrument).

Last but not least at the foremost right position of the user's tab there is a column that is constantly present despite the tab that the user is in. This column sums up all the useful information of the experimental procedure which are, the Temperature sensor values in the anode and the cathode side, the Voltage and the Current, the gas flow of each valve, and the current segment that the furnace is on. It is also indicated if a critical error occurs.

1.10 How the program works

The program is designed in a way that it starts from the foremost left tab and then by choosing the suitable Boolean options it progresses to the right. No value is mandatory to be filled in before the LabVIEW's start button. However, to activate a tab with its Boolean or its start button all the control tabs should be filled first. So, in every tab, firstly the user must define the values of the controls and then activate the tab. In the general settings are defined and the path for the saved data is created as well. Then a title for each instrument's data file is automatically created from the program. Another important thing is that the program is in a constant loop. This means that it is very crucial to select and activate every Boolean control but to have also in mind that when the process will end the program will loop, so if the Boolean controls are left in ON position the process with the ON Boolean will be repeated. For example, if we define a ramp on the Eurotherm controller and leave the Boolean of the ramp in the ON position when we will exit the infinite dwell function of the program the controller will go again to ramp mode since the Boolean is left in ON position. So, be very careful with both the start and the end of every new process that you assign to

the program. Moreover, due to the loop architecture of the program in order to execute the "Stop the program" correctly (in other words in order to stop the whole program), you must first have stopped every other process that is running in the background with its individual stop button and then hit the stop the program button. **Be careful, if you stop the program with the LabView's stop button, the program will be stopped but that doesn't mean that the processes will be stopped.** That is happening because in the Modbus protocol, that many instruments use, if you assign a value in a register and then close the program, then the register is still assigned with the value that you defined, and stopping the program will not set this value to zero or to the default value. That's why it is **very important especially with the Voegtlin valves at the end of the experiment to set all the Flow valves to zero setpoints.** Every other aspect of the program is pretty straightforward. In case of emergency, it is better to shut down the instrument rather than try to shut down the program correctly.

1.11 Quick Start of the program

1. Press the run button of LabVIEW. Till this point, nothing should have been filled.

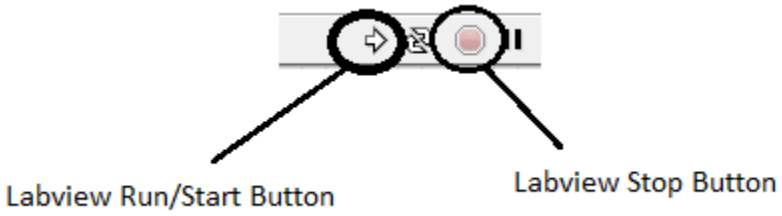

Figure A5 LabVIEW start and stop button

2. In the general tab first of all fill the choose PC control with the admin… option of the dropdown menu.
3. Fill the Fuel, Fuel Humidity, Experiment's temperature, and Sample name controls.
4. In the Timestamp control press the calendar button and choose the Set time to now option.
5. Fill the experiment procedure short text
6. Hit the start Control (if you operate the program in a small screen you have to scroll down to see the start control button)

Till this point, the general settings have been filled and the file that all the data will be saved has been created and includes a text file that describes the experiment's procedure.

7. Click to Eurotherm furnace tab
8. Assign the correct Visa resource name (which can be found via the device manager)
9. The Unit Address should be 1
10. Click to the Program tab
11. Fill the Ramp and Dwell time units (Minutes is the predefined value)
12. Fill in the Number of segments and the starting temperature
13. The take action should be in "False" position (Boolean light off)
14. Index the desired furnace program in the array (see page 3, how to fill in an array)

!! It is a good idea to control manually the start of the furnace with the enable/disable resistances buttons because, in the beginning, the readings have steep rates that confuse the controller. However, it is not a must the equilibrium will be reached anyway.

15. Turn on the Program Boolean control
16. Turn on the Eurotherm Boolean control (if everything works correctly the Eurotherm light should turn on and off that indicates that the Eurotherm has opened)

At this point the screen of Eurotherm should start the configuration and after a few seconds start executing the program

17. Hit the Voegtlin flow valves (if a hardware error occurs in the valves, that means that a red light will be permanently open in the valves, you have to solve it with the original get red-y program, this program)
18. Assign the correct COM Port (which can be found via the device manager)
19. The Baud rate must be 9600
20. Turn on the Get Red-y Valves Boolean control, again the light of the Boolean should turn on and off, if not the valves haven't started correctly
21. Hit the set valves tab
22. Index the desired inputs
23. Turn on the Boolean controls of each valve that you want to write in
24. Turn on write and/or the send email and save gas readings Booleans

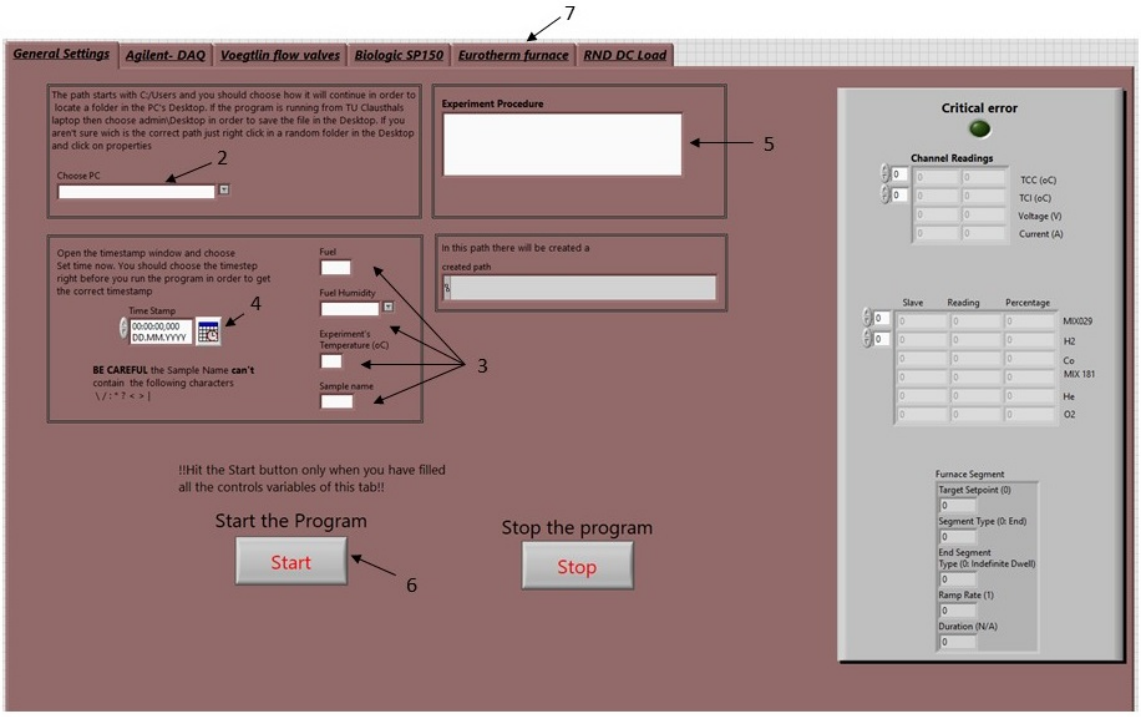

Figure A6 LabVIEW general tab

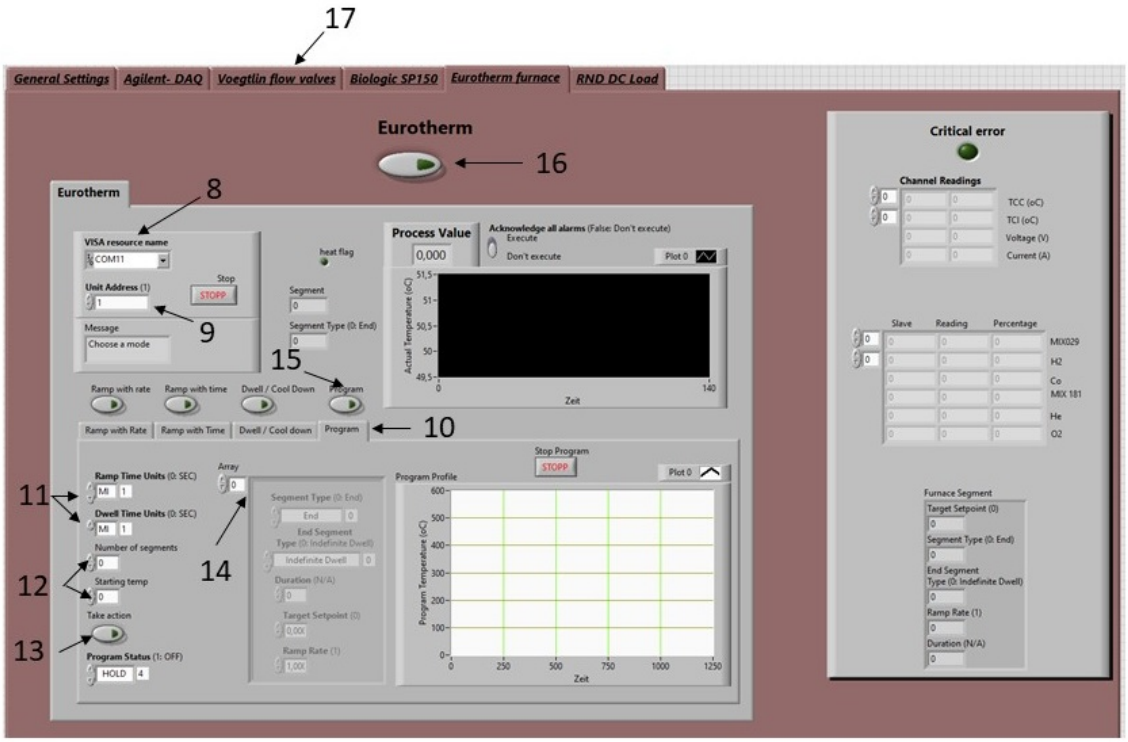

Figure A7 LabVIEW Eurotherm tab

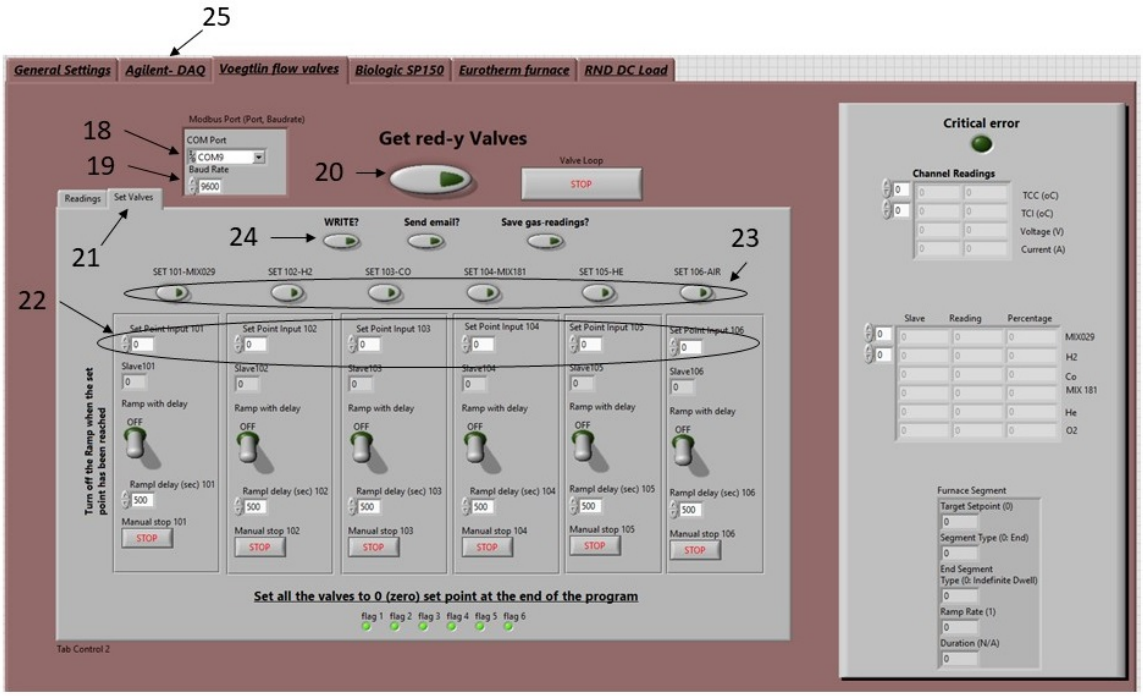

Figure A8 LabVIEW valves tab

At this point, you should see the LED lights of the valves going and off and read in the values of each valve from LabVIEW

25. Hit Agilent DAQ tab
26. Check that the resource name is GPIB0::9::INSTR
27. Index the seconds per iteration (the default value is 120, which means measure every 2 minutes)
28. Check that all the other settings are as follows:

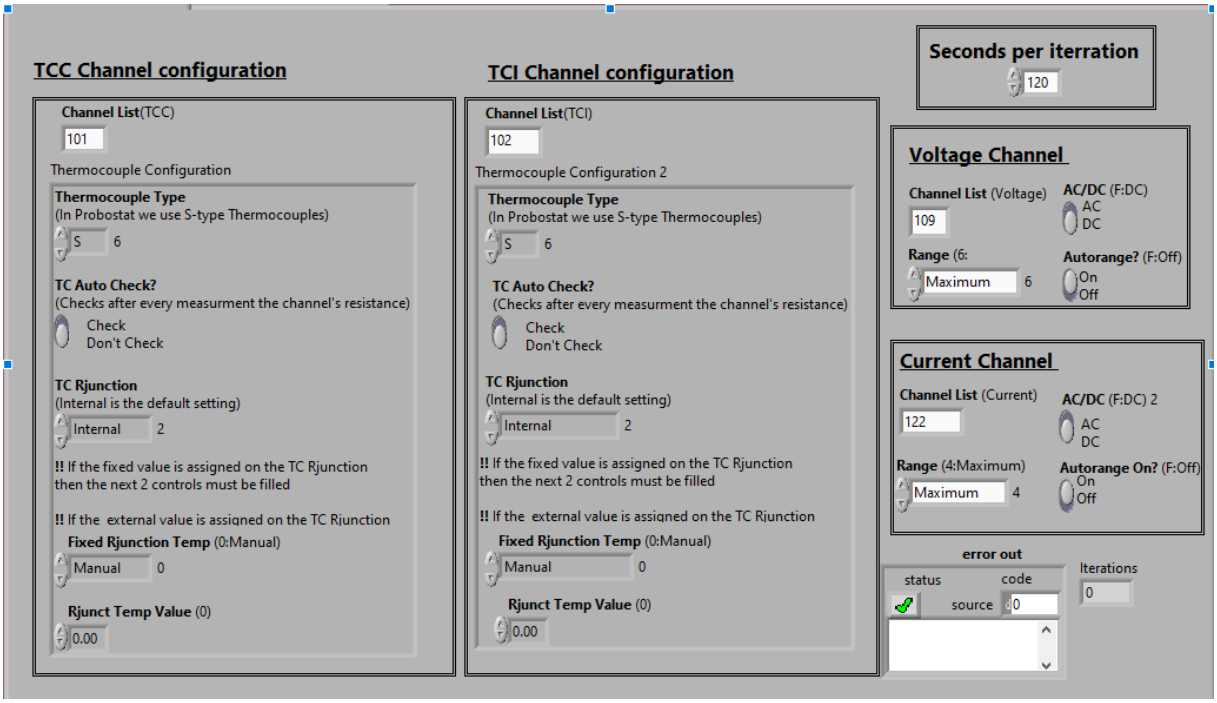

Figure A9 LabVIEW Agilent tab

29. Turn on the Agilent Boolean. (Again the Light of the Boolean should turn on and off)
30. Last but not least, start the cooling device

At this point, the program is working and the important measured values (anode, cathode temperature, furnace temperature cell open-circuit voltage, gases flows) are presented at the right side of the program. The program can run like this till the time that current should be drawn from the cell. It is important to understand the main structure of the program which is, first fill whatever information or command you want to give to the measuring instruments and then open the corresponding Boolean control to pass it via the LabVIEW to the instrument. All the tabs for every instrument work this way.

Assuming that the testing temperature has been reached and it is time for more specific tests. If you want to insert a new furnace program, fill in the new information (new number of segments, and new segments details) leave the program Boolean in the on position and press stop in the furnace program's tab. After 20 sec the new program will start automatically.

31. OCV Test. The following image shows how an OCV for 15 seconds is set. After 15 seconds of the test, the potentiostat stops automatically. You should press the stop button only in case you want to stop the program earlier. A 15-second OCV should be done before the PEIS test.

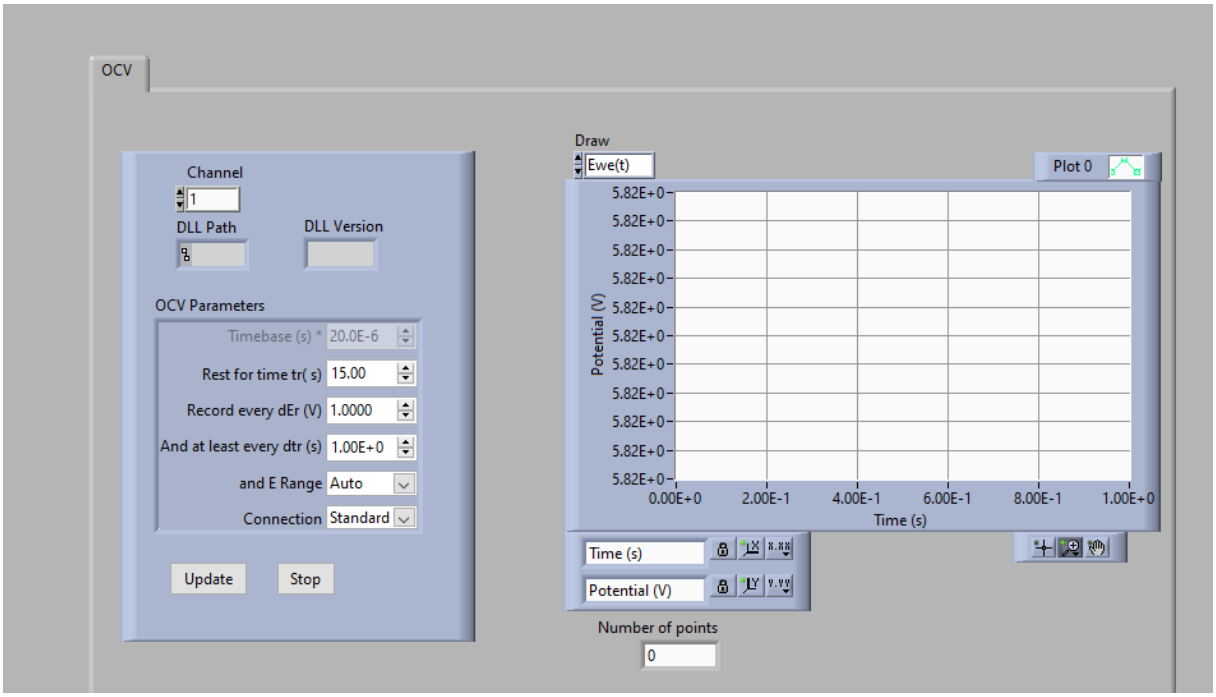

Figure A10 LabVIEW OCV tab

What represents each variable is pretty self-explained, but it is also mentioned above in detail. After filling these values in the variables, turn on the OCV Boolean and then turn on the Potentiostat Boolean. The light of potentiostat's Boolean control should be turned on and off. In another way it is not working properly.

32. PEIS Test. The following image shows the details of a PEIS test. The procedure for starting the test is the same as with OCV. It is important that you have to open again the potentiostat's Boolean control and its light should blink. Otherwise, something is not going as planned. It is possible the previous test to haven't stop, so try to stop the previous test manually.

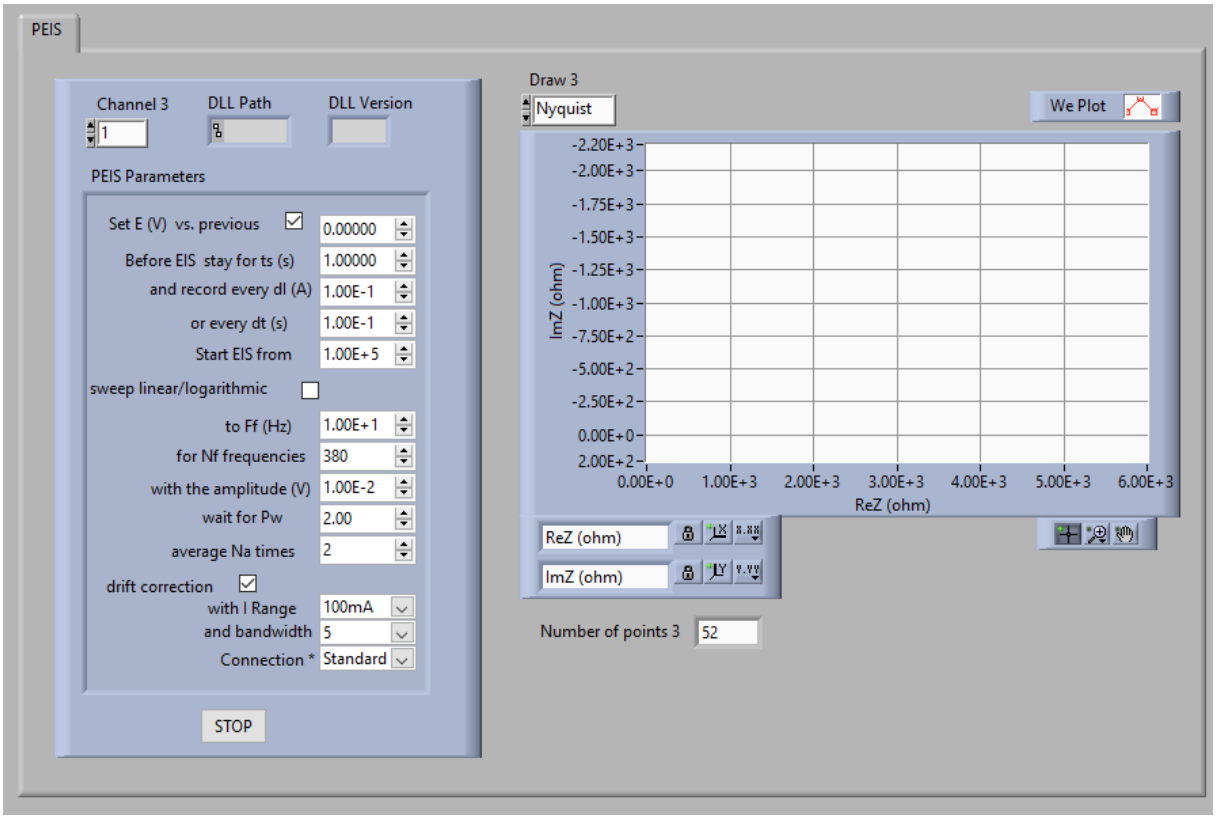

Figure A11 LabVIEW PEIS tab

33. V-I Step (from DC Load). The following image shows a common V-I test with a 10 mA current step. Each step lasts for 150 seconds and one measurement is taken every 50 seconds. When the voltage drops lower than 0.35 V the procedure will stop and it will not start again.

DON'T FORGET to check that the Visa resource name is correct according to the device manager. The Baud rate must be 115200.

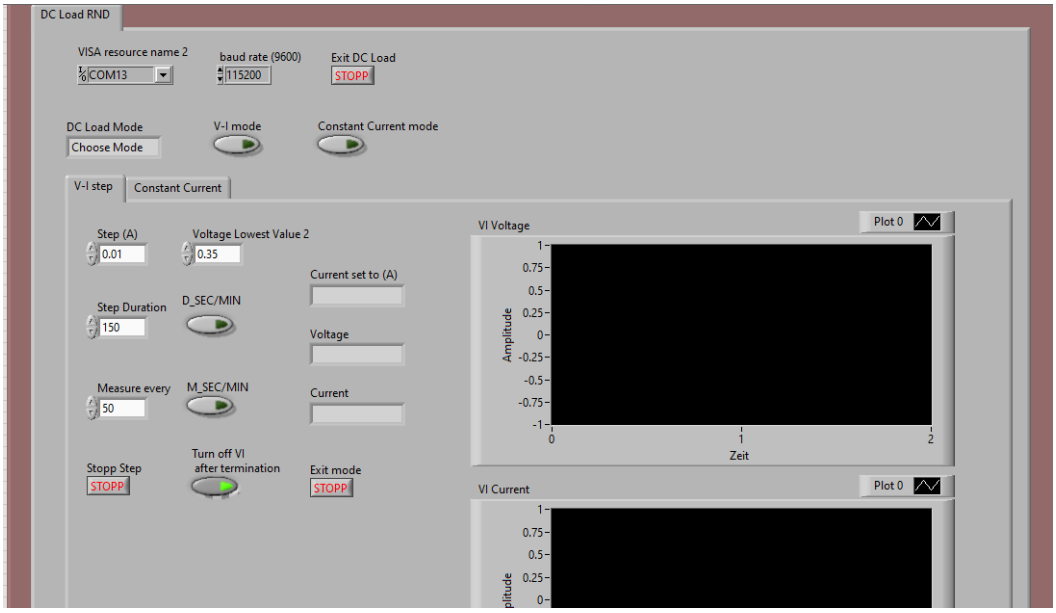

Figure A12 LabVIEW RND V-I tab

After filling in the details shown above, turn on V-I mode Boolean and then turn on DC Load RND Boolean. Be careful what is shown to the DC Load Mode. If it says Open DC Load you have to click on the DC Load RND Boolean. If it says choose Mode you must not click on the DC Load RND Boolean, just to activate the correct mode. The same applies to the Constant Current mode.

34. Constant Current test. In the picture below is shown a typical constant current procedure. In this picture, the Desired Voltage for the Constant Current is 0.6V and the DC load will approach these values with steps of 10 mA (they adjust later automatically in order to reach the Voltage Value) that last for 150 seconds. The accepted range is from 0.591 to 0.609 Volt and when the Voltage drops lower than 5.7 Volt the procedure starts again automatically. The sampling rate is 1 measurement per 60 seconds.

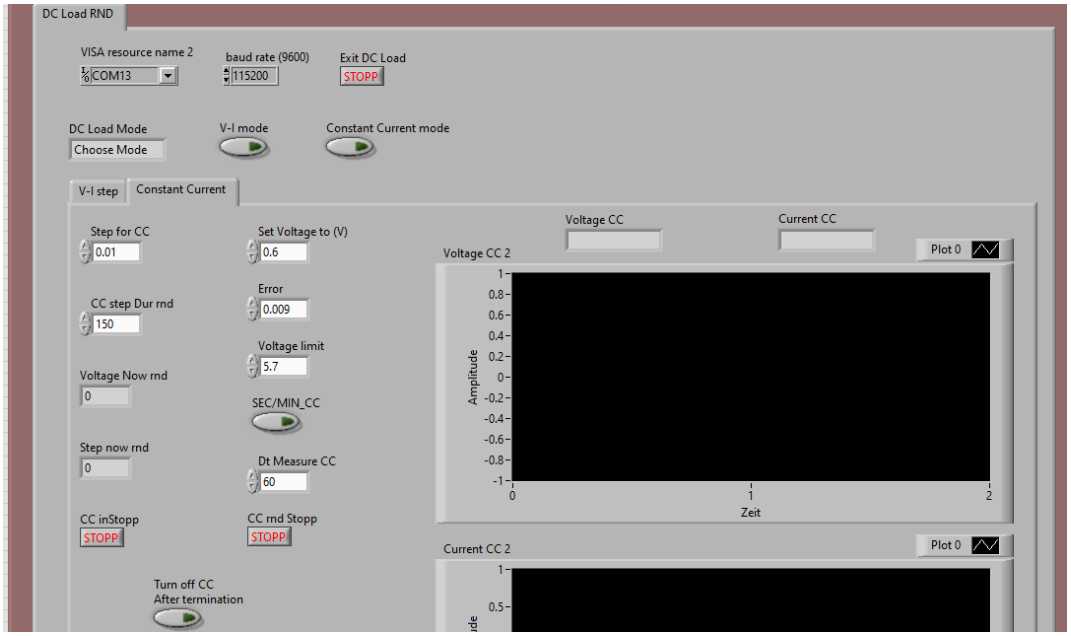

Figure A13 LabVIEW RND CC tab

If something goes not as planned the LabVIEW program can shut down manually from the LabVIEW stop button. If the furnace is in hold mode, then nothing bad will happen. The Voegtlin valves keep their flow rate despite the unexpected stop of the program. That is very important and you will be aware when the experiment ends you should index 0 flow rate to all the flow valves.

In order to terminate the program:

1. Make sure that you have set all the flow rates to 0 ml/min.
2. Stop every instrument independently by its stop button. That may be take several minutes, because when the program is in the loop it has to end its current iteration and then stop. So for example for the Agilent instrument with sampling rate 1 sample per 2 minutes the stop command can take up to 2 minutes to complete. (Tip when the stop button has been pressed it turns in a darker color, when the stop has been red from the program the stop button turns back to its regular gray color. So only when the stop button is back in its normal color the loop has been stopped).
3. Press the stop button in the General tab to terminate the whole program.

1.12 Drivers that are required

1.12.1 Agilent 34970 (connected with GPIB)

1. IOLibSuite (contains all the drivers required for the proper connection of the Agilent with the PC)
2. NI 488.2 driver
3. NI Max, you must enable NiVisa Tulip passport
4. Agilent 34970 LabVIEW driver (it can be downloaded directly from LabVIEW and contains all the VIs that are specified in the communication of Agilent with the LabVIEW, it also contains simple examples of reading and writing commands)

1.12.2 Voegtlin Flow valves

1. Modbus communication driver
2. Red-y LabVIEW driver

1.12.3 Biologic SP150

1. EC-Lab developers' package from biologic (contains the USB driver for Biologic, all the specified Vis, and simple examples)

1.12.4 Eurotherm 2416

1. For the Eurotherm connection the only driver that is required is the et24xx driver from LabVIEW. It is not supported from the LabVIEW NI so it should be downloaded independently
2. Be careful, if you are using the Eurotherm for the first time on a new PC you have to activate the COM Port from the Eurotherm's program 'itools'

1.12.5 RND 320

1. This device uses USB or RS232 connection. In windows 10 the USB driver of the device is preinstalled in the system or it is found automatically. However, if there is a problem with the connection, RND provides the USB driver in its website and in a CD
2. NI Visa driver

1.13 7. Experiment's wiring diagram

Below it is shown the wiring connection diagram of the experiment.

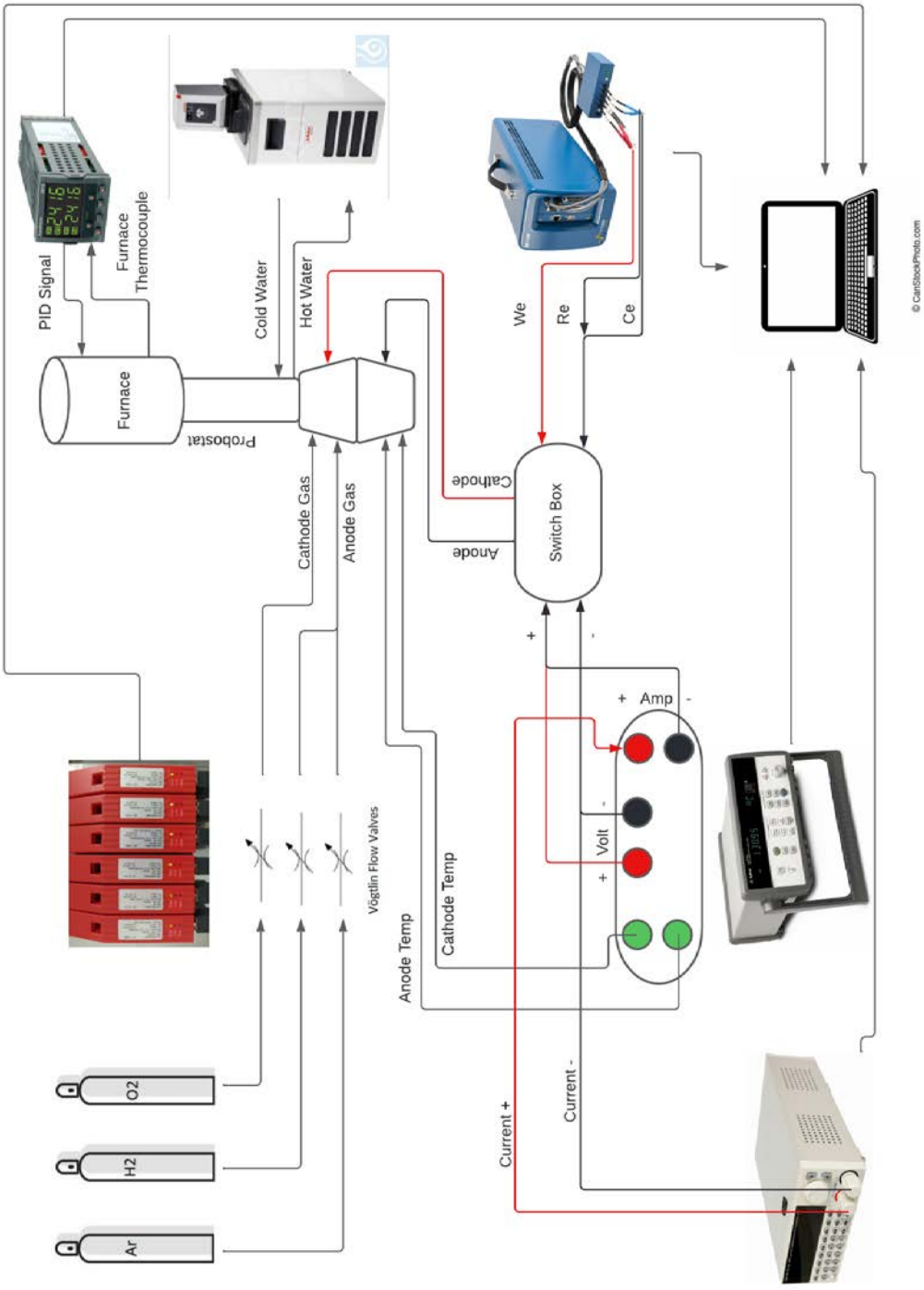

Figure A14 Test rig connection diagram